



<https://theses.gla.ac.uk/>

Theses Digitisation:

<https://www.gla.ac.uk/myglasgow/research/enlighten/theses/digitisation/>

This is a digitised version of the original print thesis.

Copyright and moral rights for this work are retained by the author

A copy can be downloaded for personal non-commercial research or study, without prior permission or charge

This work cannot be reproduced or quoted extensively from without first obtaining permission in writing from the author

The content must not be changed in any way or sold commercially in any format or medium without the formal permission of the author

When referring to this work, full bibliographic details including the author, title, awarding institution and date of the thesis must be given

Enlighten: Theses

<https://theses.gla.ac.uk/>
research-enlighten@glasgow.ac.uk

ISOMERISATION AND SUBSTITUTION REACTIONS
OF DIMOLYBDENUM COMPLEXES

A Thesis submitted to
the University of Glasgow
for the Degree of

Doctor of Philosophy

by

ANDREW McVITIE (BSc)

Department of Chemistry,
University of Glasgow.

May 1988

©

ProQuest Number: 10997948

All rights reserved

INFORMATION TO ALL USERS

The quality of this reproduction is dependent upon the quality of the copy submitted.

In the unlikely event that the author did not send a complete manuscript and there are missing pages, these will be noted. Also, if material had to be removed, a note will indicate the deletion.



ProQuest 10997948

Published by ProQuest LLC (2018). Copyright of the Dissertation is held by the Author.

All rights reserved.

This work is protected against unauthorized copying under Title 17, United States Code
Microform Edition © ProQuest LLC.

ProQuest LLC.
789 East Eisenhower Parkway
P.O. Box 1346
Ann Arbor, MI 48106 – 1346

To Mum and Dad

Dear Mum and Dad,

I'm writing to you because I want to tell you how much I love you and how much I appreciate everything you do for me. You are the best parents anyone could ask for. You always make me feel safe and loved, and you are always there for me when I need you. I know you're busy, but you always find time to spend with me. I love the way you laugh and the way you talk to me. You are my heroes and I look up to you both. I hope you're having a great day. I love you both very much.

Love,
 [Name]

I hope you're both well and happy. I miss you both very much and I can't wait to see you again. You are my world and I love you both so much. I hope you're both having a great day. I love you both very much.

Acknowledgements

I would like to express my gratitude to Dr.R.D. Peacock for his advice and encouragement during this project and also for allowing me to type this thesis on his word-processor. I would also like to thank all of the staff and students in laboratory 281 for their help in making the project an enjoyable one. I am indebted to Dr. Farrugia for determining the crystal structure of $[\text{Mo}_2(\text{O}_2\text{CCH}_3)_2(\text{dmpe})_2][\text{BF}_4]_2$ and providing the programme for carrying out the Hückel calculation on $\text{Mo}_2\text{Cl}_4(\text{PH}_3)_4$.

My special thanks to my family for their support throughout the whole of my university life. My thanks to Pat for her encouragement and love.

I thank the SERC for a studentship.

Ligand Abbreviations

dmpe	1,2-bis(dimethylphosphino)ethane
dppe	1,2-bis(diphenylphosphino)ethane
dptpe	1,2-bis(diparatoylphosphino)ethane
dmpm	bis(dimethylphosphino)methane
dppm	bis(diphenylphosphino)methane
depe	1,2-bis(diethylphosphino)ethane
dppp	1,3-bis(diphenylphosphino)propane
dpdt	(1-(diphenylphosphino)-2-(di-p- tolylphosphino)ethane)
R-phenphos	R-1,2-bis(diphenylphosphino)phenylethane
R-dppp	R-1,2-bis(diphenylphosphino)propane
S,S-dppb	S,S-2,3-bis(diphenylphosphino)butane
S-chairphos	S-1,3-bis(diphenylphosphino)butane
S,S-skewphos	S,S-2,4-bis(diphenylphosphino)pentane
en	1,2-diaminoethane
R-pn	R-1,2-diaminopropane
DIOP	2,3-O-isopropylidene-2,3-dihydroxy-1,4- bis(diphenylphosphino)butane
TPP	tetraphenylporphyrin
tmtaa	dibenzotetramethyltetraaza[14]annulene
TFMS	trifluoromethanesulphonate

CONTENTS

Dedication	i
Acknowledgements	ii
Abbreviations	iii
Contents	iv
Summary	v
<u>Chapter One</u>	1
Introduction	
<u>Chapter Two</u>	46
Experimental	
<u>Chapter Three</u>	76
Isomerisation Reactions of Dimolybdenum Complexes Containing Diphosphine Ligands	
<u>Chapter Four</u>	109
Substitution Reactions of Dimolybdenum Complexes	
<u>Chapter Five</u>	141
Optical Activity in Dimolybdenum Complexes Containing Bridging Bidentate Ligands	
<u>References</u>	183

Summary

The work in this thesis deals with quadruply bonded dimolybdenum compounds. Many new complexes have been synthesised and characterised by various spectroscopic techniques.

Complexes of general formula $\text{Mo}_2\text{X}_4(\text{P}\sim\text{P})_2$ where $\text{X} = \text{Cl}$ or Br and $\text{P}\sim\text{P}$ is a diphosphine ligand, can exist as two geometric isomers. In many cases the α (chelated) isomer isomerises to the β (bridged) form in dry dichloromethane solution. This transformation has also been observed for $\text{Mo}_2\text{Cl}_4(\text{dppe})_2$ in the solid state. Kinetic parameters have been collected for the solution isomerisation of $\alpha\text{-Mo}_2\text{Cl}_4(\text{dppp})_2$ and for the solid state isomerisation of $\alpha\text{-Mo}_2\text{Cl}_4(\text{dppe})_2$. The kinetic data are compared with those obtained for other dimolybdenum complexes. The possible mechanisms for the isomerisation reactions are reviewed and discussed in the light of the new data obtained for the solid state reaction.

Many quadruply bonded complexes contain weakly bound ligands which can easily be displaced. The complex $\text{Mo}_2(\text{TFMS})_4$ contains very labile ligands. Reactions of this complex with ligands such as DMF or acetonitrile lead to total ligand substitution. $[\text{Mo}_2(\text{O}_2\text{CCH}_3)_2(\text{CH}_3\text{CN})_6]^{2+}$ has labile acetonitrile ligands and partial ligand substitution was observed when the cation was reacted with diphosphine or diamine ligands. The product from the reaction of $[\text{Mo}_2(\text{O}_2\text{CCH}_3)_2(\text{CH}_3\text{CN})_6]^{2+}$ and dmpe gives

$[\text{Mo}_2(\text{O}_2\text{CCH}_3)_2(\text{dmpe})_2]^{2+}$, the latter complex has a trans arrangement of acetate ligands while the former has cis. A mechanism for this reaction is presented.

Optical activity in quadruply bonded complexes has generated considerable interest in recent years. The configurations and conformations of a variety of complexes of the general formula $\beta\text{-Mo}_2\text{Cl}_4(\text{P}\sim\text{P})_2$ and $[\text{Mo}_2(\text{O}_2\text{CCH}_3)_2(\text{L}\sim\text{L})_{4-2x}(\text{CH}_3\text{CN})_6]^{2+}$ ($x = 1$ or 2), where $\text{P}\sim\text{P}$ is a chiral diphosphine ligand and $\text{L}\sim\text{L}$ can be either a chiral diamine or diphosphine ligand, have been studied.

Chapter One: INTRODUCTION

1. Multiple Bonds Between Metal Atoms

1.1 General Overview on Multiple Metal Bonds

The revival in inorganic chemistry which began in the 1950's has been greatly supplemented by the discovery that metals can form multiple bonds. In 1964 Cotton *et al* first proposed the nature of the bonding scheme in the quadruply bonded species ^{1,2}, $[\text{Re}_2\text{Cl}_8]^{2-}$. Since then a vast amount of research has been carried out in this area and hundreds of complexes have been synthesised which contain a multiple metal bond.

In spite of the fact that the first synthesis and structure determination of a quadruply bonded complex was that of a dirhenium species ³, molybdenum is the most prolific former of multiple metal bonds. Table 1.1 lists the transition metals which are known to form multiple bonds ⁴. In addition to this, several heteronuclear complexes containing quadruple bonds have been formed between chromium and molybdenum ⁵⁻⁷, and also between molybdenum and tungsten ⁸⁻¹¹.

1.2 Bonding Scheme for Multiple Metal Bonds

The components of a multiple metal bond are made up from interactions of the valence metal d orbitals as shown in figure 1.1 ¹².

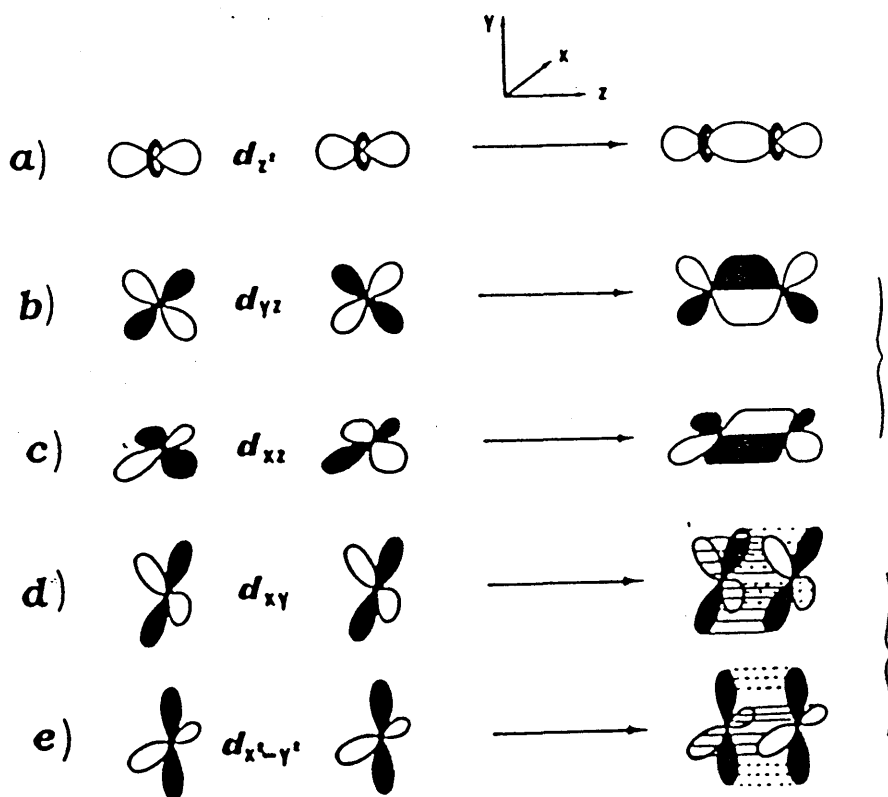


Figure 1.1 Five non-zero d orbital overlaps forming metal-metal bonds.

Table 1.1 Transition Metals which Exhibit Multiple Metal Bonding

V	Cr				
3	4				
	Mo	Tc	Ru	Rh	
	3,3.5,4	3.5,4	2,2.5,3	1	
	W	Re	Os		Pt
	3,3.5,4	3,3.5,4	3		1

When two metal atoms approach each other, there are five non-zero overlaps possible between the pairs of d orbitals. The overlap between the d_{z^2} orbitals on each atom give rise to a strong σ bonding orbital. The overlap between each pair of d_{xz} and d_{yz} orbitals give rise to a pair of equivalent, intermediate strength, π bonding orbitals; these bonds are orthogonal and degenerate. Finally, the overlap between each pair of d_{xy} and $d_{x^2-y^2}$ orbitals give rise to a pair of weak δ bonds, these are also orthogonal and degenerate. There are five corresponding antibonding orbitals which arise from the negative overlaps of the above orbitals. The overlap integrals of these molecular orbitals increase in the order $\delta \ll \pi < \sigma$. Assuming that the energies of these orbitals are proportional to the overlap integrals, then the ordering of the orbital energies will be

$$\sigma < \pi \ll \delta < \delta^* \ll \pi^* < \sigma^*$$

This system applies to the simple diatomic molecule M_2 which has cylindrical symmetry $D_{\infty h}$. When eight ligand atoms are introduced around the metal dimer in a cubic array as in figure 1.2¹³, then the symmetry of the system is lowered to a square prismatic M_2L_8 (D_{4h}). A set of coordinate axes are chosen such that the metal-metal bond lies along the z-axis as in figure 1.2. It then arises that the $d_{x^2-y^2}$ orbitals on the metal atoms become involved in metal-ligand bonding and therefore will not contribute to any metal-metal interaction.

A quadruple bond is achieved when the bonding orbitals are completely filled and there is no occupancy of the antibonding orbitals. Therefore the two metal atoms require eight d electrons between them to attain this state. Dinuclear species which fit this requirement are, for example, the $[Mo_2Cl_8]^{4-}$ anion and $Mo_2Cl_4(PEt_3)_4$ where molybdenum is in the +2 oxidation state (d^4); also the $[Re_2Cl_8]^{2-}$ anion where rhenium is in the +3 oxidation state (d^4). These species have the electronic configuration $\sigma^2\pi^4\delta^2$ which corresponds to a formal metal-metal quadruple bond. Two striking aspects of quadruply bonded complexes are the extreme shortness of the metal-metal bond and their tendency to form eclipsed structures. The shortness of the bond is due to the high bond order.

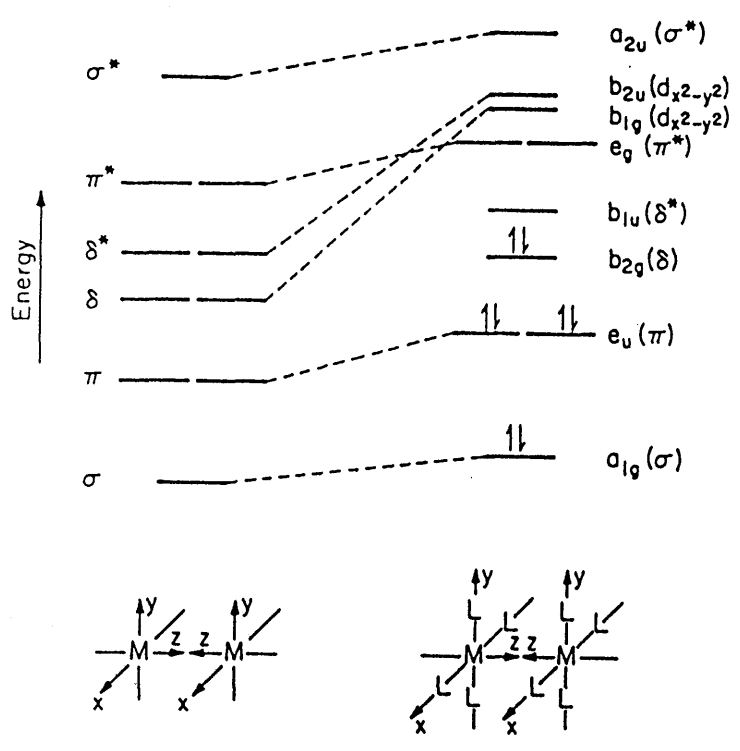


Figure 1.2 Relative energies for d molecular orbitals in $D_{\infty h}$ and D_{4h} symmetries.

Figure 1.3 depicts the structure of the $[\text{Mo}_2\text{Cl}_8]^{4-}$ anion. Here the metal-metal separation is extremely short (2.14 Å)¹⁴, this can be compared with the metal-metal distance in elemental molybdenum (2.7 Å). Therefore the combined effects of the components of the quadruple bond markedly decrease the metal-metal bond length. The propensity for quadruply bonded complexes to have both halves of the molecule eclipsed with respect to each other is shown to good effect in figure 1.3. The repulsions between the opposite halides are at a maximum in the eclipsed conformation and one might expect the staggered conformation to be more favourable. This can be explained by the fact that the δ bond is angle sensitive. The dependence of the δ overlap on the torsion angle (X)¹⁵ is shown in figure 1.4, where X is the angle of internal rotation between the two halves of the molecule when viewed down the metal-metal bond. The δ overlap follows a $\cos^2 X$ relationship¹⁶, so as X increases from 0° to 45° , the δ overlap decreases from unity to zero. Thus in the eclipsed conformation there is maximum δ overlap and therefore although the repulsions between the opposite ligands are maximised in this conformation, the energy gained from forming the δ bond must outweigh this steric hindrance. It can be seen from the graph that at $X=45^\circ$, the δ overlap will be zero and there will be a net triple bond.

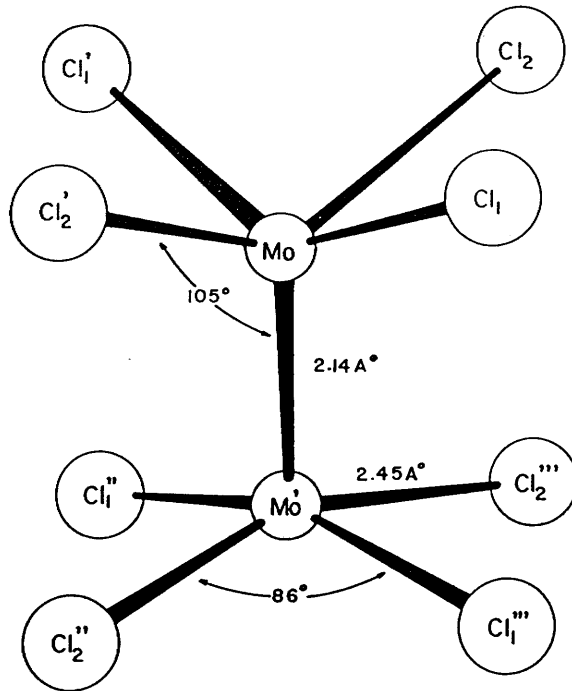


Figure 1.3 Crystal structure of the $[\text{Mo}_2\text{Cl}_8]^{4-}$ anion.

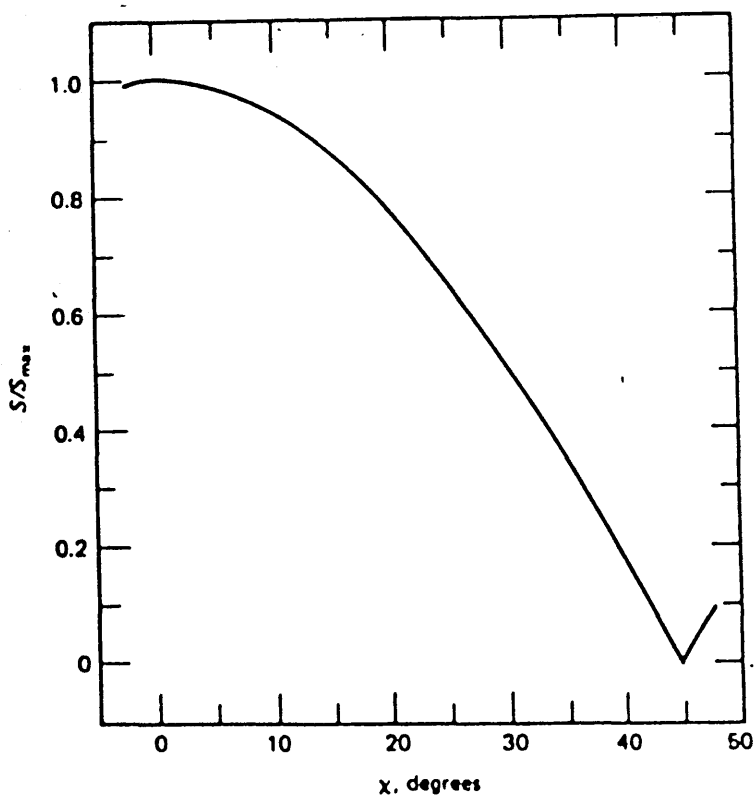


Figure 1.4 Plot of δ overlap vs. torsion angle, x .

The bonding orbitals may not always be completely filled and it is possible to get bond orders of less than four. Triple bonds can be formed when there are only six d electrons available for bonding. The electronic configuration for complexes of this type is $\sigma^2\pi^4$, which is very similar to the carbon-carbon triple bond and will therefore be insensitive to any internal rotation. An example of this is $\text{Mo}_2(\text{NMe}_2)_6$ ¹⁷; this molecule has a staggered conformation as this is the less sterically hindered. There is another type of triple bond, the electron rich triple bond. This occurs when electrons fill the δ^* antibonding orbital to give complexes with the electronic configuration $\sigma^2\pi^4\delta^2\delta^{*2}$ where the two electrons in the antibonding δ^* orbital cancel out the two electrons in the bonding δ orbital to give a net triple bond. An example of this is $\text{Re}_2\text{Cl}_4(\text{PEt}_3)_4$ ^{18,19}, shown in figure 1.5. This complex has an eclipsed conformation in order to alleviate the steric crowding.

A very interesting electron rich triply bonded species is the recently synthesised $[\text{Os}_2\text{Cl}_8]^{2-}$ anion^{20,21}. Since there is no barrier to internal rotation, the expected conformation for this anion would be the staggered structure as this minimises the halide repulsions. However table 1.2 shows that there are several conformations in the solid state.

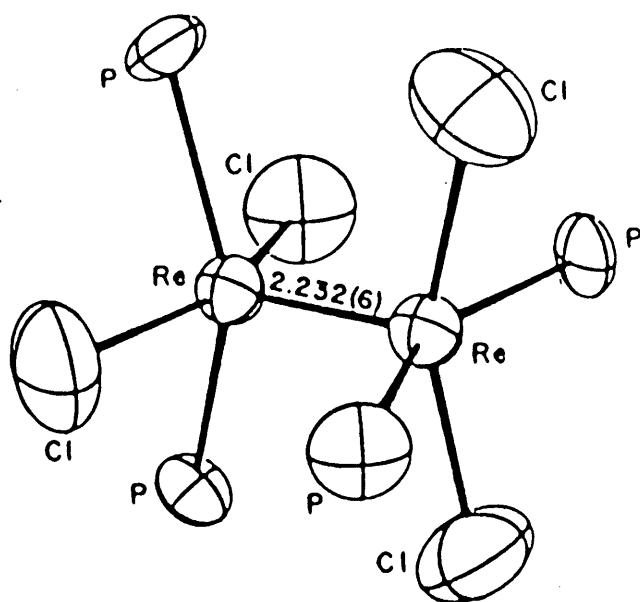


Figure 1.5 Crystal structure of $\text{Re}_2\text{Cl}_4(\text{PEt}_3)_4$.

Table 1.2 Selected Structural Parameters for Salts of the
 $[\text{Os}_2\text{Cl}_8]^{2-}$ Anion

<u>Complex</u>	<u>Os-Os (Å)</u>	<u>χ (°)</u>
(n-Bu ₄ N) ₂ Os ₂ Cl ₈	2.182	49.0
green (PPN) ₂ Os ₂ Cl ₈		
major orientation	2.206	11.4
minor orientation	2.18	39.8
brown (PPN) ₂ Os ₂ Cl ₈		
major orientation	2.212	0.0
minor orientation	2.211	0.0

The shortest bond lengths are for the staggered conformations, as expected. However the fact that there are several conformations easily stabilised indicates that the halide repulsions might not be of major importance in determining the structure but that other factors are responsible e.g. crystal packing forces or the nature of the cation used or even the method of preparation. In solution the colour of the anion is green, this suggests that a staggered structure is present. Thus the staggered conformation is the most preferred, however the difference in energy between various conformers is small because several can be readily stabilised.

1.3 Electronic Spectra of Quadruply Bonded Complexes

Many types of spectroscopy have been utilised to study metal-metal bonded species including electronic absorption and emission spectroscopy, infrared, nmr, vibrational, Raman, photoelectron spectroscopy and many more. One of the most regularly used tools for investigating quadruply bonded complexes is electronic absorption spectroscopy which will be discussed below.

The lowest energy electronic transition observed for complexes containing a quadruple bond is the δ - δ^* transition ($^1A_{1g}$ - $^1A_{2u}$) shown in figure 1.6. This transition is characteristic of the electronic absorption spectra of quadruply bonded species. The transition is fully electric dipole allowed and involves a linear movement of charge along the metal-metal bond, i.e. the transition is polarised along the metal-metal bond (z-axis) and can only be excited by light propagated perpendicular to the bond and with electric vector parallel to it. The energy and intensity of the δ - δ^* transition are semi-quantitatively related to δ overlap, although this statement must be treated with extreme caution as will be seen later.

The intensity of the δ - δ^* transition is relatively weak considering that it is a fully allowed transition. This

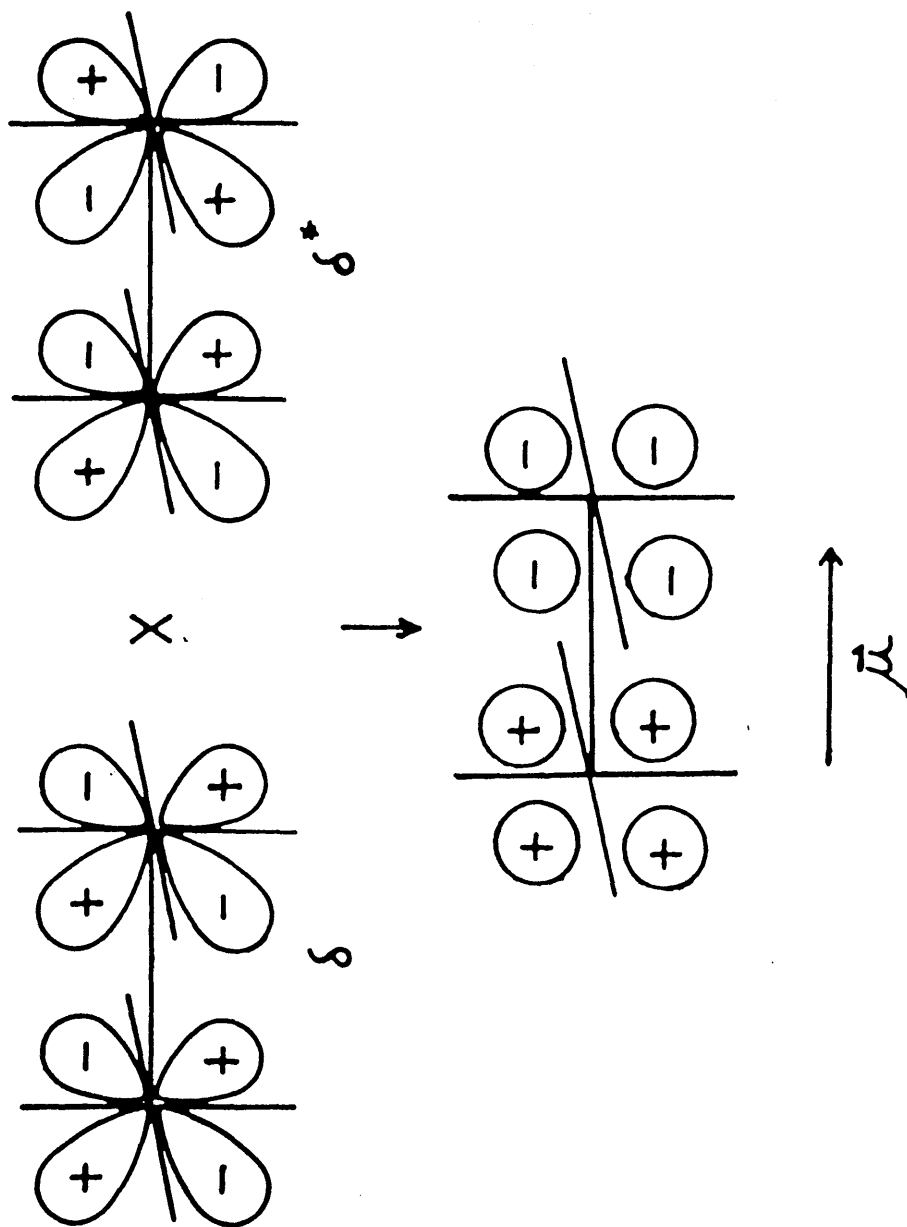


Figure 1.6 Phase multiplication and transient charge distribution for the δ - δ^* transition.

can be explained as a consequence of the small d-orbital overlap that makes up the δ bond ¹³. Mulliken ²² has shown that oscillator strength in a transition of this nature is approximately proportional to the square of the overlap integral. Thus the weak intensity is directly linked to the small δ overlap.

The position of the δ - δ^* transition for d^4 - d^4 complexes occurs between 10000-23000 cm^{-1} . The δ - δ^* transition energy does not follow a linear relationship with $\cos 2X$. Cotton et al have shown for families of complexes with different twist angles that a non-linear relationship is observed ²³. This is shown in figure 1.7. From theory it would be expected that at the fully staggered conformation ($X=45^\circ$), then the δ - δ^* transition energy should be zero. However $\beta\text{-Mo}_2\text{Cl}_4(\text{dmpe})_2$ which has a conformation close to zero overlap, ($X=40^\circ$) ²³, has in fact a δ - δ^* transition at 12500 cm^{-1} . This is close to the value of 17200 cm^{-1} for the stoichiometrically similar complex $\text{Mo}_2\text{Cl}_4(\text{PMe}_3)_4$ ^{24,25}, which has an eclipsed structure. Thus even at zero δ overlap there will be a considerable δ - δ^* transition energy. This can be assigned to the orbital overlap dependence of the one and two electron interactions in these systems. Cotton has discussed this electron correlation problem ²³.

The relationship between the position and intensity of the δ - δ^* transition of quadruply bonded complexes is very

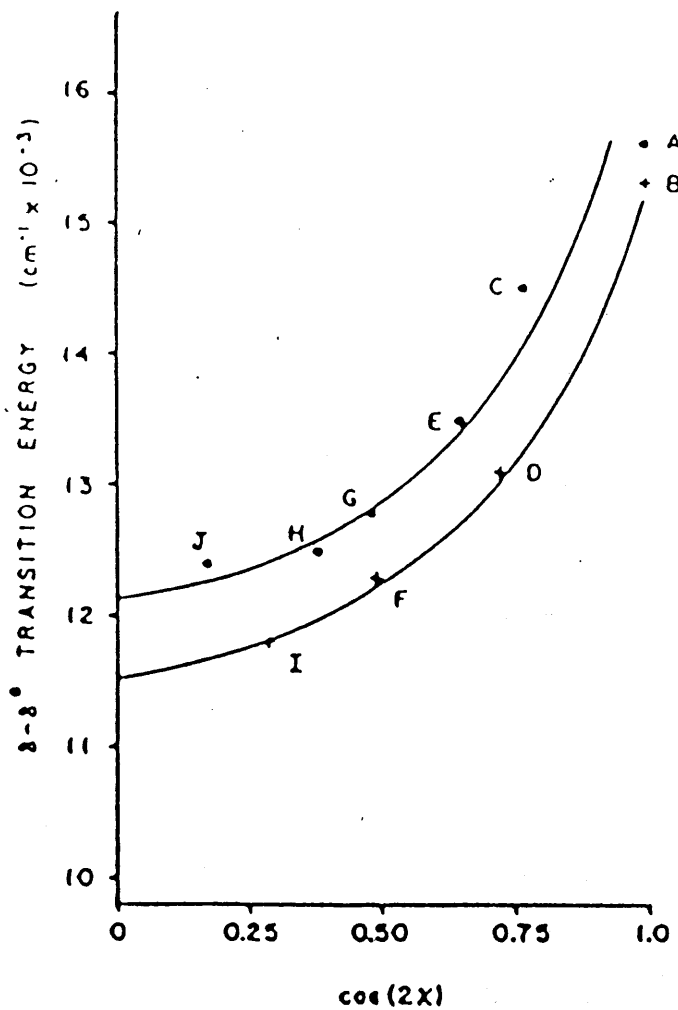


Figure 1.7 $\delta-\delta^*$ transition energy vs. $\cos^2 2X$ for $\beta\text{-Mo}_2\text{X}_4(\text{P}\sim\text{P})_2$ complexes.

poor. The $\text{Mo}_2(\text{O}_2\text{CR})_4$ complexes have among the shortest known Mo-Mo bond distances ($\sim 2.09 \text{ \AA}$) and also the highest energies for the $\delta\text{-}\delta^*$ transition ($\sim 23000 \text{ cm}^{-1}$); however the intensities of the transition are extremely weak ($\epsilon \sim 100 \text{ M}^{-1} \text{ cm}^{-1}$). On the other hand, the complex $\text{Mo}_2\text{I}_4(\text{PMe}_3)_4$ ²⁶ ($R_{\text{m-m}} = 2.127 \text{ \AA}$) has the $\delta\text{-}\delta^*$ transition occurring at 15720 cm^{-1} and has intensity $\epsilon = 5250 \text{ M}^{-1} \text{ cm}^{-1}$ which is the largest observed intensity for a $\delta\text{-}\delta^*$ transition in a quadruply bonded dimolybdenum species. Why is there such different values for the intensity of this transition? An explanation has recently been put forward in which it is suggested that the vast majority of the intensity of the $\delta\text{-}\delta^*$ transition of the latter complex is stolen from the ligand to metal charge transfer (LMCT) transitions²⁷. Mononuclear transition metal complexes have shown this phenomenon and it is explained in greater detail in reference 27. The actual intrinsic intensity of the $\delta\text{-}\delta^*$ transition is thought to be close to that seen in the dimolybdenum tetracarboxylates. These complexes can steal little intensity from the LMCT transitions because the oxygen donor ligands have very high energy LMCT states which makes the intensity stealing mechanism unfavourable. Also the structure of these complexes impose Mo-Mo-O angles of very close to 90° which means that there can be very little ligand character mixed into the δ and δ^* orbitals. Therefore in these complexes the intensity of the $\delta\text{-}\delta^*$ transition will almost exclusively result from the metal localised δ orbitals.

The low temperature absorption and Raman spectra can be used to give a value for $\nu(M-M)$ in the ground and excited electronic states of quadruply bonded complexes. $\nu(M-M)$ is the totally symmetric stretching wavenumber of the metal-metal bond and is a measure of the strength of the bond. It is calculated from the difference in energy between the first and second vibronic energy levels in a particular electronic state. The room temperature electronic absorption spectrum is of little use in yielding the desired information because only a gaussian band is observed for the $\delta-\delta^*$ transition because many of the vibronic levels are populated and therefore many transitions are observed. This is illustrated in figure 1.8. Therefore it is essential that only the first vibronic level is populated in the ground state. This can be achieved by recording the spectrum at a very low temperature (e.g. 10 K) where there is negligible population of any other vibronic level except the first. At this temperature the absorption spectrum will take the form of sharp, virtually equidistant peaks corresponding to the transitions $0-0'$, $0-1'$, $0-2'$ etc, this is illustrated in figure 1.9. The separation between the $0-0'$ and $0-1'$ peaks will give the symmetric stretching vibration for the excited state (i.e. the $\delta\delta^*$ state). In this case the excited state is triply bonded as the electron in the antibonding orbital will cancel out the electron in the bonding orbital to give a net triple bond.

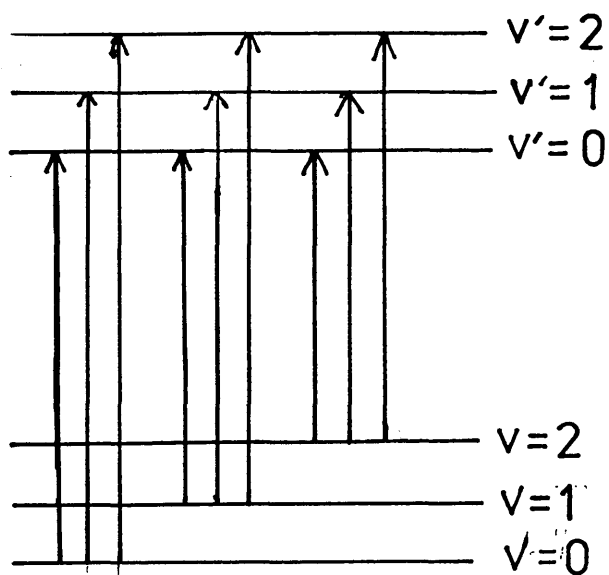


Figure 1.8 The absorption process at room temperature.

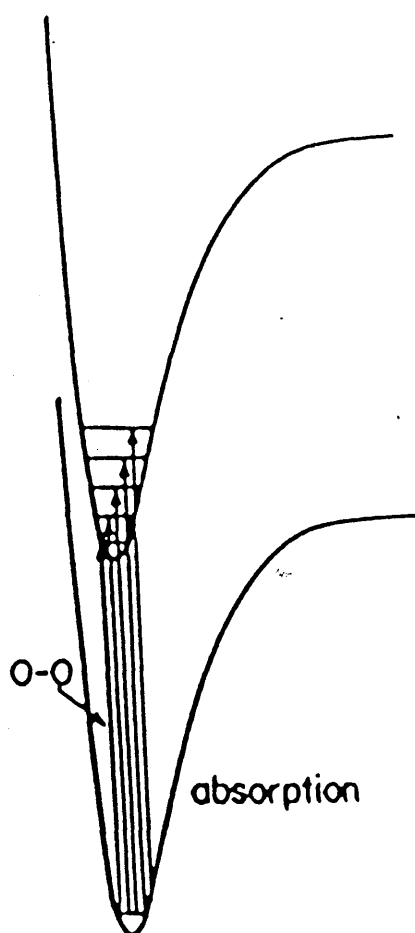


Figure 1.9 The absorption process at very low temperatures.

The $\nu(\text{M-M})$ value for $[\text{Mo}_2\text{Cl}_8]^{4-}$ in the excited state ²⁸ is 336 cm^{-1} . However in the Raman spectrum the electrons are excited into a virtual excited state, this lies between the ground state and the first excited electronic state. When the electrons fall back to the ground state, then the 0-1 separation can be calculated and the $\nu(\text{M-M})$ value for $[\text{Mo}_2\text{Cl}_8]^{4-}$ in the ground state ²⁹ is 346 cm^{-1} . The difference in $\nu(\text{M-M})$ for the triply bonded and the quadruply bonded states is small compared to the overall value. This indicates that the δ component makes only a small contribution to the quadruple bond.

1.4 Theoretical Calculations of Electronic Structure and δ - δ^* Transition Energies of M-M Bonded Complexes

The most widely used theoretical method of calculating the electronic structure of multiply bonded metal-metal complexes has been the X α scattered wave treatment (SCF-X α -SW). Background information on the details of this method are given elsewhere ³⁰⁻³³. These calculations have been performed on numerous real and model complexes ³⁴⁻⁴⁹. This method treats a molecule as a group of touching or slightly overlapping spherical atoms, assigns potentials within each atomic sphere and in the interstices, and solves the wave equation subject to the appropriate boundary conditions. It is the treatment of this problem in terms of the meeting of waves (eigenfunctions) from

separate origins that gives rise to the scattered wave (SW) description. The term X α refers to an approximate way of evaluating the mean exchange energy. The calculations on $[\text{Mo}_2\text{Cl}_8]^{4-}$ give excellent quantitative descriptions of the ground electronic structure ^{35,36} and is in good agreement with the original description of the quadruple bond based on the orbital overlap considerations ². This method can also be used to give an estimate of the δ - δ^* transition energy. For systems with bond order 3.5, (i.e. with electronic configuration $\sigma^2\pi^4\delta^1$ or $\sigma^2\pi^4\delta^2\delta^*1$, e.g. $[\text{Tc}_2\text{Cl}_8]^{3-}$ the transition is estimated to occur at $6.0 \times 10^3 \text{ cm}^{-1}$ compared with the experimental value of $5.9 \times 10^3 \text{ cm}^{-1}$, and here the agreement is excellent. However for species of bond order 4 the agreement is not so good. The experimental value for the δ - δ^* transition for $[\text{Mo}_2\text{Cl}_8]^{4-}$ is $18.8 \times 10^3 \text{ cm}^{-1}$ compared to the calculated value of $9.2 \times 10^3 \text{ cm}^{-1}$. This is an electron correlation problem because singlet-singlet and singlet-triplet transitions are possible in quadruply bonded species whereas in $[\text{Tc}_2\text{Cl}_8]^{3-}$ only a doublet-doublet is possible. An attempt to overcome this problem was undertaken by Noodleman and Norman ⁵⁰, who introduced valence bond (VB) concepts to the calculation to give an X α -VB method. An application of this method gave a tremendous improvement in the δ - δ^* transition energy to $15.2 \times 10^3 \text{ cm}^{-1}$.

2. Structures and Properties of Dimolybdenum Complexes

2.1 Carboxylates and Substituted Derivatives

The dimolybdenum tetracarboxylates, $\text{Mo}_2(\text{O}_2\text{CR})_4$, are a very important class of complexes containing a Mo-Mo quadruple bond. Their significance is that they can be synthesised ⁷³⁻⁷⁹ in very good yields from a mononuclear starting material, $\text{Mo}(\text{CO})_6$, which is easily available and relatively inexpensive. The most important member of this family is dimolybdenum tetraacetate, $\text{Mo}_2(\text{O}_2\text{CCH}_3)_4$, the initial structural characterisation ⁸⁰ of which was carried out in 1965, soon after the recognition of the quadruple bond. Since then the structure has been redetermined more accurately ⁵³ and is shown in figure 1.10. The complex has all four acetate groups in the bridging mode and has a rigorously eclipsed conformation between the two halves of the molecule when viewed down the metal-metal bond.

The tetracarboxylate complexes contain very short Mo-Mo distances as is shown in table 1.3. These short metal-metal bonds arise from the fact that in these species the Mo-Mo-O angle is always very close to 90° and also the small ligand backbone will favour a short metal-metal separation.

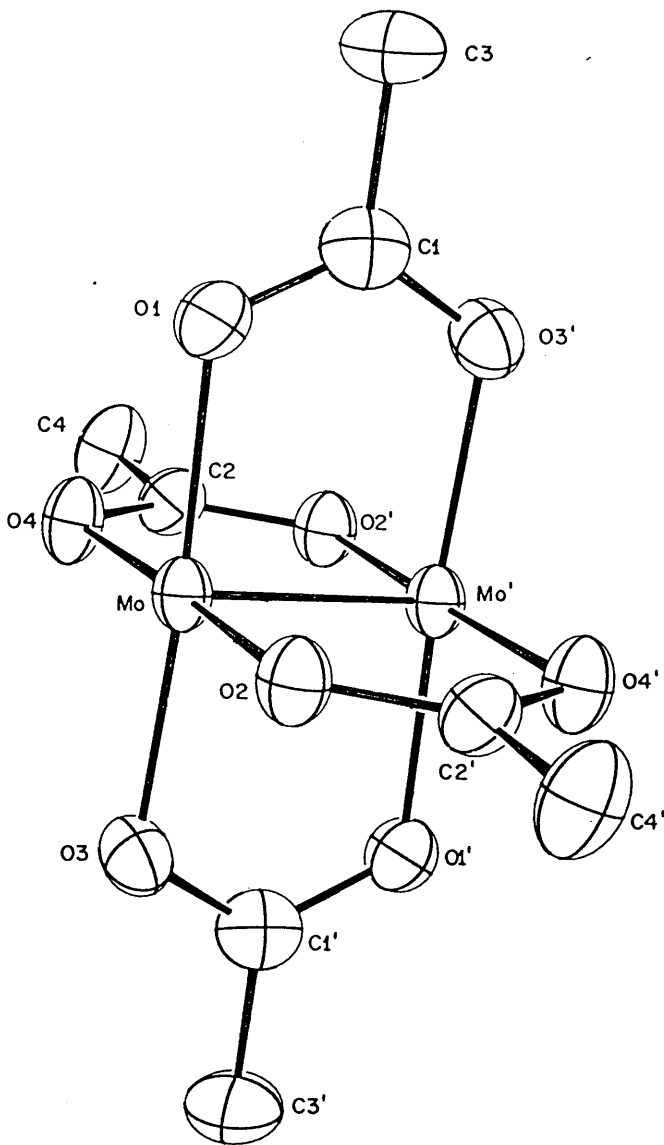


Figure 1.10 Crystal structure of $\text{Mo}_2(\text{O}_2\text{CCH}_3)_4$.

Table 1.3 Dimolybdenum Complexes with Carboxylate

Ligands

<u>R_m-m</u> <u>Å</u>	<u>Complex</u>	<u>Ref.</u>
<u>Complexes with Four Carboxylate Ligands</u>		
2.091	Mo ₂ (O ₂ CH) ₄	51
2.105	Mo ₂ (O ₂ CH) ₄ .KCl	52
2.0934	Mo ₂ (O ₂ CCH ₃) ₄	53
2.090	Mo ₂ (O ₂ CCF ₃) ₄	54
2.129	Mo ₂ (O ₂ CCF ₃) ₄ (py) ₂	55
2.088	Mo ₂ (O ₂ CCMe ₃) ₄	56
2.096	Mo ₂ (O ₂ CC ₆ H ₅) ₄	56
2.100	Mo ₂ (O ₂ CC ₆ H ₅) ₄ (diglyme) ₂	57
<u>Complexes with Two Trans Carboxylate Ligands</u>		
2.065	Mo ₂ (O ₂ CCH ₃) ₂ [o-(NMe ₂)C ₆ H ₄ CH ₂] ₂	58
2.079	Mo ₂ (O ₂ CCH ₃) ₂ [(OCHMe ₂) ₄ Al] ₂	59
2.086	(Ph ₄ As) ₂ [Mo ₂ (O ₂ CCH ₃) ₂ Cl ₄].2CH ₃ OH	60
2.091	Mo ₂ Br ₂ (O ₂ CC ₆ H ₅) ₂ (PBu ⁿ ₃) ₂	61
2.091	Mo ₂ Cl ₂ (O ₂ CCH ₃) ₂ (PPh ₃) ₂	62
2.098	[NBu ⁿ ₄] ₂ [Mo ₂ (O ₂ CCF ₃) ₂ Br ₄]	63
2.098	Mo ₂ Cl ₂ (O ₂ CCMe ₃) ₂ (PEt ₃) ₂	64
2.099	Mo ₂ Cl ₂ (O ₂ CCH ₃) ₂ (PBu ⁿ ₃) ₂	65
2.107	Mo ₂ (O ₂ CCH ₃) ₂ {[(2,6-xylyl)N] ₂ CCH ₃ } ₂ .4THF	66
2.114	Mo ₂ (O ₂ CCH ₃) ₂ (OSiMe ₃) ₂ (PMe ₃) ₂	67

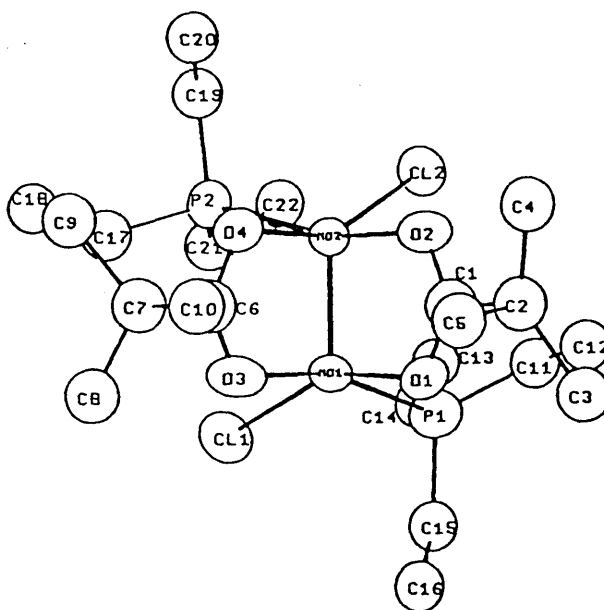
Table 1.3 ctd.

Complexes with Two Cis Carboxylate Ligands

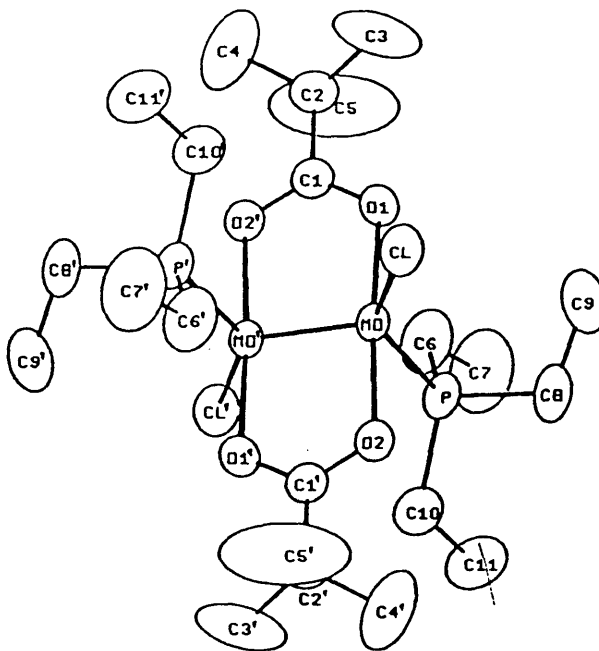
2.113	$\text{Mo}_2\text{Cl}_2(\text{O}_2\text{CCMe}_3)_2(\text{PEt}_3)_2$	64
2.127	$\text{Mo}_2\text{Cl}_2(\text{O}_2\text{CCF}_3)_2(\text{C}_2\text{H}_5\text{CN})_2$	68
2.129	$\text{Mo}_2(\text{O}_2\text{CCH}_3)_2(\text{acac})_2$	60
2.129	$\text{Mo}_2(\text{O}_2\text{CCH}_3)_2[(\text{pz})_2\text{BEt}_2]_2 \cdot \text{CS}_2$	69
2.131	$\text{Mo}_2(\text{O}_2\text{CCH}_3)_2[\text{PhNC}(\text{CH}_3)\text{CHC}(\text{CH}_3)\text{O}]_2$	70
2.134	$\text{Mo}_2(\text{O}_2\text{CCH}_3)_2(\text{CH}_3\text{CN})_6[\text{BF}_4]_2$	71,72

The most important property of the tetracarboxylate family is that they are extremely useful in the synthesis of so many other quadruply bonded species e.g. in the synthesis of the $[\text{Mo}_2\text{Cl}_8]^{4-}$ 14,81 anion, which is itself used as a precursor for many other dimolybdenum complexes.

An interesting class of dimolybdenum carboxylates are those that contain two carboxylate ligands; this can lead to different isomers arising. Figure 1.11 depicts the two structurally characterised isomers of $\text{Mo}_2\text{Cl}_2(\text{O}_2\text{CCMe}_3)_2(\text{PEt}_3)_2$ 64. The A isomer has the carboxylate groups in a cis arrangement while the B isomer has a trans disposition of the carboxylate ligands. Table 1.3 shows the Mo-Mo bond length for sixteen such isomers. There is a trend that the trans isomers have significantly shorter bond lengths than the cis isomers. The most reasonable explanation for this is that there is less steric crowding in the trans isomers.



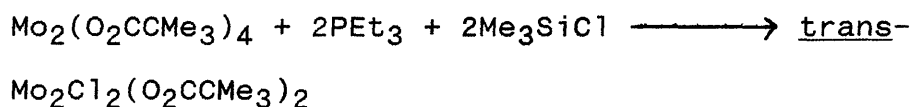
ORTEP drawing of isomer A.



ORTEP drawing of isomer B.

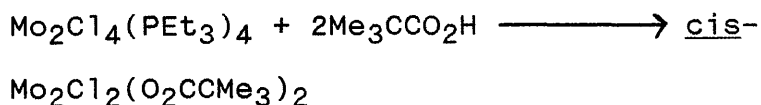
Figure 1.11 Cis(A) and trans(B) isomers of $\text{Mo}_2\text{Cl}_2(\text{O}_2\text{CCMe}_3)_2(\text{PET}_3)_2$.

The only pair of isomers to be isolated are those shown in figure 1.11 where the Mo-Mo bond length in the trans isomer is 0.015 Å shorter than in the cis form. The preparative routes for each isomer are completely different. The trans isomer is made as follows



Here the pivalates in $\text{Mo}_2(\text{O}_2\text{CCMe}_3)_4$ will probably be stepwise substituted thereby favouring formation of the less sterically crowded trans isomer.

Cis- $\text{Mo}_2\text{Cl}_2(\text{O}_2\text{CCMe}_3)_2(\text{PEt}_3)_2$ is synthesised in the following way



The cis isomer will form from $\text{Mo}_2\text{Cl}_4(\text{PEt}_3)_4$ because in the latter complex ⁸² the phosphine and chloride ligands are set up in the same configuration that is present in cis- $\text{Mo}_2\text{Cl}_2(\text{O}_2\text{CCMe}_3)_2(\text{PEt}_3)_2$. Thus the slightly less favourable cis isomer is formed in this case. However the energy difference between the two isomers must be fairly small because they appear to be interconvertible in solution, although the rates and mechanisms of these processes have not yet been reported ⁶⁴.

In figure 1.11, the non-acetate ligands are monodentate, this is not always the the case and the formation of either the cis or trans dicarboxylate is sometimes heavily dependent on the nature of the ligands involved. For example in $\text{Mo}_2(\text{O}_2\text{CCH}_3)_2(\text{acac})_2$, $\text{Mo}_2(\text{O}_2\text{CCH}_3)_2[(\text{pz})_2\text{BEt}_2]_2 \cdot \text{CS}_2$ and $\text{Mo}_2(\text{O}_2\text{CCH}_3)_2[\text{PhNC}(\text{CH}_3)\text{CH}(\text{CH}_3)\text{O}]_2$, both ends of the non-acetate ligands chelate to the molybdenum atoms. In these situations a cis dicarboxylate structure must be formed because a trans isomer is impossible with chelating ligands. There are no cis dicarboxylates where the two non-acetate ligands are in the bridging mode. The reasons for this must be because it is sterically unfavourable.

The $[\text{Mo}_2(\text{O}_2\text{CCH}_3)_2\text{Cl}_4]^{2-}$ anion ⁶⁰ is extremely interesting because the metal-metal separation is 2.086 Å, this is shorter than either $\text{Mo}_2(\text{O}_2\text{CCH}_3)_4$ ⁵¹, where the distance is 2.093 Å, or $\text{K}_4\text{Mo}_2\text{Cl}_8$ ¹⁴, which has a separation of 2.139 Å. However the δ - δ^* transition occurs at 20200 cm^{-1} which is between that of $\text{Mo}_2(\text{O}_2\text{CCH}_3)_4$, 23000 cm^{-1} , and $\text{K}_4\text{Mo}_2\text{Cl}_8$, 18800 cm^{-1} . This illustrates the unreliability of the relationship between $R_{\text{m-m}}$ and the energy of the δ - δ^* transition.

2.2 Complexes with Diphosphine Ligands

There has been extensive research into quadruply bonded complexes containing phosphine ligands in the last decade. Complexes of the general formula $\text{Mo}_2\text{X}_4(\text{L}^{\sim}\text{L})_2$ (where L^{\sim}L is a diphosphine ligand and X is a halide) have been of particular interest. These species can exist in two isomeric forms which are shown in figure 1.12. In the α form both ends of the diphosphine ligand chelate to the same molybdenum atom; when viewed down the metal-metal bond the ligands take up an eclipsed conformation and therefore the complex has maximum δ overlap. All multiply bonded α species which have been characterised to date have this conformation including $\alpha\text{-Mo}_2\text{Cl}_4(\text{dppe})_2$ ⁸⁷, $\alpha\text{-W}_2\text{Cl}_4(\text{dppe})_2$ ⁹⁶, $\alpha\text{-W}_2\text{Cl}_4(\text{dmpe})_2$ ^{82,97}, $\alpha\text{-Re}_2\text{Cl}_4(\text{dmpe})_2$ ⁹⁸ and $\alpha\text{-Re}_2\text{Cl}_4(\text{dppp})_2$ ⁹⁹. In the β isomer, the diphosphine ligand bridges across the metal-metal bond and depending on the nature of the backbone of the ligand then the two halves of the molecule may be staggered with respect to each other. This staggering will reduce the α overlap (see figure 1.4).

In certain quadruply bonded dimolybdenum species the α isomer has been shown to isomerise to the β form in solution ^{89,100,101} and in the solid state ⁸⁷. This isomerisation process is thermodynamically favourable despite the resulting decrease in δ overlap as a result of

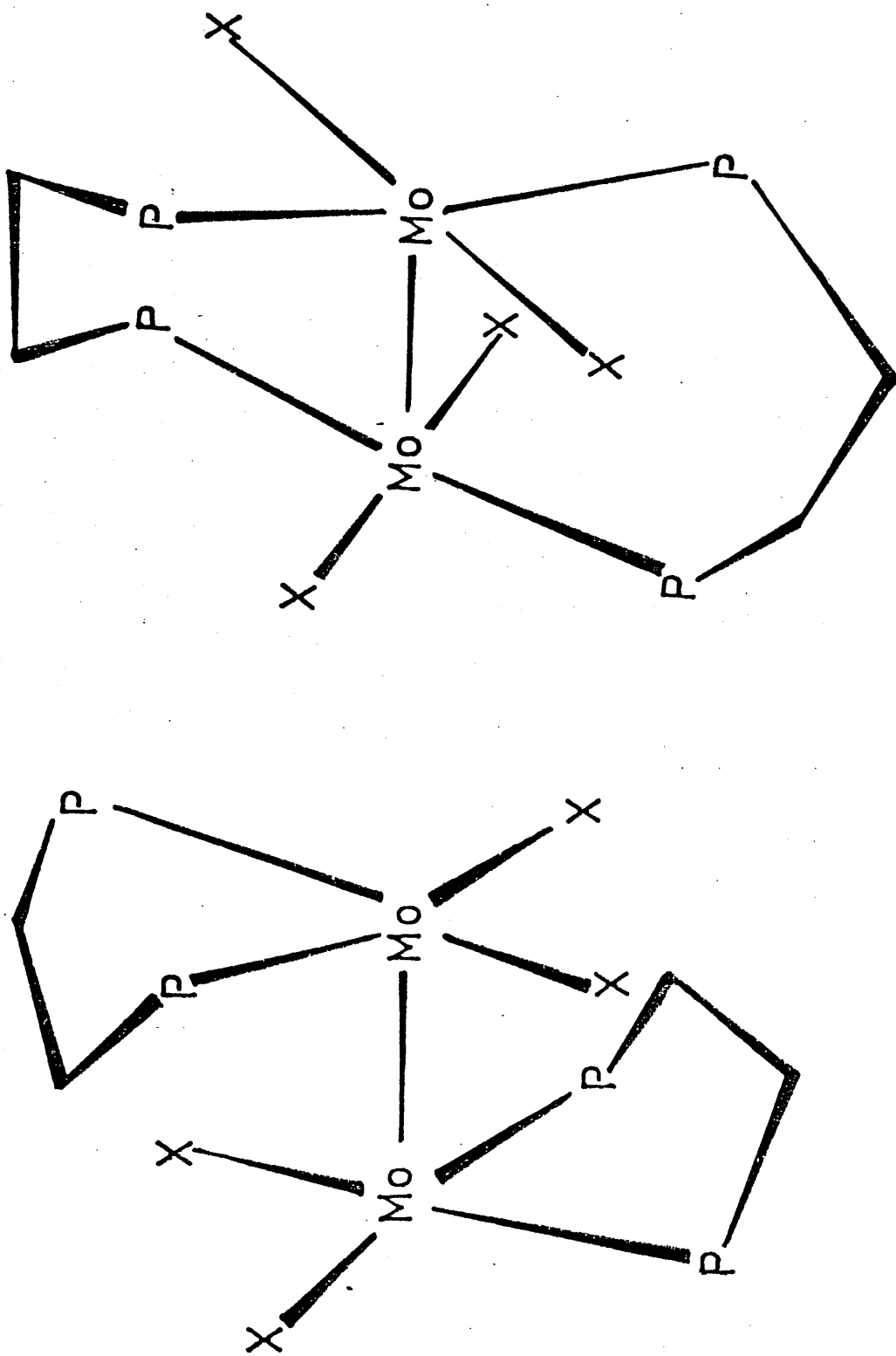


Figure 1.12 Schematic representations of α and β isomers of $\text{Mo}_2\text{Cl}_4(\text{P}\sim\text{P})_2$.

the staggering in the β isomers. This favourability is thought to be due to the conformational stability of the rings formed by the ligands bridging across the metal-metal bond in the β isomer. Also in the α isomer the chelating rings take up an unfavourable envelope conformation in which the carbon backbone lies over the metal-metal bond and in close proximity to the halide atoms; this occurs in order that the substituents on the phosphorus atoms point away from the halides. The crystal structure of $\beta\text{-Mo}_2\text{Cl}_4(\text{dppe})_2$ ⁸⁸, illustrated in figure 1.13, has two heteronuclear Mo-Mo-P-C-C-P six-membered rings. These rings take up a stable chair conformation and the two fused rings give an overall cis-decalin type structure. The conformational stability of these rings will be the driving force for the isomerisation reaction and will more than compensate for any decrease in the δ bonding. The mechanism for this process has received considerable attention^{87,89,100} and will be discussed later in this thesis.

Table 1.4 shows a list of metal-metal bond lengths of structurally characterised complexes of the general formula $\text{Mo}_2\text{X}_4(\text{L}\sim\text{L})_2$ and $\text{Mo}_2\text{X}_4\text{L}_4$; the twist angle (X) is also given in each case. This illustrates the difference in the α and β isomers of $\text{Mo}_2\text{Cl}_4(\text{dppe})_2$, the only pair of these dimolybdenum isomers to be structurally characterised. The eclipsed α isomer has a significantly

shorter bond length than the staggered β isomer. A graph of R_{m-m} vs $\cos 2X$ has been plotted for certain β isomers taking into account the differences of the $-PMe_2$ and the $-PPh_2$ ligands. This yields an excellent linear relationship⁹² and the least squares fit plot has a very good correlation coefficient (0.9547). This plot is shown in figure 1.14. For this family of complexes the plot can be extrapolated to show that the increase in bond length for the loss of the δ bond (i.e. going from $X = 0^\circ$ to $X = 45^\circ$) would be 0.097 Å. This again illustrates that the δ component of the quadruple bond is fairly weak and that its contribution to the overall bond shortening caused by the quadruple bond is small.

It is worth comparing the quadruply bonded dimolybdenum complexes with analogous triply bonded dirhenium species to observe any differences caused by the δ bond. The structure of $\beta\text{-Mo}_2\text{Cl}_4(\text{dppm})_2$ ⁸³ is shown in figure 1.15(a), this has an envelope conformation with a twist angle of zero and therefore maximum δ overlap. This complex is one of the few eclipsed β isomers. However the structure of $\beta\text{-Re}_2\text{Cl}_4(\text{dppm})_2$ ⁹⁸ has an essentially staggered conformation with $X = 56^\circ$, this is depicted in figure 1.15(b), the bridging ring has a twist-boat structure. This staggering arises because the complex has a triple bond and therefore no formal barrier to rotation about the metal-metal bond. This twisted structure must

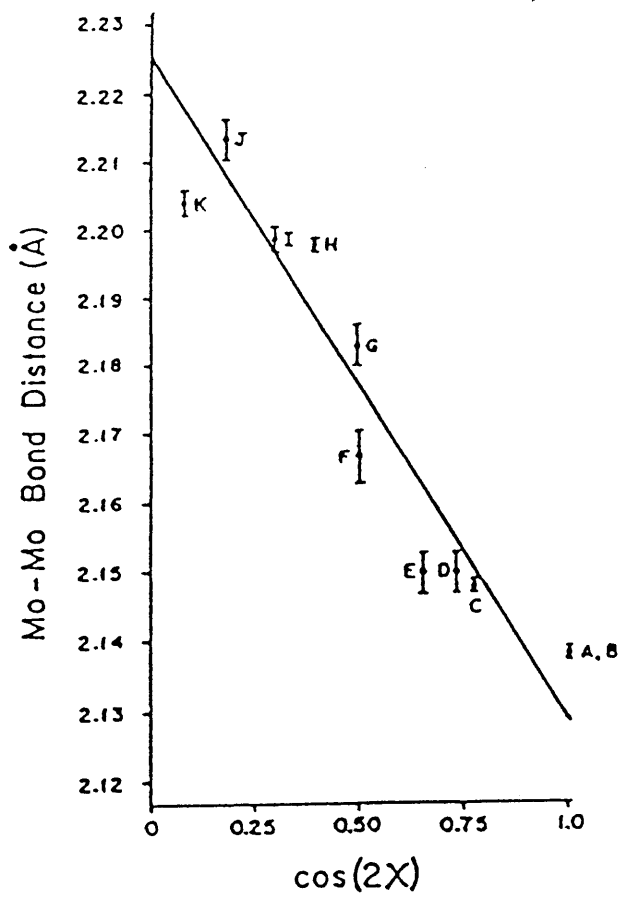


Figure 1.14 R_{m-m} vs. $\cos 2X$ for $\beta\text{-Mo}_2\text{X}_4(\text{P}\sim\text{P})_2$ complexes.

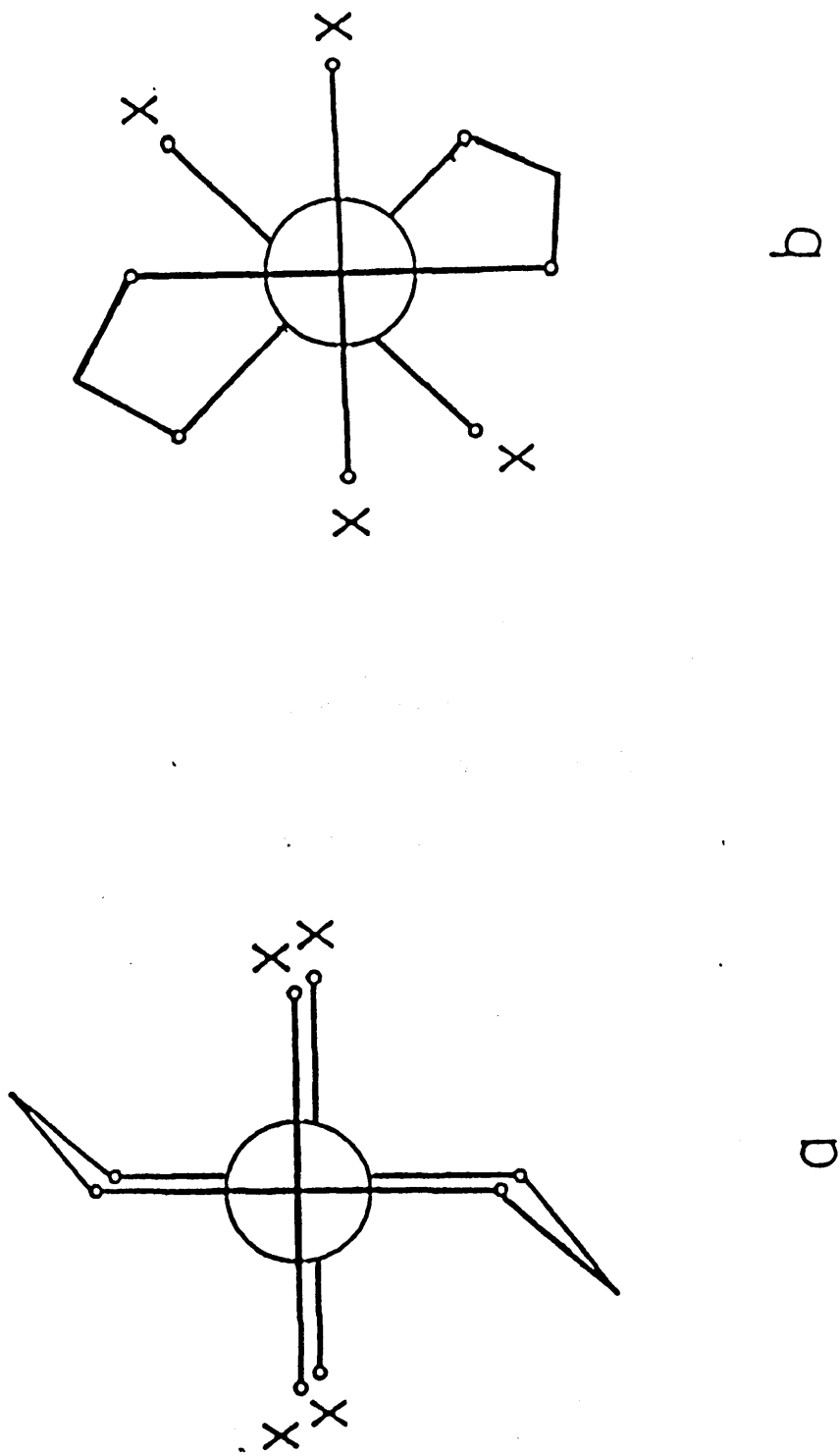


Figure 1.15 Eclipsed(a) and staggered(b) arrangement of ligands in

$\beta\text{-M}_2\text{X}_4(\text{P}\sim\text{P})_2$ complexes, where P~P has a three atom backbone.

Table 1.4 Structural Data for some Dimolybdenum Complexes
Containing Phosphine Ligands

R_{m-m} (Å)	χ (°)	Complex	Ref.
<u>Complexes with Monophosphine Ligands</u>			
2.130	0	$\text{Mo}_2\text{Cl}_4(\text{PMe}_3)_4$	82
2.125	0	$\text{Mo}_2\text{Br}_4(\text{PMe}_3)_4$	26
2.127	0	$\text{Mo}_2\text{I}_4(\text{PMe}_3)_4$	26
<u>Complexes with Diphosphine Ligands with a 3-atom Backbone</u>			
2.138	0	$\beta\text{-Mo}_2\text{Cl}_4(\text{dppm})_2 \cdot 2(\text{CH}_3)_2\text{CO}$	83
2.167	13.3	$\beta\text{-Mo}_2(\text{NCS})_4(\text{dppm})_2 \cdot 2(\text{CH}_3)_2\text{CO}$	83
2.148	20	$\beta\text{-Mo}_2\text{Cl}_4(\text{tdpm})_2 \cdot 2\text{CH}_2\text{Cl}_2$	84
2.1253	0	$\beta\text{-Mo}_2\text{Cl}_4(\text{dmpm})_2$	85
2.134	0	$\beta\text{-Mo}_2\text{Cl}_4(\text{dmpm})_2 \cdot 0.5\text{H}_2\text{O} \cdot 1.25\text{CH}_3\text{OH}$	85
2.138	0	$\beta\text{-Mo}_2\text{Br}_4(\text{dppm})_2$	84
2.139	0	$\beta\text{-Mo}_2\text{I}_4(\text{dppm})_2$	86
<u>Complexes with Diphosphine Ligands with a 4-atom Backbone</u>			
2.140	0	$\alpha\text{-Mo}_2\text{Cl}_4(\text{dppe})_2 \cdot \text{OC}_4\text{H}_8$	87
2.183	59.5	$\beta\text{-Mo}_2\text{Cl}_4(\text{dppe})_2$	88
2.177	58.7	$\beta\text{-Mo}_2\text{Br}_4(\text{dppe})_2$	89
2.129	0	$\beta\text{-Mo}_2\text{I}_4(\text{dppe})_2 \cdot 0.67\text{CH}_2\text{Cl}_2$	90
2.180	27.9	$\beta\text{-Mo}_2\text{I}_4(\text{dppe})_2 \cdot 0.67\text{CH}_2\text{Cl}_2$	90
2.179	25.7	$\beta\text{-Mo}_2\text{I}_4(\text{dppe})_2 \cdot \text{C}_7\text{H}_8$	90
2.183	40.0	$\beta\text{-Mo}_2\text{Cl}_4(\text{dmpe})_2$	91
2.168	33.8	$\beta'\text{-Mo}_2\text{Cl}_4(\text{dmpe})_2$	23
2.169	36.5	$\beta\text{-Mo}_2\text{Br}_4(\text{dmpe})_2$	23

Table 1.4 ctd.

Complexes with Diphosphine Ligands with a 4-atom Backbone

2.173	42.7	$\beta\text{-Mo}_2\text{Cl}_4(\text{depe})_2$	92
2.150	24.6	$\beta\text{-Mo}_2\text{Cl}_4(\text{S,S-dppb})_2\cdot\text{OC}_4\text{H}_8$	93
2.143	22.9	$\beta\text{-Mo}_2\text{Cl}_4(\text{S,S-dppb})_2\cdot 4\text{CH}_3\text{CN}$	93
2.147	21.7	$\beta\text{-Mo}_2\text{Br}_4(\text{S,S-dppb})_2\cdot\text{OC}_4\text{H}_8$	94
2.180	25.8	$\beta\text{-Mo}_2(\text{NCS})_4(\text{S,S-dppb})_2$	95

represent the energy minimum conformation. The energy difference between the conformations in figure 1.15(a) and (b) will be small because the δ bond must be decisive in forcing the eclipsed structure in the dimolybdenum case as this is the only difference between the complexes. The complex $\beta\text{-Re}_2\text{Cl}_5(\text{dppm})_2$ ¹⁰², which has bond order 3.5, has an eclipsed conformation. The structure of this complex is identical to $\beta\text{-Mo}_2\text{Cl}_4(\text{dppm})_2$ except that it has a chloride in an axial position to the metal-metal bond, so even half a δ bond may be enough to cause eclipsing in the above complexes. The structure of $\beta\text{-Re}_2\text{Cl}_4(\text{dppe})_2$ ¹¹⁷ is very similar to that of $\beta\text{-Mo}_2\text{Cl}_4(\text{dppe})_2$ (see figure 1.13). The only difference is that the twist angle in the former complex is 52.4° while it is 59.5° in the latter. Here the δ bond makes no impact in determining the conformation. It is the affinity of the bridging six-membered rings to be in the chair conformation which determines the structure.

It is clear that the δ bond is very weak and that there are many other factors which can influence the conformation of these complexes. Table 1.4 shows that $\beta\text{-Mo}_2\text{I}_4(\text{dppe})_2$ has three different conformations in the solid state with twist angles of 0° , 25.7° and 27.9° respectively. The first and third of these conformations occur in the same crystal. The eclipsed structure ($X = 0^\circ$) of $\beta\text{-Mo}_2\text{I}_4(\text{dppe})_2$ has the only example of a heteronuclear bridging six-membered ring taking up a boat conformation. This leads to a short metal-metal (2.129 Å) which is significantly shorter than the two staggered conformations which do not have maximum δ overlap. The fact that there are two markedly different rotamers in the same crystal illustrates how little energy difference there must be between them. So what is determining the structure in this case? Small intermolecular packing forces may be important in stabilising the two different conformers, each one at a different site in the crystal. Another factor which may be decisive in forming the eclipsed form of $\beta\text{-Mo}_2\text{I}_4(\text{dppe})_2$ is that in this conformation the phenyl groups must adopt a face to face arrangement which could be important in stabilising this conformation. This is depicted in figure 1.16. However in solution the complex gives only one band in the $\delta\text{-}\delta^*$ electronic transition region at 11600 cm^{-1} , which suggests a twisted conformation of roughly 27° is most stable in this phase. The ^{31}P nmr solution spectrum of this complex displays a temperature dependence

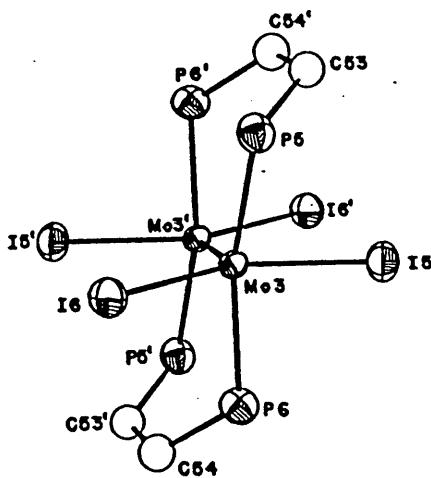
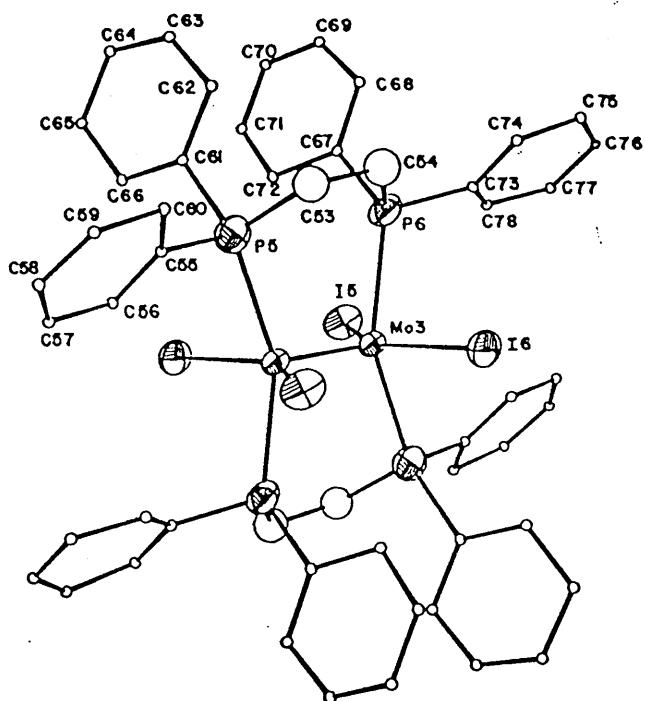


Figure 1.16 Crystal structure of $\beta\text{-Mo}_2\text{I}_4(\text{dppe})_2$ where $X = \text{O}^\ominus$.

suggesting a low energy fluxional process interconverting various rotamers ⁹⁰. This seems very likely when one considers that several rotamers can easily be stabilised in the solid state.

An interesting recent development has been the isolation of α and β isomers of $\text{Mo}_2\text{X}_4(\text{dppee})_2$ ¹⁰³ ($\text{X} = \text{Cl}, \text{Br}$ and I), although the rhenium analogues are already known ¹⁰⁴. The β isomers present a unique situation of a fused decalin-like ring system which contains both C=C and quadruple Mo-Mo bonds

Much of the above information confirms the weak strength of the δ bond. In molecules containing diphosphine ligands there are many factors involved in determining the conformation. Since the δ overlap is very weak, other factors will have a greater contribution in determining the structure, this is illustrated by many of the examples given above.

2.3 Complexes with Nitrogen Ligands

Despite the vast amount of research on quadruply bonded dimolybdenum species, there have been relatively few complexes made in which all eight coordinating ligand atoms are nitrogen i.e. complexes having the Mo_2N_8 moiety.

The first example of this type was $\text{Mo}_2(\text{en})_4\text{Cl}_4$ which was synthesised in 1974 ¹¹⁰. Although a crystal structure was not reported the complex was predicted ¹¹⁰, from scale models and interpretation of various spectra, to contain four chelating en ligands (figure 1.17(a)) rather than four bridging en ligands (figure 1.17(b)). However a recent paper dealing with the optically active methylated derivative $\text{Mo}_2(\text{R-pn})_4\text{Cl}_4$ has shown that the structure almost certainly contains bridging ligands ¹¹¹. This will be explained when the optical activity of quadruply bonded complexes is discussed in a later chapter.

Several complexes of the general formula $\text{Mo}_2(\text{N}^-\text{N})_4$ have been structurally characterised where N^-N is an anionic N-C-N or N-N-N backbone species ¹⁰⁵⁻¹⁰⁹. All four ligands bridge across the metal-metal bond in all of these complexes. These species have characteristically short metal-metal bond lengths in the range 2.070-2.103 Å and have essentially eclipsed conformations, similar to the structure of $\text{Mo}_2(\text{O}_2\text{CCH}_3)_4$ as in figure 1.8.

Two complexes that have recently been studied are $\text{Mo}_2(\text{TPP})_2$ ¹¹² and $\text{Mo}_2(\text{tmtaa})_2$ ¹¹³, where both ligands are N_4 macrocyclic derivatives. The metal-metal bond length for the former complex is 2.239 Å, this is the longest recorded Mo-Mo bond length for a quadruply bonded dimolybdenum complex. The crystal structure is shown in

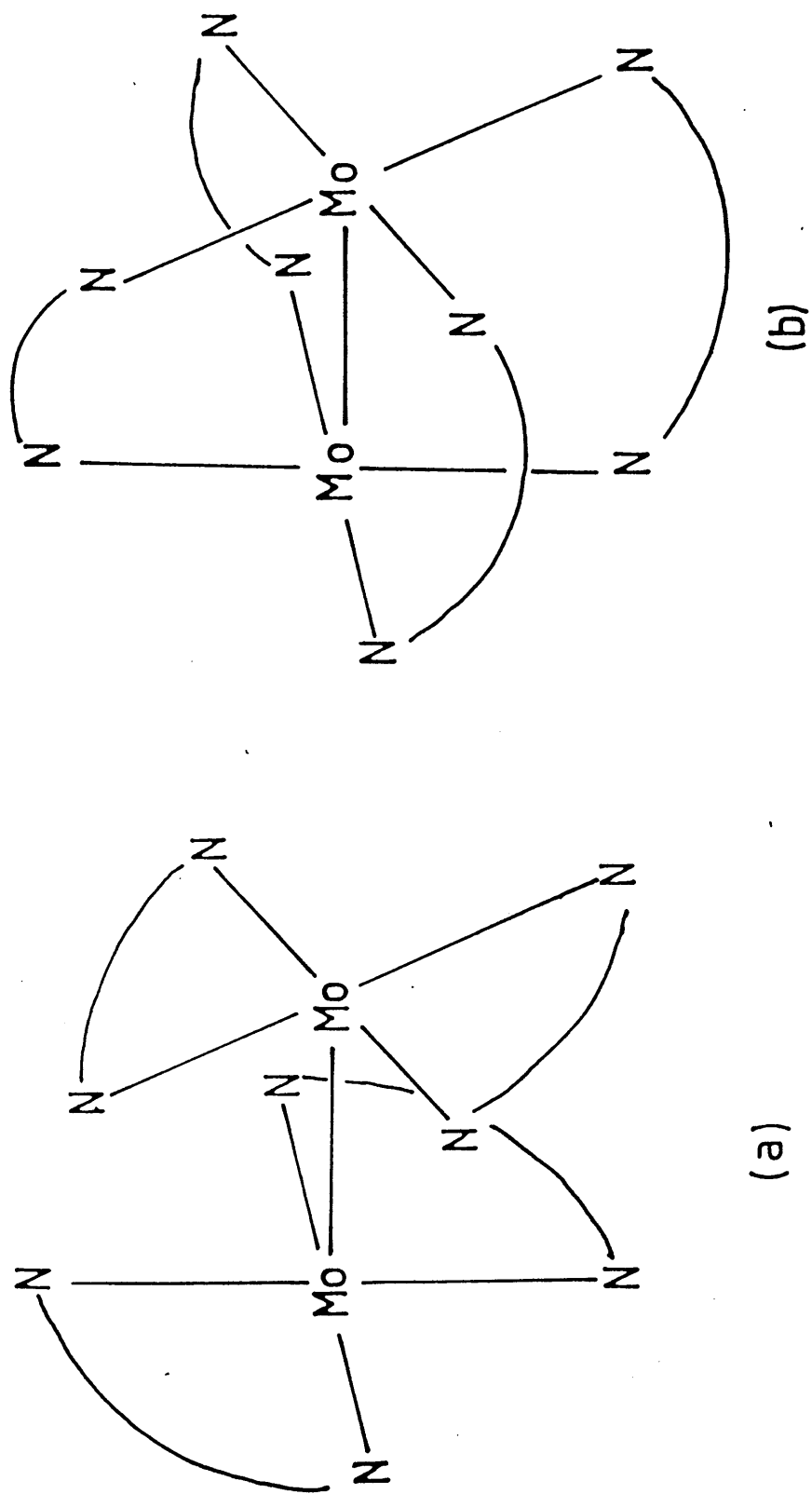


Figure 1.17 Chelating(a) and bridging(b) forms of $[\text{Mo}_2(\text{N}\sim\text{N})_4]^{4+}$ cations.

figure 1.18. The complex is rotated by 18° but the reason for the relatively long bond length is the bulkiness of the ligands which prevent close contact of the molybdenum atoms. $\text{Mo}_2(\text{tmtaa})_2$ also has a porphyrin N_4 ligand; the crystal structure of of this complex has not yet been carried out. However, $[\text{Mo}_2(\text{tmtaa})_2][\text{PF}_6]$ which has a bond order of 3.5 has been structurally characterised ¹¹³. Again, the bulkiness of the ligand explains the long metal-metal bond length (2.221 Å), but also the loss of half a δ bond will account for some of the increase. The twist angle of this complex is close to 90° in order to lessen the steric congestion. The structure of $\text{Mo}_2(\text{tmtaa})_2$ is expected to be identical.

Monodentate nitrogen ligands have not been used extensively in dimolybdenum chemistry. The complex $\text{Mo}_2(\text{CH}_3\text{CN})_8(\text{TFMS})_4$ has been synthesised although not structurally characterised ¹¹⁴. From spectroscopic data the structure has eight acetonitriles bonded through the nitrogen atoms to the dimolybdenum unit. Spectroscopy also favours ionic triflates rather than coordinating triflates as in $\text{Mo}_2(\text{TFMS})_4$ ¹¹⁵. Cotton et al have reported the synthesis of $[\text{Mo}_2(\text{CH}_3\text{CN})_8][\text{BF}_4]_4$ complex ¹¹⁶ in crystal form in a single step reaction from $\text{Mo}_2(\text{O}_2\text{CCH}_3)_4$.

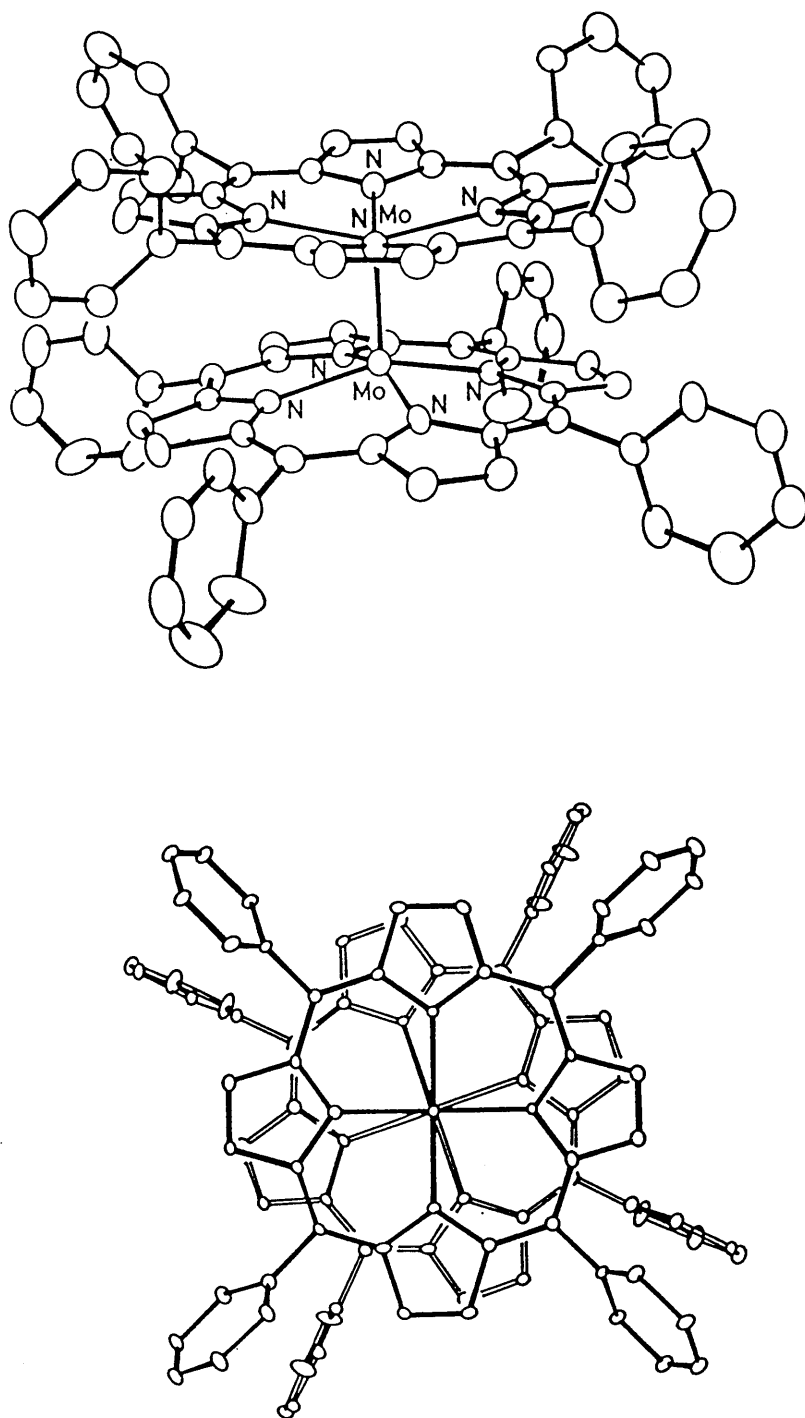


Figure 1.18 Crystal structure of Mo₂(TPP)₂.

3 Objectives

The purpose of this project was to synthesise new quadruply bonded dimolybdenum complexes. The structure and properties of these complexes were studied using various techniques. Three major areas of study were undertaken.

(1) The isomerisation reaction of $\text{Mo}_2\text{X}_4(\text{P}\sim\text{P})_2$ complexes was studied in both solution and the solid state, in order to help determine a mechanism for each phase.

(2) Substitution reactions involving replacement of labile ligands by stronger coordinating species in dimolybdenum complexes.

(3) Optical activity in quadruply bonded complexes has attracted a lot of interest in recent years. The configurations and conformations of new optically complexes will be discussed and compared with existing species.

1 Instrumentation

1.1 Electronic Absorption Spectra

All electronic absorption spectra were recorded on a Beckman UV 5270 UV-visible-NIR spectrophotometer. The absorption intensity measurements were accurate to 0.001 absorption units.

1.2 Circular Dichroism Spectra

The cd spectrometer is constructed around a Jobin-Yvon 0.6 m monochromator. The source is a 150 W horizontally mounted xenon arc lamp which is focussed by means of a parabolic reflector. The light energy from the monochromator is plane-polarised in the vertical plane by a quartz Rochon prism and it is circularly polarised by passing through a photo-elastic modulator held at 45° to its fast and slow axes. The circularly polarised light is collected by a photomultiplier after it has passed through the sample. A synchronous lock-in amplifier is used to measure the modulated signal, this is referenced to the photo-elastic modulator vibration frequency of 50 kHz. The periodic difference in light intensity which arises due to the presence of an optically active sample is detected by the lock-in amplifier. The output from the amplifier is plotted on a chart recorder as the monochromator scans the desired wavelength region. A spectrum of ΔA with wavelength is obtained, where ΔA is the fractional

circular dichroism absorbance. Values as low as 10^{-5} can be detected for ΔA .

1.3 Raman Spectra

Raman spectra were recorded on a Spex Ramalog IV instrument using coherent 52G Kr⁺ and Ar⁺ ion lasers as excitation sources. In order to prevent the sample burning in the laser beam, the rotating sample technique was used. The scattered light was collected at 180° to the incident beam.

1.4 Nuclear Magnetic Resonance Spectra

All nmr spectra were recorded on a Bruker WP 200 ST spectrometer.

1.5 Infra-Red Spectra

All ir spectra were recorded on a Perkin-Elmer 983 spectrophotometer.

2 Chemicals, Solvent Purification etc.

The purity and suppliers of some of the chemicals used in this project are listed in table 2.1. The purification methods for the solvents are given in table 2.2.

Table 2.1 Purity and Suppliers of Chemicals used in this Project

<u>Chemical</u>	<u>Purity</u>	<u>Supplier</u>
Molybdenum hexacarbonyl	Pure	B.D.H.
dppe	Pure	Strem
S,S-dppb (chiraphos)	Pure	Strem
dppp	Pure	Strem
dmpe	Pure	Strem
DIOP	Pure	Aldrich
Triphenylphosphine	Pure	Strem
Chlorodiphenylphosphine	Tech.	Aldrich
Propylenediamine	Pure	B.D.H.
Triflic acid	Pure	Fluorochem
[Me ₃ O][BF ₄]	Pure	Fluka

Table 2.2 Methods of Solvent Purification

<u>Solvent</u>	<u>Purification Method</u>
Methanol	} Distilled from CaH_2 and stored over activated 3 Å sieves.
Ethanol	
Diglyme	
Dimethylformamide	
Pyridine	Distilled from KOH.
Tetrahydrofuran	Distilled from and stored
Toluene	under Na wire.
Acetonitrile	Distilled from P_2O_5 and stored over activated 3 Å sieves.
Dichloromethane	Distilled from CaH_2 and stored over activated 3 Å sieves.

Reactions that required an inert atmosphere were performed with oxygen-free nitrogen. The nitrogen was dried by passing it through a column of sodium hydroxide pellets followed by a column of silica gel.

Certain reactions required a vacuum line. This was constructed from pyrex glass and used a Genevac rotary oil pump and a mercury diffusion pump. Pressures as low as 10^{-4} mm Hg were achieved. Some reactions had to use both a nitrogen atmosphere and a vacuum, these reactions were carried out on a Schlenk line.

Most complexes were characterised by the above spectroscopic techniques. Elemental analyses of new compounds were carried out by the Glasgow University Micro-analysis service.

3 Experimental Procedure

3.1 Preparation of $\text{Mo}_2(\text{O}_2\text{CCH}_3)_4$

The synthesis of this complex can be undertaken by either of two favoured methods.

(a) ^{79}G lacial acetic acid (10 ml), acetic anhydride (1 ml) and purified diglyme (100 ml) were placed in a round bottomed flask. This mixture was purged with nitrogen for at least 15 minutes and then $\text{Mo}(\text{CO})_6$ (2.00 g; 7.58 mmol) was added. The mixture was refluxed under nitrogen for 3 hours. During the reflux $\text{Mo}(\text{CO})_6$ sublimed on the condenser wall, this was periodically scraped to let the $\text{Mo}(\text{CO})_6$ fall back into the refluxing solution. The resulting brown solution was cooled in ice until yellow needle crystals of $\text{Mo}_2(\text{O}_2\text{CCH}_3)_4$ were formed. Addition of ethanol sometimes helped crystal formation. These crystals were filtered and washed with two 10 ml portions of ethanol and ether, then dried in vacuo. Typical yield 70%.

(b) ^{118}o -dichlorobenzene (100 ml), glacial acetic acid (10 ml), acetic anhydride (1 ml) and hexane (2 ml) were placed in a round bottomed flask. The mixture was purged with nitrogen for 15 minutes. Then $\text{Mo}(\text{CO})_6$ (2.00 g; 7.58 mmol) was added and the mixture was refluxed for 10 hours under nitrogen. The resulting brown solution was then cooled in ice and $\text{Mo}_2(\text{O}_2\text{CCH}_3)_4$ was precipitated. The crystals were washed with two 10 ml portions of ethanol and ether, then dried in vacuo. Typical yield 80%.

3.2 Preparation of $\text{Mo}_2(\text{O}_2\text{CCF}_3)_4$ 119

This reaction was carried in a nitrogen atmosphere. $\text{Mo}_2(\text{O}_2\text{CCH}_3)_4$ (2.00 g; 4.66 mmol) dissolved in a mixture of trifluoroacetic acid (30 ml) and trifluoroacetic anhydride (3 ml). This solution was heated to boiling, cooled to room temperature and then allowed to stand for two hours at -20°C . The solvent was removed by passing a stream of nitrogen over the solution. Once the crystals had been dried, they were washed with two 10 ml portions of pentane and dried in vacuo under a blanket of nitrogen. The yellow crystals of $\text{Mo}_2(\text{O}_2\text{CCF}_3)_4$ are slightly air sensitive and were stored in an inert atmosphere. Typical yield 70%. This complex could be further purified by vacuum sublimation.

3.3 Preparation of $\text{K}_4\text{Mo}_2\text{Cl}_8$ 120

In a typical reaction, $\text{Mo}_2(\text{O}_2\text{CCH}_3)_4$ (1.00 g; 2.33 mmol) and KCl (1.39 g; 18.70 mmol) were added to 12M HCl (50 ml) which had been saturated with HCl gas at 0°C . The reactants were stirred in a beaker covered with a watchglass for 40 minutes at room temperature. The red $\text{K}_4\text{Mo}_2\text{Cl}_8$ that formed was filtered and washed with two 15 ml portions of ethanol and dried in vacuo. Typical yield 70%.

3.4 Preparation of R-phenphos 121

The R-phenphos ligand, $(C_6H_5)_2PCH(C_6H_5)CH_2P(C_6H_5)_2$, was prepared in three stages from mandelic acid.

(1) (S)-phenyl-1,2-ethanediol

L-mandelic acid (43 g; 0.8 mol) dissolved in 125 ml was added dropwise to a suspension of 6.7 g (0.17 mol) of $LiAlH_4$ in 250 ml of diethyl ether at a rate sufficient to maintain a rapid reflux. After about one hour this addition was complete. The reaction mixture was refluxed for a further 30 minutes, cooled and treated with 18 ml of ethyl acetate to destroy excess $LiAlH_4$. The resulting mixture was then hydrolysed by addition of 7 ml of water, then 7 ml of 15% aqueous sodium hydroxide and finally 20 ml of water. The precipitate that formed was filtered and washed with diethyl ether. This diethyl ether solution was dried over $MgSO_4$ and then concentrated under 25 mm Hg pressure. The residue was crystallised from a mixture of diethyl ether and 35-60°C petroleum ether to give 7.0 g (65% yield) of (S)- $C_6H_5CH(OH)CH_2OH$.

(2) (S)-1-phenyl-1,2-ethanediol bis(toluenesulphonate)

A solution of 7.0 g (0.05 mmol) of (S)-phenyl-1,2-ethanediol in 40 ml of purified pyridine was treated at 0°C with 23.3 g (0.12 mmol) of p-toluenesulphonyl chloride. The mixture was stirred for three hours at this temperature and then cooled to -10°C for 16 hours. After this time the mixture was poured into 300 ml of ice water

with vigorous stirring. The resulting fine suspension was poured into a mixture of 35 ml of concentrated HCl and excess crushed ice. A white crystalline precipitate was formed and this was filtered, washed thoroughly with water and petroleum ether to give 15.3 g (67% yield) of (S)-1-phenyl-1,2-ethanediol bis(p-toluenesulphonate).

(3) (R)-1,2-bis(diphenylphosphino)-1-phenylethane

A solution of 7.2 ml (8.8 g; 0.04 mol) of $(C_6H_5)_2PCl$ in 150 ml dioxane was boiled under reflux for 7 hours with 3.8 g (0.166 mol) of finely cut sodium metal in a nitrogen atmosphere with strong mechanical stirring. The resulting orange yellow solution reaction mixture was treated with 100 ml of anhydrous tetrahydrofuran and then decanted from unreacted sodium. A solution of (S)-1-phenyl-1,2-ethanediol bis(toluenesulphonate) (6.6 g; 0.015 mol) in 50 ml of THF was added dropwise over 30 minutes. The reaction mixture had become light yellow after this addition and was stirred for a further 30 minutes before being filtered through glass wool. The solvents were removed from the filtrate under pressure to give an oil. The oil was treated with ethanol to give a white solid. This solid was recrystallised from ethanol to give white crystalline (R)- $(C_6H_5)_2PCH(C_6H_5)CH_2P(C_6H_5)_2$ (2.8 g; 40% yield).

3.5 Preparation of S,S-skewphos 122

The S,S-skewphos ligand, $(C_6H_5)_2PCH(CH_3)CH_2CH(CH_3)P(C_6H_5)_2$, was prepared in several steps from 2,4-pentanediol.

(1) (R,R) and (S,S)-2,4-pentanediol bis(d-10-camphorsulphonate)

To a stirred solution of freshly recrystallised d-10-camphorsulphonyl chloride (55 g) in dry pyridine (50 ml) at 0°C was slowly added racemic 2,4-pentanediol (10.4 g) in dry pyridine. The mixture was stirred at this temperature for four hours and warmed to 25°C and stirred for 12 hours at this temperature. Crushed ice was then added to the reaction mixture until the product, a colourless oil, was fully formed. This mixture was poured into a stirred mixture of HCl (12N, 70 ml) in crushed ice (600 g). The product was extracted from the neutralised mixture with diethyl ether (2 x 200 ml); then the combined ether extracts were washed with water (2 X 100 ml) and then with brine (100 ml) and were dried over $MgSO_4$. The ether was removed under reduced pressure at 40°C to give a colourless oil (52 g).

(2) (R,R)-2,4-pentanediol bis(d-camphorsulphonate)

The oil from above was dissolved in diethyl ether (52 ml); this solution was stoppered and left to stand at ambient temperature for four days. Fine white crystals formed which were filtered and washed with diethyl ether.

The filtrate was set aside, and the solid (18 g) was recrystallised from dichloromethane (50 ml) and diethyl ether (100 ml) to which hexane was gradually added. The plate crystals of the pure R,R diastereomer were filtered and washed with diethyl ether and hexane.

(3) (S,S)-skewphos

To a magnetically stirred solution of freshly recrystallised triphenylphosphine (26.2 g) in THF (75 ml) at 25°C was added finely cut lithium (1.4 g). This mixture was stirred for two hours and the solution turned orange. During this stirring operation, the consumption of the lithium caused the temperature to rise to 55°C, however at the end of the two hours the temperature had returned to 25°C. Freshly distilled tertiary-butyl chloride (9.25 g) was then added dropwise to the reaction. The reaction solution became hot, and after 30 minutes stirring, the vessel was immersed in an ice bath. (R,R)-2,4-pentanediol bis(d-camphorsulphonate) (10.6 g) in THF (35 ml) was then added dropwise to the stirred, cold phosphide solution. The reaction mixture was then stirred for 30 minutes. Water (100 ml) was slowly added and then most of the THF was removed under reduced pressure. The residue was extracted with diethyl ether (2 x 100 ml) and added slowly to a stirred solution of $\text{Ni}(\text{ClO}_4)_2 \cdot 6\text{H}_2\text{O}$ (5 g) and NaNCS (5 g) in ethanol (100 ml). Yellow crystals formed at once and the slurry was stirred for 10 hours. The yellow solid

$[\text{Ni}\{(S,S)\text{-skewphos}\}(\text{NCS})_2]$ (8.8 g) was then collected and was washed with ethanol and diethyl ether.

(4) $[\text{Ni}\{(S,S)\text{-skewphos}\}(\text{NCS})_2]$

This complex was recrystallised by suspending the solid (8.8 g) in dichloromethane (170 ml). Trifluoroacetic acid (9 ml) was slowly added to this mixture and the complex dissolved. It was filtered and ethanol (170 ml) was slowly added to the now clear orange-brown filtrate. The solution was then allowed to stand for two hours during which time more ethanol (150 ml) was added. The bronze coloured plates were collected and washed with ethanol and diethyl ether. The nickel complex could be recrystallised by the above method for a second time if desired.

(5) Free (S,S)-skewphos

$[\text{Ni}\{(S,S)\text{-skewphos}\}(\text{NCS})_2]$ (4.5 g) was suspended in a mixture of ethanol (20 ml) and THF (20 ml). This mixture was stirred and brought to 80°C and then NaCN (1.5 g) in water (10 ml) was quickly added. A deep red solution formed which rapidly faded to a pale yellow colour. The ethanol and THF were removed under reduced pressure, then water (50 ml) was added to the residue, and the phosphine was extracted with diethyl ether (2 x 50 ml). The combined ether extracts were washed with water (2 x 50 ml) and then with brine (50 ml) and then dried over Na_2SO_4 . The ether was removed under reduced to leave (S,S)-skewphos (3.3 g) as an oil. The phosphine was stored under nitrogen at 0°C although it is not very air sensitive.

3.6 Preparation of $\alpha\text{-Mo}_2\text{Cl}_4(\text{dppe})_2$

There are two methods of preparing this complex

(a) ¹⁰⁰In a typical reaction $\text{K}_4\text{Mo}_2\text{Cl}_8$ (0.35 g; 0.5 mmol) and dppe (0.4 g; 1 mmol) were added to 50 ml of methanol which had been thoroughly purged with nitrogen. The reactants were refluxed under nitrogen for three hours and then cooled in ice. The green precipitate which formed was filtered and washed with two 10 ml portions of methanol and diethyl ether. Typical yield 75%. The product, $\alpha\text{-Mo}_2\text{Cl}_4(\text{dppe})_2$, is air stable.

(b) ⁸⁸ $\text{Mo}_2(\text{O}_2\text{CCF}_3)_4$ (0.32 g; 0.5 mmol) and dppe (0.4 g; 1 mmol) were added to 30 ml of degassed toluene. A rubber septum cap was placed over the reaction vessel in order to maintain a nitrogen atmosphere. Me_3SiCl (2 mmol) was then injected by syringe into the reaction mixture. The reactants were then stirred for 2-3 hours during which time a green precipitate formed. This precipitate was filtered and washed with two 10 ml portions of ether. Typical yield 50%.

3.7 Preparation of $\alpha\text{-Mo}_2\text{Cl}_4(\text{dppp})_2$

This was prepared by the same method as preparative route (a) for $\alpha\text{-Mo}_2\text{Cl}_4(\text{dppe})_2$. However only a reflux of less than an hour was necessary. The product was an air stable green solid. Analysis (found) C 61.2% (61.0), H 4.9% (4.8), P 11.7% (12.0).

3.8 Preparation of $\beta\text{-Mo}_2\text{Cl}_4(\text{R-phenphos})_2$

This complex could be prepared by either of the two preparative routes used for $\alpha\text{-Mo}_2\text{Cl}_4(\text{dppe})_2$. The solid was an air stable yellow-green solid. Analysis (found) C 59.9% (59.4), H 4.4% (4.0), Cl 11.1% (11.7).

3.9 Preparation of $\beta\text{-Mo}_2\text{Cl}_4(\text{S,S-skewphos})_2$

In a typical reaction $\text{K}_4\text{Mo}_2\text{Cl}_8$ (0.35 g; 0.5 mmol) and S,S-skewphos (0.44 g; 1 mmol) were added to 50 ml of degassed methanol. This mixture was refluxed under nitrogen for one hour. A green solution was obtained as $\alpha\text{-Mo}_2\text{Cl}_4(\text{S,S-skewphos})_2$ is soluble in methanol. This solution was stripped of solvent to give a green solid which was washed with diethyl ether. All operations were carried out in a nitrogen atmosphere as the product is air sensitive. Analysis (found) C 57.3% (56.7), H 4.9% (4.8), P 10.2% (9.9).

3.10 Preparation of $\beta\text{-Mo}_2\text{Cl}_4(\text{DIOP})_2$

This complex was prepared by the same preparative method used for $\beta\text{-Mo}_2\text{Cl}_4(\text{S,S-skewphos})_2$. In this case the product is an air sensitive blue solid. Characterisation of this complex was based on the spectra collected.

3.11 Preparation of $\text{Mo}_2(\text{TFMS})_4$ 123

The following preparation was carried out on the vacuum line in a double limbed vessel. In one limb of the vessel was placed 1.3 g (3 mmol) of $\text{Mo}_2(\text{O}_2\text{CCH}_3)_4$ and 5 ml of purified HTFMS in the other limb. The HTFMS was then distilled into the limb containing the $\text{Mo}_2(\text{O}_2\text{CCH}_3)_4$. The reaction mixture rapidly became bright red in colour. This mixture was frequently shaken over a period of several hours and then heated to drive the remaining liquid. The product usually varied in colour from orange to tan. Typical yield 70%. Further purification could be achieved by vacuum sublimation. This air sensitive product was stored under nitrogen.

3.12 Preparation of $\text{Mo}_2(\text{DMF})_8(\text{TFMS})_4$

This reaction was carried out on the vacuum line. $\text{Mo}_2(\text{TFMS})_4$ was completely dissolved in DMF to give a bright red solution. The solvent was then removed to give an air sensitive red solid. Typical yield 80%. The complex could be recrystallised from dichloromethane. Analysis (found) C 24.5% (24.5), H 4.1% (3.9), N 8.2% (8.0).

3.13 Preparation of $\text{Mo}_2(\text{CH}_3\text{CN})_8(\text{TFMS})_4$

$\text{Mo}_2(\text{TFMS})_4$ was completely dissolved in acetonitrile on the vacuum line to give a deep purple solution. The

solvent was removed to leave an air sensitive purple solid. This solid could be recrystallised from acetonitrile.

3.14 Preparation of $\text{Mo}_2(\text{NH}_3)_8(\text{TFMS})_4$

$\text{Mo}_2(\text{CH}_3\text{CN})_8(\text{TFMS})_4$ was dissolved in acetonitrile on the vacuum line, then a couple of mls of dry ammonia was distilled into the reaction mixture to give a brown solution. The solvent was removed to give a brown solid. Characterisation of this complex was based on spectroscopy (see chp 4).

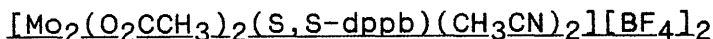
3.15 Preparation of $[\text{Mo}_2(\text{O}_2\text{CCH}_3)_2(\text{CH}_3\text{CN})_6][\text{BF}_4]_2$ ⁷²

This reaction was performed using Schlenk techniques. $\text{Mo}_2(\text{O}_2\text{CCH}_3)_4$ (1.3 g; 3 mmol) was added to a solution of $[\text{Me}_3\text{O}][\text{BF}_4]$ (1.8 g; 12 mmol) in acetonitrile (100 ml). A bright red solution formed and the mixture was stirred until all of the $\text{Mo}_2(\text{O}_2\text{CCH}_3)_4$ had dissolved. When the solvent was being removed, a red solid started to precipitate, this was increased by the addition of diethyl ether. The air sensitive solid was filtered and washed with diethyl ether. Typical yield 80%. The product could be recrystallised from acetonitrile. Analysis of this complex varied; this has been discussed elsewhere ⁷¹.

3.16 Preparation of $[\text{Mo}_2(\text{O}_2\text{CCH}_3)_2(\text{dmpe})_2][\text{BF}_4]_2$

This reaction was performed on a Schlenk line although the product is air stable. $[\text{Mo}_2(\text{O}_2\text{CCH}_3)_2(\text{CH}_3\text{CN})_6][\text{BF}_4]_2$ (0.15 g; 0.20 mmol) was completely dissolved in acetonitrile, then dmpe (0.6 g; 0.40 mmol) was added to this mixture. An orange solution formed and this was stirred for several hours. The solvent was removed to give an orange solid, this was washed with a little dichloromethane and diethyl ether. Analysis was excellent except for carbon which was somewhat high. Analysis (found) C 24.5% (21.3), H 4.85% (4.8), P 15.8% (15.8) N 0.0% (0.0). The complex was recrystallised from acetonitrile.

3.17 Preparation of



$[\text{Mo}_2(\text{O}_2\text{CCH}_3)_2(\text{CH}_3\text{CN})_6][\text{BF}_4]_2$ (0.3 g; 0.41 mmol) was completely dissolved in acetonitrile, S,S-dppb (0.33 g; 0.83 mmol) was then added. The mixture was stirred for one day and the solution darkened to a deep purple colour. The volume of solution was reduced and precipitation of a purple solid occurred, this was increased by addition of diethyl ether. The air sensitive solid was filtered and washed with diethyl ether. Analysis (found) C 44.9% (45.2), H 4.2% (4.2), P 6.4% (6.0).

3.18 Reaction of $[\text{Mo}_2(\text{O}_2\text{CCH}_3)_2(\text{CH}_3\text{CN})_6][\text{BF}_4]_2$ with NH_3

This reaction was carried out on the vacuum line. A couple of mls of ammonia was distilled into a solution of $[\text{Mo}_2(\text{O}_2\text{CCH}_3)_2(\text{CH}_3\text{CN})_6][\text{BF}_4]_2$ in acetonitrile. The resulting solution was golden yellow. The solvent was removed to give a yellow green solid. Characterisation of this complex will be discussed in chp 4.

3.19 Reaction of $[\text{Mo}_2(\text{O}_2\text{CCH}_3)_2(\text{CH}_3\text{CN})_6][\text{BF}_4]_2$ with

R-pn

This reaction almost identical to the last preparation discussed. In this case a brown solution is obtained, this will be discussed in chp 4.

3.20 Reaction of $\text{Mo}_2(\text{O}_2\text{CCH}_3)_4$ with S,S-dppb

This reaction was performed on the vacuum line. $\text{Mo}_2(\text{O}_2\text{CCH}_3)_4$ (0.2 g; 0.5 mmol), S,S-dppb (0.4 g; 1 mmol) and $[\text{Me}_3\text{O}][\text{BF}_4]$ (0.3 g; 2 mmol) were placed in a vacuum cell. Acetonitrile (5 ml) was distilled onto the mixture, a bright orange solution was observed with much unreacted $\text{Mo}_2(\text{O}_2\text{CCH}_3)_4$. This will be discussed in chp 4

3.21 Reaction of $\text{Mo}_2(\text{O}_2\text{CCH}_3)_4$ with R-pn

This reaction was very similar to the previous preparation, a golden solution was obtained. See chp 4.

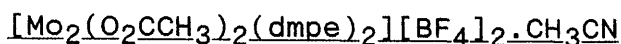
4 Crystal Structure of $[\text{Mo}_2(\text{O}_2\text{CCH}_3)_2(\text{dmpe})_2][\text{BF}_4]_2$

Details of data collection procedures and structural refinement are given in table 2.1.

$[\text{Mo}_2(\text{O}_2\text{CCH}_3)_2(\text{dmpe})_2][\text{BF}_4]_2 \cdot \text{CH}_3\text{CN}$ crystallises from acetonitrile as translucent orange prisms which rapidly cloud on removal from the mother liquor. A segment c. 0.3 x 0.3 x 0.3 mm was cut from a larger crystal and immediately coated in glue in order to prevent solvent loss. Data were collected on an Enraf-Nonius CAD4F automated diffractometer, with graphite monochromated X-radiation ($\lambda = 0.71069 \text{ \AA}$). Unit cell parameters were determined by refinement of the setting angles ($\theta \geq 12^\circ$) of 25 reflections. Standards were measured every two hours during data collection and no significant decay was observed. Lorentz/polarisation and absorption (DIFABS 124) corrections were applied. Systematic absences ($h0l$, $h + l = 2n + 1$; $0k0$, $k = 2n + 1$) uniquely indicated the monoclinic space group $P2_1/n$ (no.14 C_{2h}^5). The structure was solved by direct methods (MITHRIL 125) and subsequent electron density syntheses. All non-hydrogen atoms were allowed anisotropic thermal motion. Hydrogen atoms were included at calculated positions (C-H = 1.0 Å) and were held fixed during refinement with fixed isotropic (0.05 Å^2)

thermal parameters. Refinement was by full-matrix least-squares. Due to matrix size limitations the parameters list was divided into two sections and each refined separately. The function minimised was $w(|E_o| - |E_c|)^2$ with the weighting function $w = [\sigma^2(E_o)]^{-1}$ used and judged satisfactory. $\sigma(E_o)$ was estimated from counting statistics. Neutral atom scattering factors were from reference 126 with corrections applied for anomalous scattering. All calculations were carried out on a Gould-SEL 32/27 mini computer using GX suit of programs 127.

Table 2.1 Experimental Data for Crystallographic Study of



Formula	$\text{C}_{16}\text{H}_{38}\text{B}_2\text{F}_8\text{Mo}_2\text{O}_4\text{P}_4 \cdot \text{CH}_3\text{CN}$
M_r	825.4
Space group	$P2_1/n$ (No.14 C_{2h}^5)
Crystal system	monoclinic
$a/\text{\AA}$	16.047(8)
$b/\text{\AA}$	11.582(4)
$c/\text{\AA}$	19.067(4)
β/deg	101.03(3)
$V/\text{\AA}^3$	3478(2)
Z	4
$D_{\text{calc}}/\text{g cm}^{-3}$	1.58
$F(000)$	1658
$\mu(\text{Mo-K}\alpha), \text{cm}^{-1}$	9.5
I/K	298
Scan mode	$\theta/2\theta$
θ range/deg	$2 \leq \theta \leq 22$
Crystal size/mm	$0.3 \times 0.3 \times 0.3$
Range of trans. coeff. corr.	0.91-1.11
No. of data collected	4701
No. of unique data	4244
Std. reflections	251 251
Observability criterion n	
$I > n\sigma(I)$	3
No. of data in refinement	2874

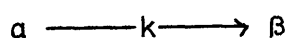
Table 2.1 ctd

No. of refined parameters	217/262
Final R	0.043
Final R_w	0.045
Largest remaining feature in elec. density map, $e \text{ \AA}^{-3}$	+0.74 (max), -0.64 (min)
Shift/esd in last cycle	0.35 (max), 0.02 (av)

5 Collection and Treatment of Isomerisation Results

In this project the kinetic parameters were collected for the α - β isomerisation of $\text{Mo}_2\text{Cl}_4(\text{dppp})_2$ in dichloromethane solution and $\text{Mo}_2\text{Cl}_4(\text{dppe})_2$ in the solid state. The isomerisation was monitored by electronic absorption spectroscopy in both phases. The treatment of this data will be discussed after a detailed study of first order isomerisation kinetics.

This α - β isomerisation follows first order kinetics and no intermediates are observed, thus



where k is the rate constant for the isomerisation.

The reaction is followed by absorption spectroscopy. Thus from the Beer-Lambert law, the absorbance at a set wavelength, at any particular time, due to the concentration of the isomers, $c_{\alpha t}$ and $c_{\beta t}$, is

$$A_t = \epsilon_{\alpha} c_{\alpha t} l + \epsilon_{\beta} c_{\beta t} l \quad (2.1)$$

where ϵ_{α} and ϵ_{β} are the extinction coefficients for the respective α and β isomers at the set wavelength. The path length of the cell is denoted by l .

Since there are no intermediates involved and there can only ever be two species in solution, then

$$c_{\alpha t} + c_{\beta t} = c_0 \quad (2.2)$$

where c_0 is the total concentration and it is equal to the initial concentration of the α isomer. The cells used in this project all have path length of 1 cm. Using this information and equation (2.2), then equation (2.1) can be rewritten as

$$A_t = \epsilon_{\alpha} c_{\alpha t} + \epsilon_{\beta} (c_0 - c_{\alpha t})$$

The rate of the reaction is equal to the rate of disappearance of the α isomer or the rate of formation of the β isomer. This can be written as

$$\text{rate} = -\frac{dc_{\alpha t}}{dt} = \frac{dc_{\beta t}}{dt} = kc_{\alpha t}$$

$$\rightarrow \frac{dc_{\alpha t}}{dc_{\alpha t}} = - \int_0^t k dt$$

$$\rightarrow \ln \frac{c_{\alpha t}}{c_0} = -(kt) \quad (2.3)$$

The absorbance at any particular wavelength at a time, t , is given in equation (2.1). When $t = \infty$, $c_{\alpha t} = 0$, the absorbance at this time will be

$$A_{\infty} = \epsilon_{\beta} c_0$$

Thus at any time, t ,

$$A_{\infty} - A_t = \epsilon_{\beta} c_0 - (\epsilon_{\alpha} c_{\alpha t} + \epsilon_{\beta} c_{\beta t})$$

Substituting $c_0 = c_{\alpha t} + c_{\beta t}$ in this equation gives

$$A_{\infty} - A_t = \epsilon_{\beta} (c_{\alpha t} + c_{\beta t}) - (\epsilon_{\alpha} c_{\alpha t} + \epsilon_{\beta} c_{\beta t})$$

$$A_{\infty} - A_t = \epsilon_{\beta} c_{\alpha t} + \epsilon_{\beta} c_{\beta t} - \epsilon_{\alpha} c_{\alpha t} - \epsilon_{\beta} c_{\beta t}$$

$$A_{\infty} - A_t = c_{\alpha t} (\epsilon_{\beta} - \epsilon_{\alpha}) \quad (2.4)$$

There are certain wavelengths in the isomerisation spectra where the absorbance does not change with time. At these points $A_{\infty} - A_t = 0$, thus from equation (2.4) ξ_{α} will be equal to ξ_{β} at these particular wavelengths. Therefore for a set concentration, no matter what the relative proportion of α and β isomer, the electronic spectrum will pass through this isosbestic point. These isosbestic points are certain signs that there are only two species in solution, thus intermediates can be ruled out.

Equation (2.4) can be rearranged to give

$$c_{\alpha t} = \frac{(A_{\infty} - A_t)}{(\xi_{\beta} - \xi_{\alpha})}$$

Now $c_{\alpha t}$ can be substituted into equation (2.3) to give

$$\ln \left\{ \frac{(A_{\infty} - A_t)}{c_0(\xi_{\beta} - \xi_{\alpha})} \right\} = -(kt)$$

$$\rightarrow \ln(A_{\infty} - A_t) = -kt + \ln[c_0(\xi_{\beta} - \xi_{\alpha})] \quad (2.5)$$

In order to simplify this equation, wavelengths are chosen where only one isomer absorbs. Thus equation (2.5) now becomes

$$\ln(A_{\infty} - A_t) = -(kt) + \ln(c_0 \epsilon_{\alpha})$$

where ξ_n is ξ_α or ξ_β depending on the wavelength chosen. Now both $\xi_\alpha c_0$ and $\xi_\beta c_0$ are equal to the initial absorbance, $A_{0\alpha}$ and $A_{0\beta}$, of each respective isomer. Therefore the final version of the equation can be expressed as

$$\ln(A_\infty - A_t) = -(kt) + \ln(A_{0n}) \quad (2.6)$$

Now a plot of $\ln(A_\infty - A_t)$ versus time will give a straight line with gradient, $-k$, and intercept, $\ln(A_{0n})$, if the reaction is a first order process.

This procedure can be repeated over a range of temperatures in order to obtain a value for the activation energy from the Arrhenius equation.

$$\ln(k) = - \frac{E_a}{RT} + \ln(A) \quad (2.7)$$

where k (in sec^{-1}) is the rate constant, A is the pre-exponential factor, R is the gas constant ($8.314 \text{ JK}^{-1}\text{mol}^{-1}$), T (in K) is the temperature and E_a is the activation energy (in Jmol^{-1}). A plot of $\ln(k)$ versus $1/T$ gives a straight line with gradient $(-E_a/R)$ and intercept $\ln(A)$.

Another equation can be employed to give the entropy of activation, this is

$$\ln(A) = \frac{RT}{Nh} e^{(\Delta S^\ddagger/R)} \quad (2.8)$$

where A is the pre-exponential factor, R is the gas constant ($8.314 \text{ JK}^{-1}\text{mol}^{-1}$), T (in K) is the temperature, e is the base of natural logarithms (~ 2.71828), N is Avogadro's constant ($6.022 \times 10^{23} \text{ mol}^{-1}$), h is Planck's constant ($6.626 \times 10^{-34} \text{ Js}$) and ΔS^\ddagger is the entropy of activation (in $\text{JK}^{-1}\text{mol}^{-1}$).

The collection of the kinetic data in solution is easy because the the isomerisation of a single sample can be monitored from start to finish by spectroscopy. Treatment of the results is followed as above. In fact the isomerisation of $\alpha\text{-Mo}_2\text{Cl}_4(\text{dppp})_2$ was studied at five different temperatures in the range $15.2 - 29.2^\circ\text{C}$. A thermostated electronic absorption cell was used to keep the temperature constant, the temperatures were accurate to $+ 0.1^\circ\text{C}$.

In the solid state isomerisation it is not as easy to collect the results because of the more extreme conditions (i.e. under vacuum and at high temperatures). It is impractical to study just one sample at a particular temperature. This is because of the difficulty involved in removing the sample several times from the oven, breaking the vacuum seal and recording the extent of isomerisation

by running the electronic spectrum of part of the sample in dichloromethane. Then the sample would have to be re-evacuated and put back in the oven where it would require time to equilibrate to the oven temperature. It is obviously unwise to repeat this procedure several times. The simplest method is to start with several evacuated vessels containing the α isomer, these are put in the oven together at a set temperature. After a suitable time interval has elapsed, one of the vessels is removed from the oven. Great care is taken when opening the oven to be as quick as possible in order to avoid any temperature drop in the oven which is undesirable. The seal on the cooled vessel is then broken, the sample is dissolved in dichloromethane and the electronic spectrum is run immediately in order to avoid any isomerisation occurring in solution. From this spectrum, the ratio of the α and β isomers can be derived after that particular period in the oven. The weights of the sample are checked with the spectrum to ensure that no decomposition takes place during the isomerisation. Thus from several samples taken out at different time intervals, a picture emerges of the different ratios at these time intervals. This can be used to obtain a rate constant for a particular temperature, from equation (2.3) a plot of $\ln(c_{\alpha t}/c_0)$ versus time will yield the rate constant for the α decay. Thus it does not matter if the weights of the samples are different at a set temperature, it is the ratio of the isomers at the time interval that is important. The vessels cannot just be placed on the oven shelf because where the shelf comes into contact with the vessel causes uneven heat

distribution and this is undesirable. This can be overcome by suspending the vessels by an iron wire from a grid in the oven, making sure that all of the sample is at one end of the vessel and the wire is tied to the other end. The temperature range studied for $\alpha\text{-Mo}_2\text{Cl}_4(\text{dppe})_2$ in the solid state was 211 - 250°C. The temperature is controlled by a fan to ensure that there is no temperature gradient and the temperatures were correct to + 1°C.

**Chapter Three: ISOMERISATION REACTIONS OF DIMOLYBDENUM
COMPLEXES CONTAINING DIPHOSPHINE LIGANDS**

1 The Isomerisation Reaction of $\text{Mo}_2\text{X}_4(\text{P}\sim\text{P})_2$ Complexes

In chapter 1 it was noted that complexes with the general formula $\text{Mo}_2\text{X}_4(\text{P}\sim\text{P})_2$ can exist as two geometric isomers (figure 1.12). These are a chelated (α) form, in which the two diphosphine ligands chelate different molybdenum atoms, and a bridged (β) form in which the diphosphine ligands bridge across the metal-metal bond. Fraser *et al* ¹⁰⁰ found that the α form isomerises to the appropriate β isomer in dry dichloromethane solution and subsequently Agaskar and Cotton ⁸⁷ have shown that the isomerisation of $\alpha\text{-Mo}_2\text{Cl}_4(\text{dppe})_2$ occurs in the solid state. The solution isomerisation proceeds with a half life of between several minutes and a few hours depending on the complex and has been studied for $\text{Mo}_2\text{Cl}_4(\text{dppe})_2$, $\text{Mo}_2\text{Br}_4(\text{dppe})_2$, $\text{Mo}_2\text{Cl}_4(\text{dptpe})_2$, $\text{Mo}_2\text{Br}_4(\text{dptpe})_2$ and $\text{Mo}_2\text{Cl}_4(\text{R-dppp})_2$ ¹⁰⁰. In all cases the isomerisation follows first order kinetics for both α decay and β formation. The only complex that has been studied in the solid state is $\text{Mo}_2\text{Cl}_4(\text{dppe})_2$. Here the α form was shown to isomerise cleanly to the β isomer at 250°C under a static vacuum with no detectable side products. The rate of isomerisation was not reported.

In this chapter the solid state isomerisation is studied in detail and the kinetic parameters are compared with those previously measured for the solution process.

Kinetic results are also presented for the isomerisation of α - $\text{Mo}_2\text{Cl}_4(\text{dppp})_2$ in solution and the parameters obtained for this complex with a five atom ligand backbone are compared with those with only four atoms in the ligand backbone. The possible mechanisms for the isomerisation reaction will be discussed in the light of the new results.

2 Electronic Spectra and Kinetics of Isomerisation of $\text{Mo}_2\text{X}_4(\text{P}^{\sim}\text{P})_2$ Complexes

Table 3.1 shows the δ - δ^* transition energies for various α and β isomers of the general formula $\text{Mo}_2\text{X}_4(\text{P}^{\sim}\text{P})_2$. The most noticeable fact in this table is that the transition energies of the β isomers are at a lower energy than their corresponding α isomers. This is because most of the β isomers are twisted (table 1.4) which results in a partial loss of δ overlap and figure 1.7 shows the non-linear relationship between $\cos 2X$ and the δ - δ^* transition energy. All the α isomers are eclipsed and therefore have maximum δ overlap. However the complexes with the highest δ - δ^* transition energies in this series are the β isomers with three atom backbone ligands i.e. dppm and dmpm . Here the short backbone leads to an eclipsed β isomer with a short metal-metal bond. There are no α isomers containing these ligands because the phosphorus atoms cannot get close enough to chelate to the same metal atom.

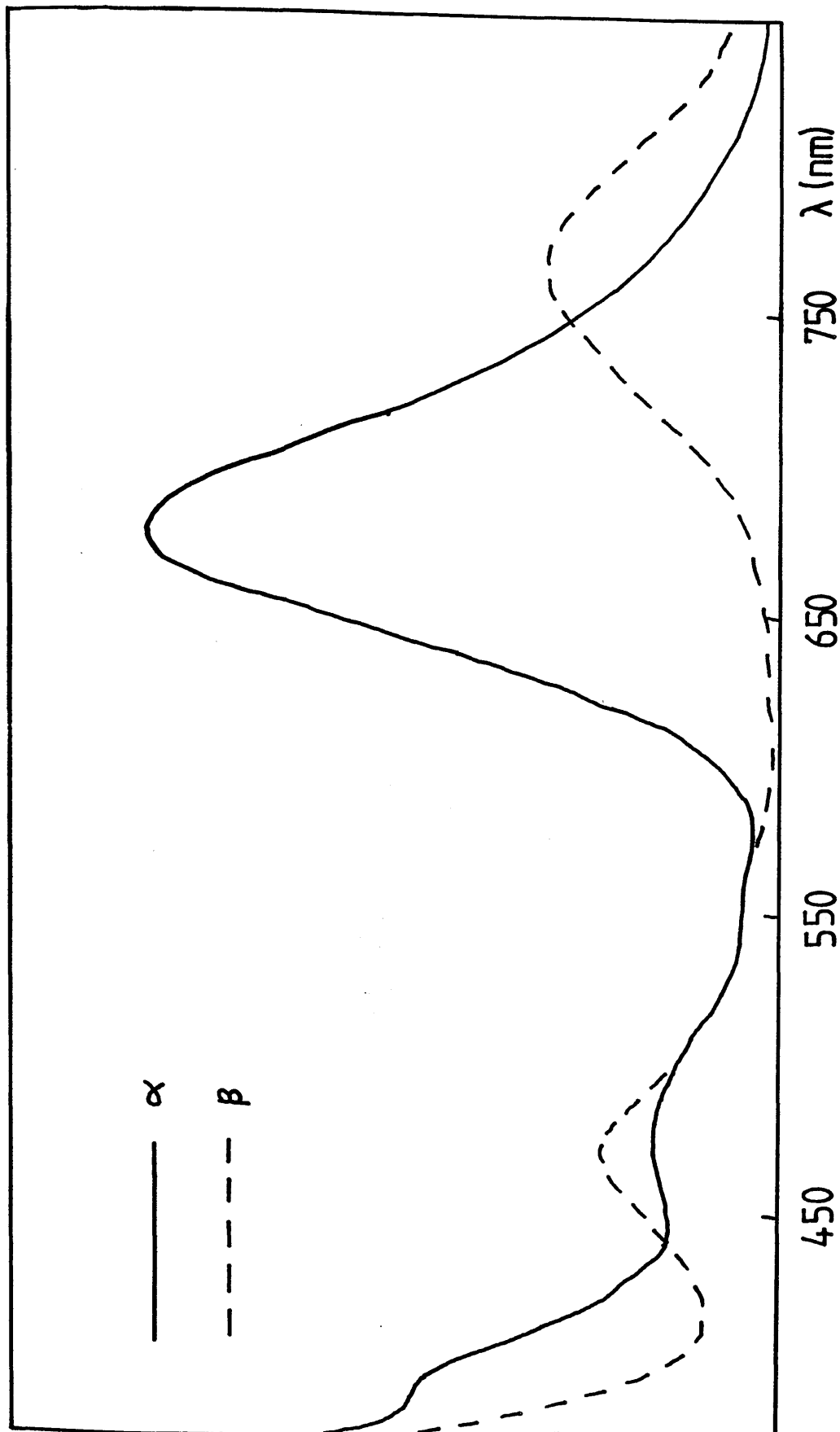
Table 3.1 The δ - δ^* Transition Energies of $\text{Mo}_2\text{X}_4(\text{P}\sim\text{P})_2$
Complexes in Dichloromethane Solution

<u>Complex</u>	<u>λ (nm)</u>	<u>$\tilde{\nu}$ (cm^{-1})</u>	<u>Ref.</u>
$\alpha\text{-Mo}_2\text{Cl}_4(\text{dppe})_2$	675	14815	100
$\alpha\text{-Mo}_2\text{Cl}_4(\text{dmpe})_2$	666	15015	128
$\alpha\text{-Mo}_2\text{Cl}_4(\text{dptpe})_2$	675	14815	129
$\alpha\text{-Mo}_2\text{Cl}_4(\text{R-dppp})_2$	670	14925	129
$\alpha\text{-Mo}_2\text{Cl}_4(\text{dppp})_2$	648	15432	this work
$\alpha\text{-Mo}_2\text{Br}_4(\text{dptpe})_2$	685	14598	129
$\beta\text{-Mo}_2\text{Cl}_4(\text{dppm})_2$	634	15772	83
$\beta\text{-Mo}_2\text{Cl}_4(\text{dmpm})_2$	604	16556	85
$\beta\text{-Mo}_2\text{Cl}_4(\text{dppe})_2$	760	13158	100
$\beta\text{-Mo}_2\text{Cl}_4(\text{dmpe})_2$	803	12453	91
$\beta\text{-Mo}_2\text{Cl}_4(\text{dptpe})_2$	760	13158	129
$\beta\text{-Mo}_2\text{Cl}_4(\text{R-dppp})_2$	750	13333	129
$\beta\text{-Mo}_2\text{Cl}_4(\text{S, S-dppb})_2$	725	13793	93
$\beta\text{-Mo}_2\text{Cl}_4(\text{R-phenphos})_2$	755	13245	this work
$\beta\text{-Mo}_2\text{Cl}_4(\text{dppp})_2$	682	14662	this work
$\beta\text{-Mo}_2\text{Br}_4(\text{dppm})_2$	650	15384	84
$\beta\text{-Mo}_2\text{Br}_4(\text{dppe})_2$	790	12658	129
$\beta\text{-Mo}_2\text{Br}_4(\text{dmpe})_2$	843	11862	23
$\beta\text{-Mo}_2\text{Br}_4(\text{dptpe})_2$	790	12658	129
$\beta\text{-Mo}_2\text{Br}_4(\text{R-dppp})_2$	775	12903	129
$\beta\text{-Mo}_2\text{Br}_4(\text{S, S-dppb})_2$	755	13245	129
$\beta\text{-Mo}_2\text{I}_4(\text{dppm})_2$	684	14619	86
$\beta\text{-Mo}_2\text{I}_4(\text{dppe})_2$	860	11600	90

The electronic absorption spectra of the α and β isomers of $\text{Mo}_2\text{Cl}_4(\text{dppe})_2$ are shown ¹⁰⁰ in figure 3.1. This illustrates the higher energy δ - δ^* transition of the α isomer. It is also a more intense transition. This is mainly due to the greater δ overlap in the α species although comparisons of intensity must be treated with caution (chp 1 sect.1.3). As stated earlier, α - $\text{Mo}_2\text{Cl}_4(\text{dppe})_2$ isomerises to the β form when dissolved in dry dichloromethane. This reaction can be monitored by electronic absorption spectroscopy as shown ¹⁰⁰ in figure 3.2. The isomerisation reaction is a first order process with no intermediates involved, the sharp isosbestic points indicate that only two species are present in solution. In order to obtain a rate constant for α isomer decay, the absorbance is monitored at a wavelength where the α isomer absorbs strongly and the β isomer does not. The absorbance of an isomer is directly proportional to its concentration. A plot of $\log \text{Abs}(\alpha)$ vs time will give a straight line for a first order process; the gradient giving the rate constant k . The same procedure can be repeated for β isomer formation. An Arrhenius plot is obtained if the isomerisation is studied at several different temperatures. The activation energy (E_a) and the entropy of activation (ΔS^\ddagger) can be calculated from this plot.

The α - β isomerisation of $\text{Mo}_2\text{Cl}_4(\text{dppp})_2$ in dichloromethane is shown in figure 3.3, here the δ - δ^*

Absorbance

Figure 3.1 Electronic absorption spectra of α and β - $\text{Mo}_2\text{Cl}_4(\text{dppe})_2$ in CH_2Cl_2

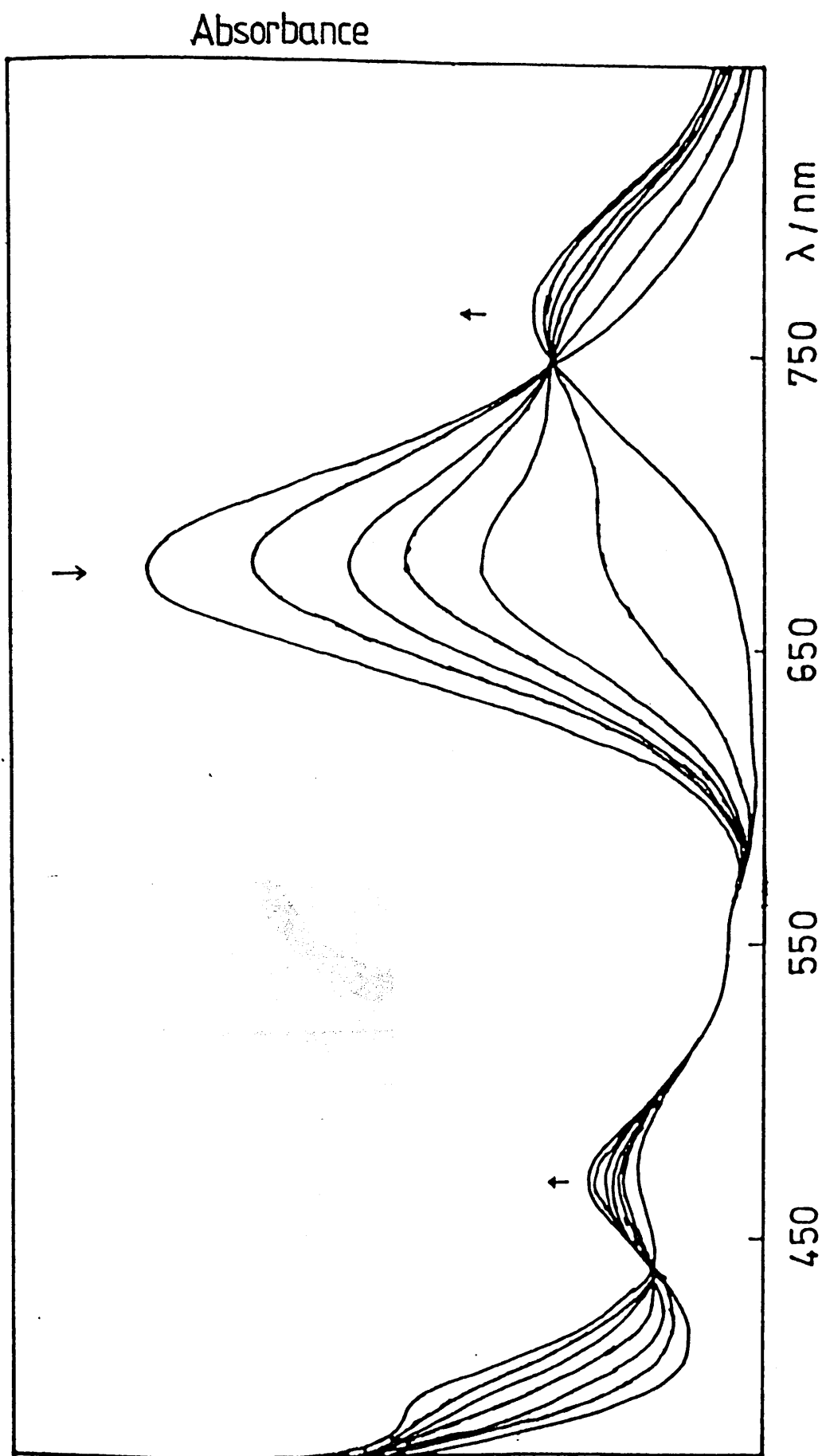


Figure 3.2 $\alpha \rightarrow \beta$ isomerisation of $\text{Mo}_2\text{Cl}_4(\text{dppe})_2$ in CH_2Cl_2 .

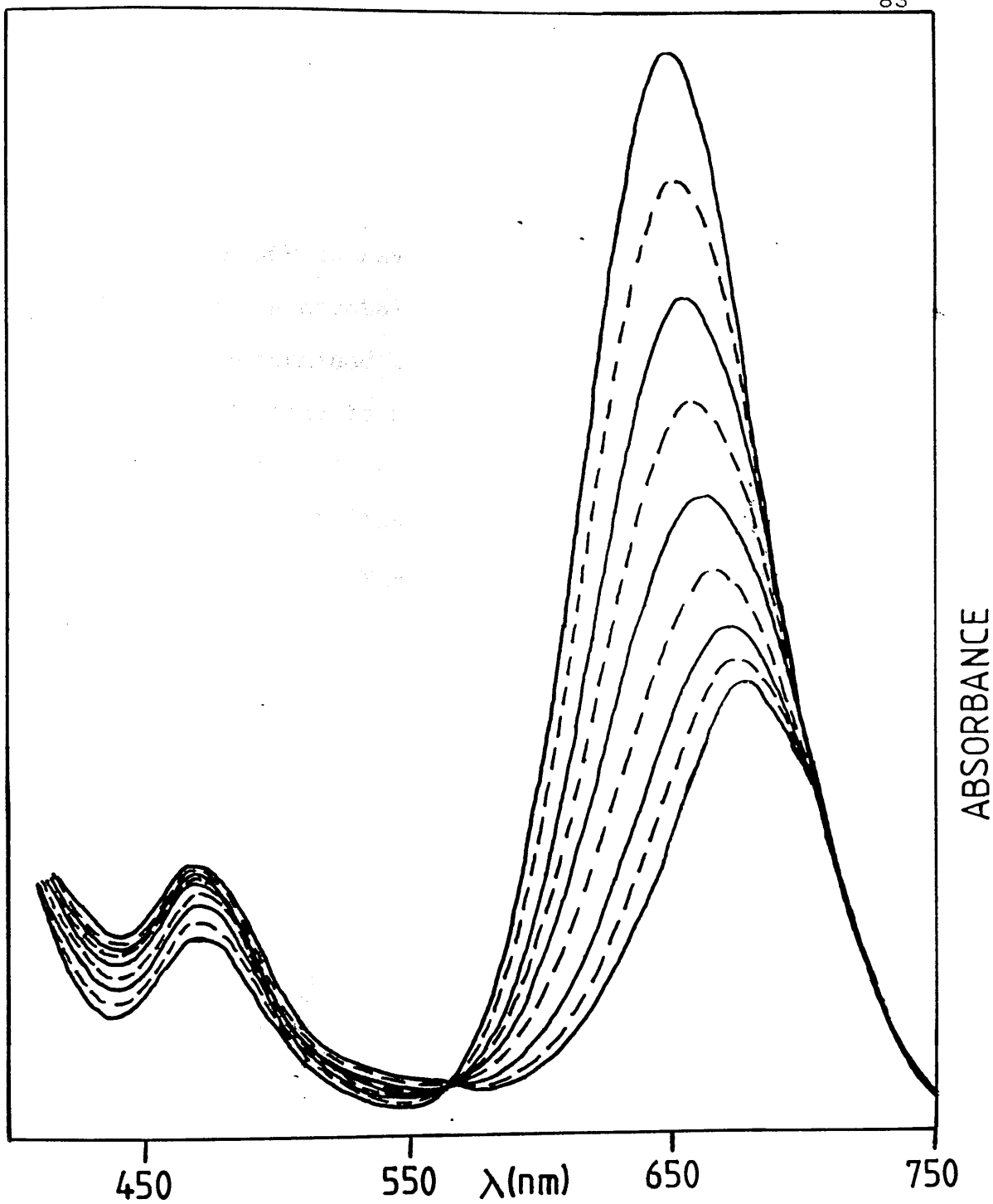


Figure 3.3 $\alpha \rightarrow \beta$ isomerisation of $\text{Mo}_2\text{Cl}_4(\text{dppp})_2$ in CH_2Cl_2 .

transition energies of both isomers are very close together. The twist angle of the β isomer must be very close to 0° or 90° to have such a high transition energy. Unfortunately the crystal structure of the β isomer has not yet been determined but scale models indicate that a twist angle of close to 90° rather than 0° would be more favourable. This is because the seven membered ring formed by the bridging dppp ligand is likely to be more stable in a seven atom chair type conformation rather than a structure which is close to eclipsed. Therefore from the graph of $\delta-\delta^*$ transition energies vs $\cos 2X$, a conformation with a twist angle of 72° would appear to be most favourable. Figure 3.4 shows a plot of $\alpha\text{-Mo}_2\text{Cl}_4(\text{dppp})_2$ decay vs time at 21.6°C and the Arrhenius plot for this isomerisation is shown in figure 3.5.

$\alpha\text{-Mo}_2\text{Cl}_4(\text{dppe})_2$ isomerises to the β form in the solid state ⁸⁷. The conditions for this transformation to occur are that it is performed at a high temperature ($\sim 250^\circ\text{C}$) and under static vacuum. The kinetic parameters for this solid state process were collected as part of this project in order to compare it with the results in solution. Obtaining the data for the solid state reaction was much more difficult than in the case of the solution isomerisation because of the more extreme conditions. The procedure is explained in detail in chapter 2. A plot of β formation at 228°C is shown in figure 3.6 and the Arrhenius plot for this process is given in figure 3.7.

Figure 3.4 Plot of $\ln(A_t^{630} - A^{630})$ vs. time for $\text{Mo}_2\text{Cl}_4(\text{dppp})_2$ following a decay (21.6°C).

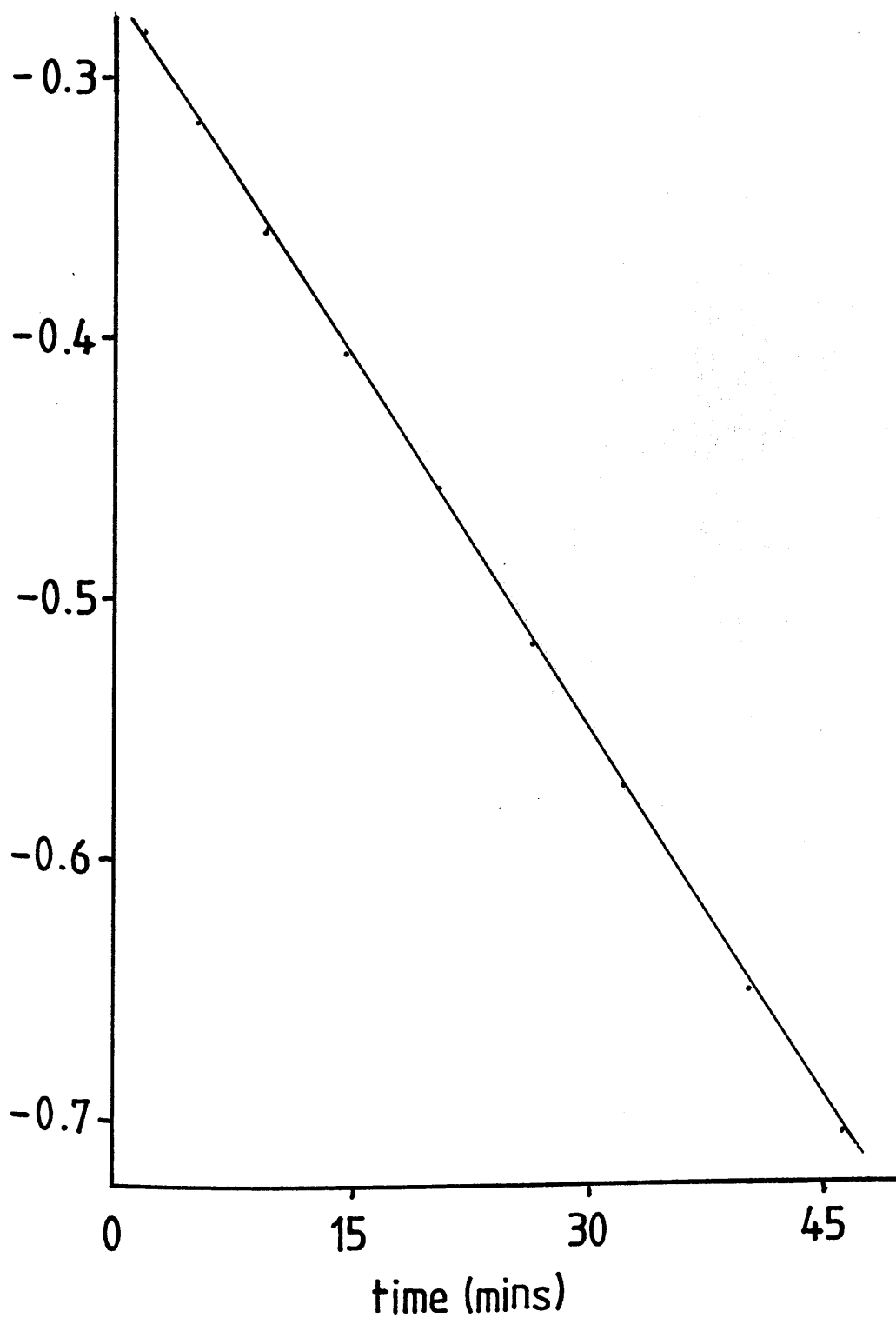


Figure 3.5 Arrhenius plot for isomerisation of $\text{Mo}_2\text{Cl}_4(\text{dppp})_2$ in CH_2Cl_2 .

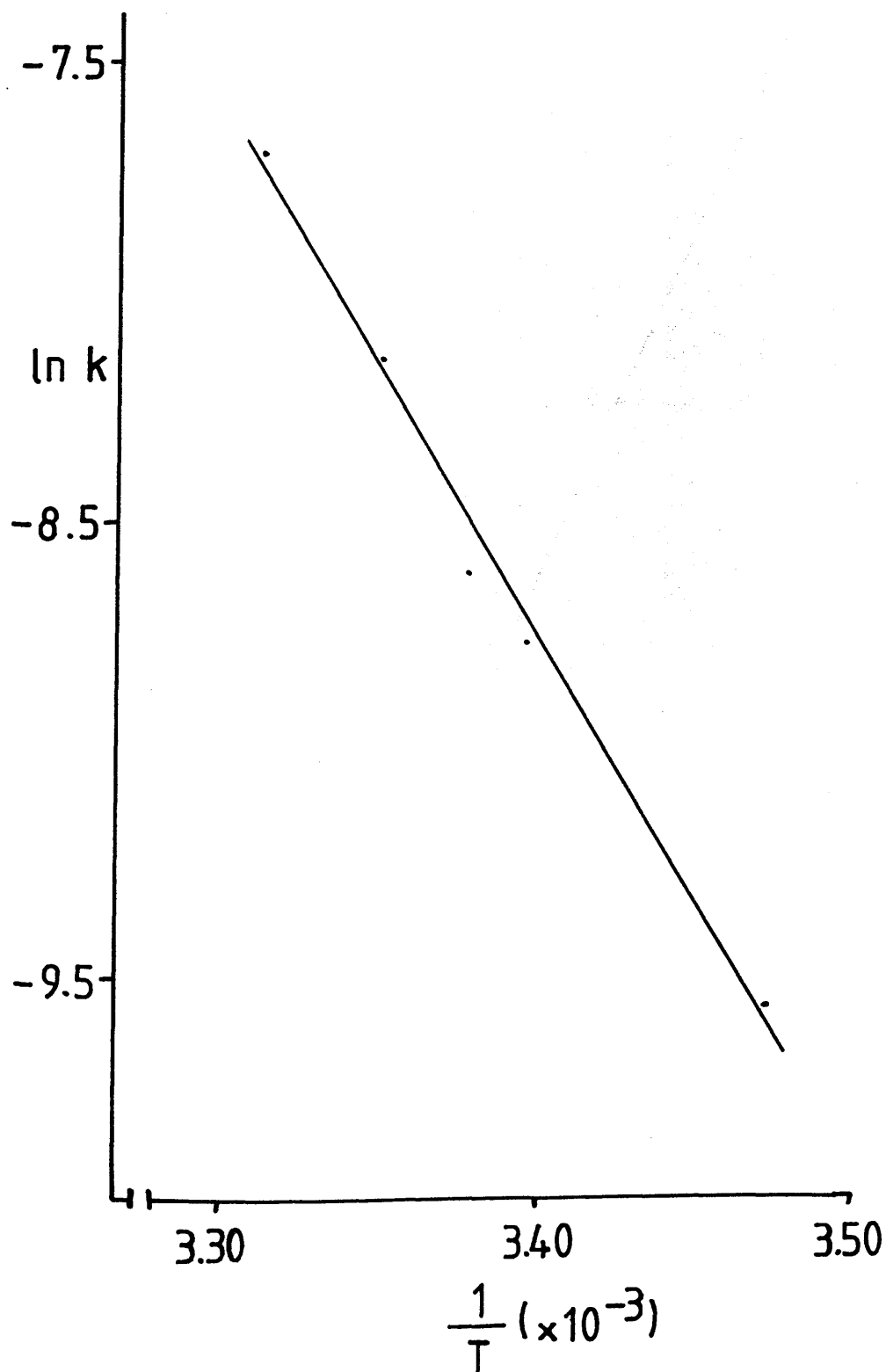


Figure 3.6 Plot of $\ln(c_a/c_a + c_\beta)$ vs. time for $\text{Mo}_2\text{Cl}_4(\text{dppe})_2$ in the solid state (228°C).

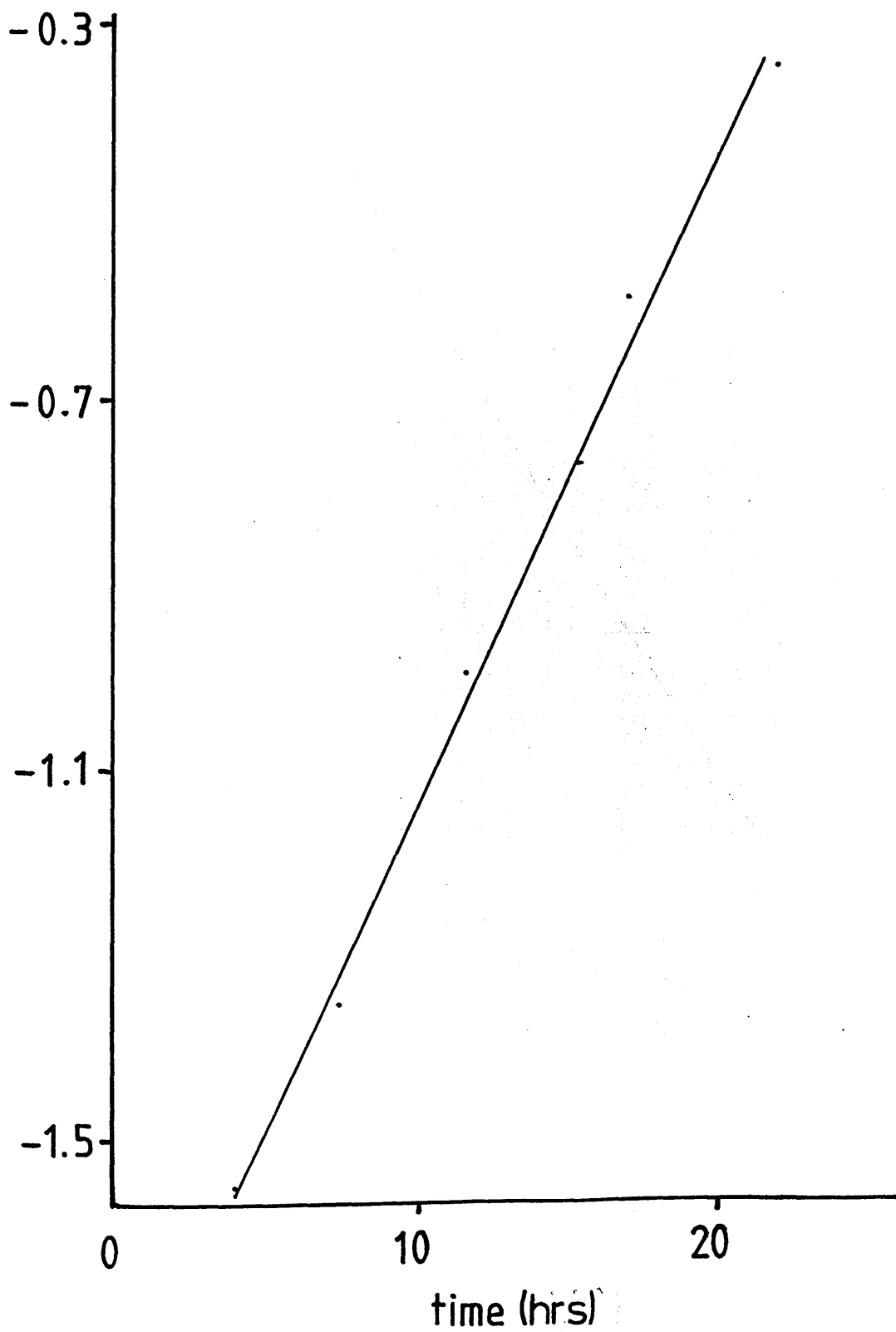
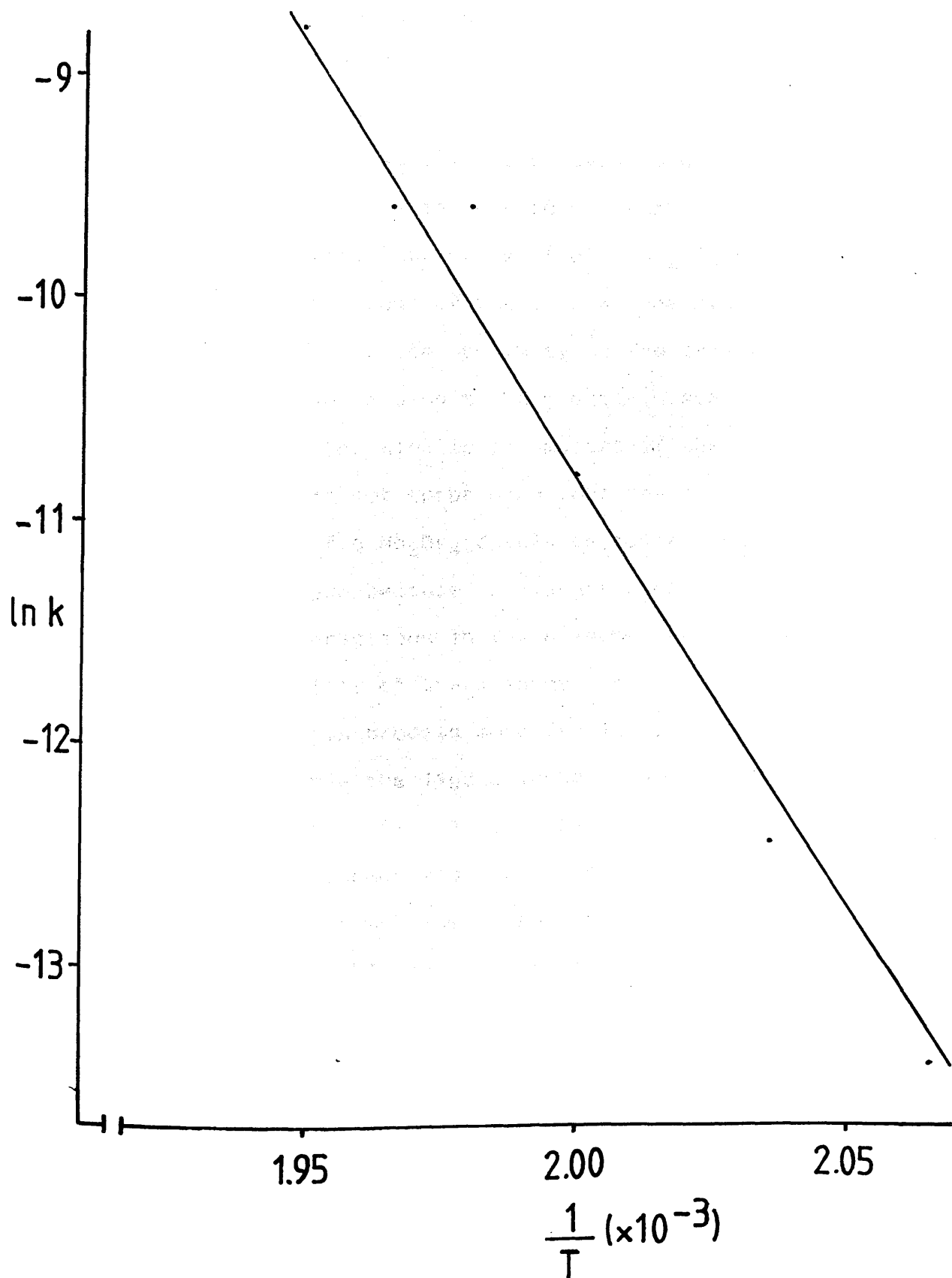


Figure 3.7 Arrhenius plot for isomerisation of Mo₂Cl₄(dppe)₂ in the solid state.



The kinetic data for the α - β isomerisation reactions of all complexes studied to date are summarised in table 3.2. A cursory interpretation of these results is presented here before looking at possible mechanisms. The main driving force for the isomerisation is thought to be the conformational stability of the bridging rings in the β isomers and also possibly the unfavourable steric interactions in the α isomers (chp 1 sect.2.2). Figure 3.8 depicts the crystal structure ⁸⁷ of α - $\text{Mo}_2\text{Cl}_4(\text{dppe})_2$, this shows how the backbone of the ligand lies over the metal-metal bond and in close proximity to the halide atoms. This picture can be used to help explain some of the differences in the kinetic parameters of the different complexes. It is not surprising that the rate of isomerisation of α - $\text{Mo}_2\text{Br}_4(\text{dppe})_2$ is faster than the chloride analogue because the larger bromide means that the steric interactions in the α isomer are increased. Thus the stability of the α isomer is decreased and makes the isomerisation process more facile. In α - $\text{Mo}_2\text{Cl}_4(\text{R-dppp})_2$ the ligand backbone has a methyl substituent, this will markedly decrease the stability of the chelated α isomer and the isomerisation rate for this complex is very fast. The α isomers of $\text{Mo}_2\text{X}_4(\text{R-phenphos})_2$ and $\text{Mo}_2\text{X}_4(\text{S,S-dppb})_2$ have not been isolated, this is almost certainly due to the severe steric congestion in the respective α isomers which makes the isomerisation extremely fast even at very low temperatures.

Table 3.2 Kinetic parameters for $\alpha \rightarrow \beta$ isomerisation of $\text{Mo}_2\text{X}_4(\text{P}^-\text{P})_2$ complexes

	E_a (kJmol ⁻¹)	$t_{1/2}$ (298K)	$\log_{10}A$	ΔS^\ddagger (JK ⁻¹ mol ⁻¹)*	ref
$[\text{Mo}_2\text{Cl}_4(\text{dppe})_2]$ solution	121	19 hrs	16.2	57	100 and this work
$[\text{Mo}_2\text{Cl}_4(\text{dppe})_2]$ solid state	330		29.7	315	this work
$[\text{Mo}_2\text{Cl}_4(\text{dptpe})_2]$	113	24 hrs	14.7	28	100
$[\text{Mo}_2\text{Cl}_4(\text{R-dppp})_2]$	107	8 mins	15.9	51	100
$[\text{Mo}_2\text{Cl}_4(\text{dppp})_2]$	96	39 mins	13.3	1	this work
$[\text{Mo}_2\text{Br}_4(\text{dppe})_2]$	82	43 mins	10.8	-46	100
$[\text{Mo}_2\text{Br}_4(\text{dptpe})_2]$	114	7 hrs	15.4	42	100

* at 298K

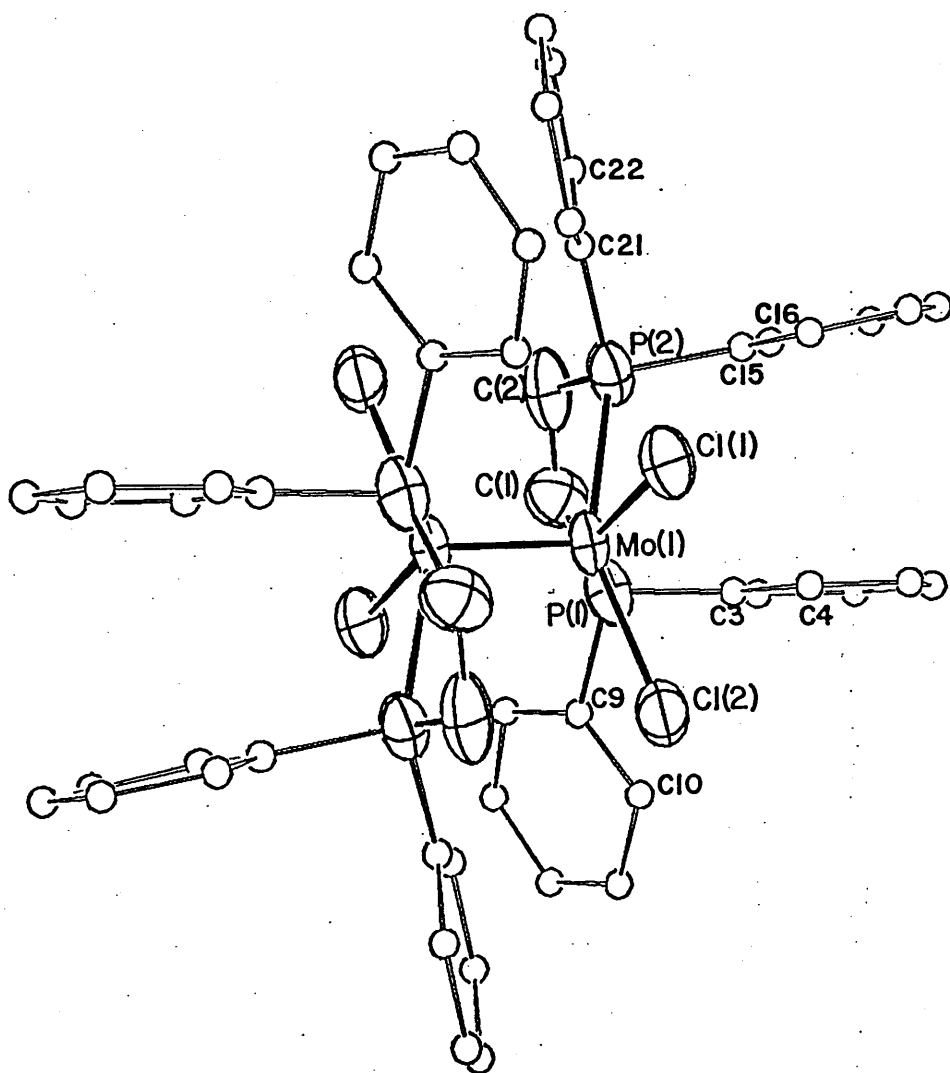


Figure 3.8 Crystal structure of $\alpha\text{-Mo}_2\text{Cl}_4(\text{dppe})_2$.

The isomerisation rate of $\alpha\text{-Mo}_2\text{Cl}_4(\text{dppp})_2$ is perhaps more difficult to explain. The crystal structure of this complex has not been determined. However the structure of the triply bonded species $\alpha\text{-Re}_2\text{Cl}_4(\text{dppp})_2$ ⁹⁹ is known, here the six membered rings formed by chelating diphosphines take up the chair conformation. If it is assumed that the dimolybdenum complex has the same structure as its dirhenium analogue (and this is most likely), then $\alpha\text{-Mo}_2\text{Cl}_4(\text{dppp})_2$ might be expected to be relatively stable as the chair conformation relieves some of the steric congestion even in the α isomer. Therefore the isomerisation rate should be relatively slow. The fact that this is not the case means that some other factor must be responsible for the isomerisation rate.

Interpretation of the kinetic parameters of $\alpha\text{-Mo}_2\text{Cl}_4(\text{dppe})_2$ in the solid state will be undertaken after possible mechanisms are reviewed.

3 Mechanism

Isomerisation reactions involving quadruply bonded dimolybdenum complexes have been relatively few and possible mechanisms have not been widely discussed. Therefore it is perhaps best to look at the possible mechanisms for intramolecular rearrangements of O_h complexes. Figure 3.9 illustrates the four ways¹³⁷ that

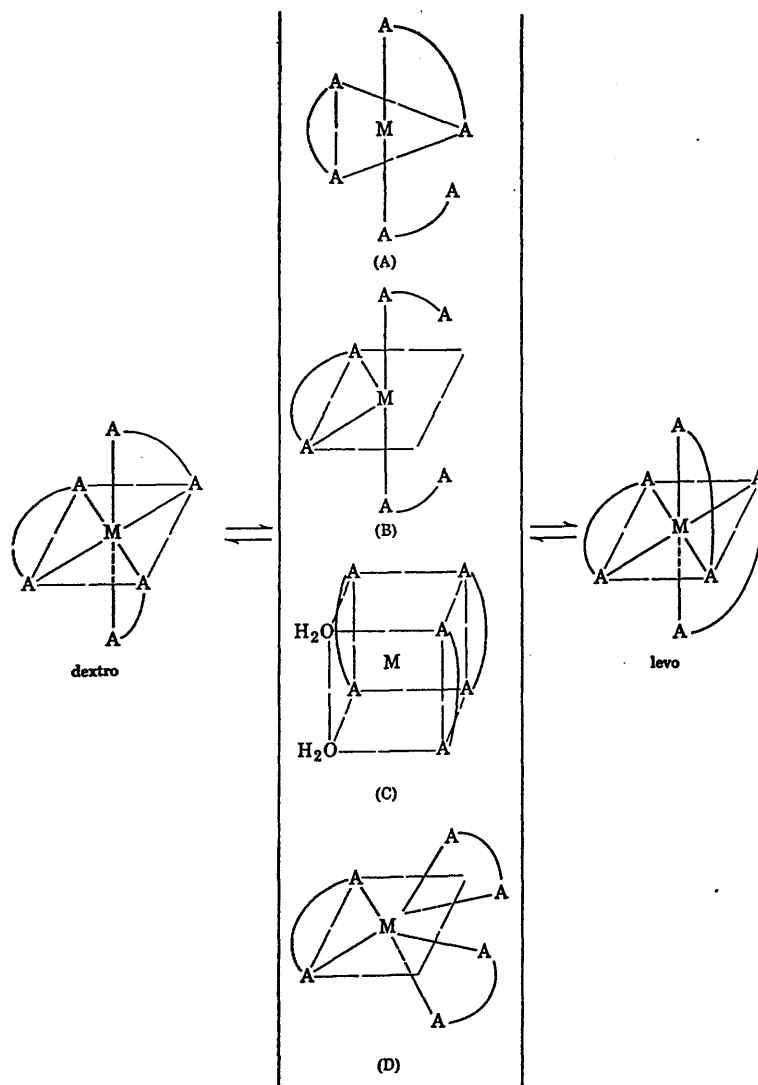


Figure 3.9 Possible rearrangements involved in intramolecular racemisation of octahedral $[M(N\sim N)_3]^{2+}$ complexes.

$M(N\sim N)_3$ can racemise to the opposite configuration. The mechanisms shown in figures 3.9(a) and (b) involve metal-ligand bond rupture, while those in figures 3.9 (c) and (d) proceed by twisting motions of the chelate rings and appear to involve no formal metal-metal bond cleavage. It is difficult to assign which mechanism occurs for a particular rearrangement and few processes have been classified as having only one mechanism.

Two possible mechanisms have been put forward for the α - β isomerisation of $Mo_2X_4(P\sim P)_2$ complexes, these two mechanisms are similar to the two classes of mechanism described above. One involves a Mo-P bond rupture¹⁰⁰ and the other proceeds by an internal flip⁸⁷ of the dimolybdenum unit. The former mechanism was suggested by Fraser et al after the observation of the solution isomerisation of the $Mo_2X_4(P\sim P)_2$ complexes. Agaskar and Cotton proposed the internal flip mechanism on the basis that α - $Mo_2Cl_4(dppe)_2$ isomerises in the solid state and that this mechanism would also operate in the solution phase. Both mechanisms are described in detail below.

The bond dissociation mechanism is illustrated in figure 3.10. The initial step involves a Mo-P bond rupture. This is followed by rotation of the two halves of the molecule about the metal-metal bond. The third step is an S_N2 type attack by the free end of the diphosphine

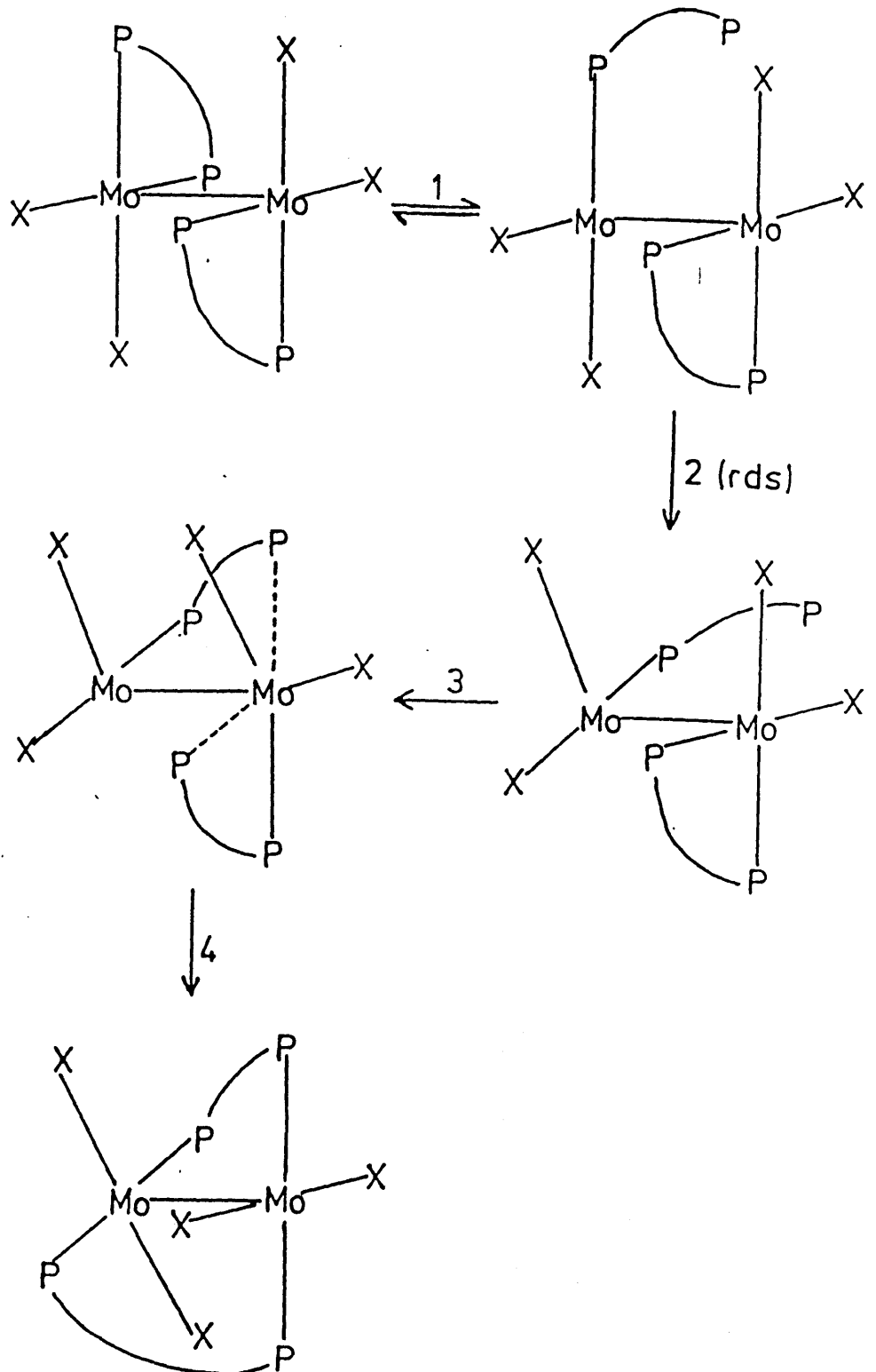


Figure 3.10 Possible mechanism for α - β isomerisation involving Mo-P bond rupture.

ligand between the halide atoms on the opposite molybdenum atom, thus displacing one end of the other diphosphine ligand. The β structure is completed in the final step when the free phosphine end forms a second bridging ring. The final two steps may well be concerted. The rate determining step is probably step (2), as only a rotation about the metal-metal bond will dramatically affect the position and intensity of the δ - δ^* transition and this is what is being monitored when the isomerisation is followed by electronic spectroscopy in solution.

Figure 3.11 illustrates the internal flip mechanism. In the α isomer the eight ligands can be considered as forming the eight corners of a cube as in figure 3.11(a) (this almost occurs in the crystal structure of α - $\text{Mo}_2\text{Cl}_4(\text{dppe})_2$). The two molybdenum atoms each reside at the centre of opposite faces such that each diphosphine ligand chelates to only one molybdenum atom. If the dimetal unit rotates in the plane parallel to the paper as in figure 3.11(b), this involves no blatant metal-ligand bond cleavage, only a gradual elongation of the bonds. Figure 3.11(c) shows when the rotation has completed 90° , this is essentially a β structure with the diphosphine ligands now bridging the dimolybdenum unit. Depending on the nature of the ligand some rearrangement may occur as in figure 3.11(d) and this may well be concerted with the flip.

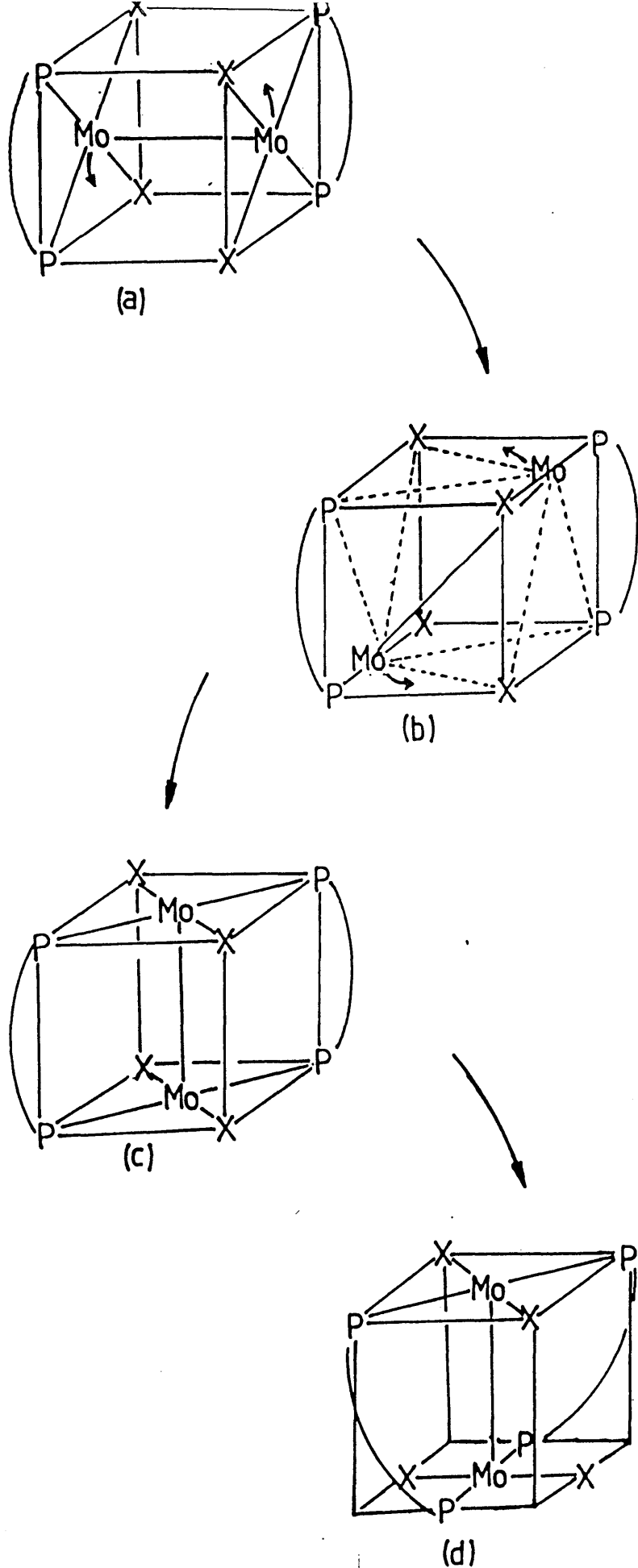


Figure 3.11 Possible mechanism for α - β isomerisation involving an Mo_2 internal flip.

Which mechanism is occurring in which phase? The flip mechanism is the most plausible in the solid state because it is unlikely that the bond rupture mechanism could proceed so cleanly at such high temperatures. These studies have been complemented by extended Hückel calculations on a simple model complex, $\text{Mo}_2\text{Cl}_4(\text{PH}_3)_4$, in order to obtain an estimate of the activation energy for the flip mechanism in the solid state. The activation energy for the flip mechanism is the difference in energy between the ground state and the activated state, i.e. the difference in energy between figures 3.11(a) and (b). The ground state for this model complex is an α -type molecule with each bidentate diphosphine ligand replaced by two monophosphines. The activated state is when the rotation is at 45° , here the ligands may have to splay back to let the metal atoms pass through. This Hückel calculation estimates the activation energy as being approximately 400 kJmol^{-1} . Obviously this is a very crude value as only electronic factors are considered and the calculation does not take into account any steric factors or conformational considerations. However it is of the same order of magnitude as the experimental value (330 kJmol^{-1}), and this can be considered a good piece of evidence for favouring the flip mechanism in the solid phase.

Rotating metal fragments within ligand cages also occur in metal cluster complexes. One such example is $\text{Fe}_3(\text{CO})_{12}$,

here the Fe_3 unit was first postulated ¹³¹ then proven ¹³² to rotate within the fixed ligand cage in the solid phase by solid state nmr. The structure of $\text{Fe}_3(\text{CO})_{12}$ in the solid ¹³³ has been determined and is shown in figure 3.12. The molecule is disordered consisting of a close to icosahedral arrangement of carbon monoxide ligands with two possible orientations of the iron triangle related by an inversion centre, this is schematically represented in figure 3.13. The solid state nmr ¹³² is consistent with a fluxional process involving a rotation of the iron triangle between these two orientations as in figure 3.13. There are six signals in the solid state ¹³C nmr in the ratio 2:2:2:2:2:2. This fits the scheme in figure 3.13 where the equivalent pairs are 1 and 5, 2 and 6, 3 and 8, 4 and 7, 9 and 12 and 10 and 11. This process may also occur in solution but it is not the only mechanism as all twelve carbon monoxide ligands are equivalent in the solution nmr ¹³⁴, there may be several viable mechanisms in this phase.

Thus the evidence appears to favour the internal flip mechanism for the solid state isomerisation of $\alpha\text{-Mo}_2\text{Cl}_4(\text{dppe})_2$. However the mechanism for the solution isomerisation of $\alpha\text{-Mo}_2\text{X}_4(\text{P}^{\sim}\text{P})_2$ complexes is not so clear cut. Relevant experiments ¹⁰⁰ that have been carried out in order to help determine which mechanism is occurring in solution are discussed here. When a large excess of halide

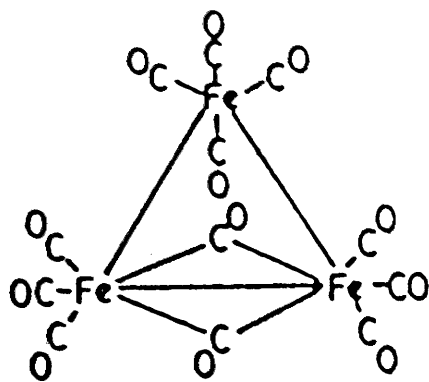


Figure 3.12 Structure of $\text{Fe}_3(\text{CO})_{12}$ in the solid state.

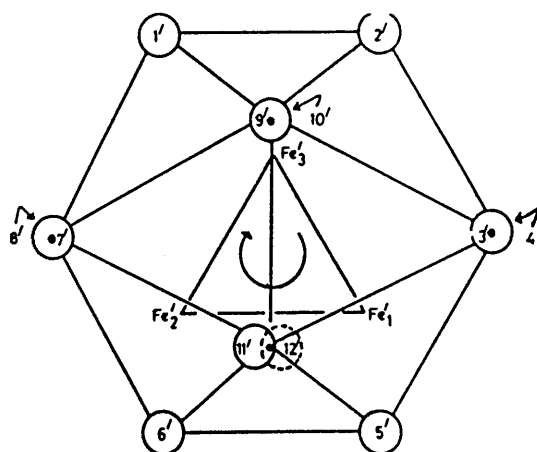
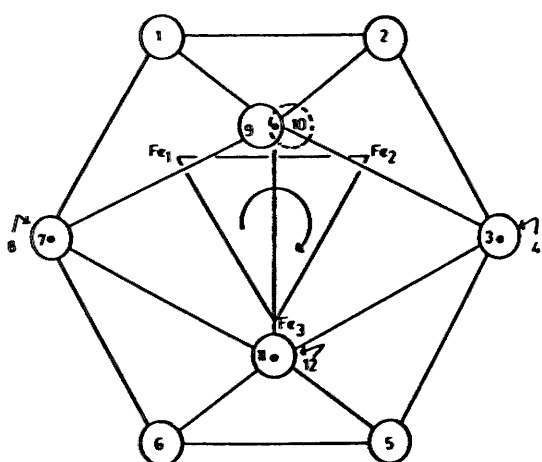
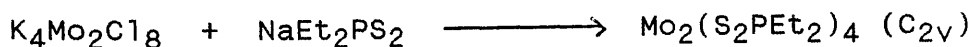


Figure 3.13 Two observed orientations of Fe_3 in $\text{Fe}_3(\text{CO})_{12}$.

(e.g. Ph_4PX) is added to a solution of an α isomer, then the rate of isomerisation is unaffected. This rules out any mechanism that involves halide dissociation during isomerisation. Also when an excess of diphosphine ligand is added to a solution of an α isomer, again the rate is unaffected. This rules out any mechanism involving complete dissociation of the diphosphine ligand during isomerisation as the rate would be retarded if this was the case. However excess diphosphine should not affect the rate if the mechanism involves only one end of the diphosphine being dissociated. This last piece of information favours neither mechanism as the flip mechanism would also not be affected by any excess diphosphine ligand. When PBU^n_3 is added to a solution of an α isomer then $\text{Mo}_2\text{X}_4(\text{PBU}^n_3)_4$ is formed in preference to the β isomer, this means that the α isomer is substitutionally labile. A solution of the β isomer is unaffected by any PBU^n_3 . Thus the Mo-P bond must be easily cleaved in the α isomer for this substitution to take place. This makes the bond rupture mechanism a very feasible process. Also this probably rules out the Mo-P bond rupture as being the rate determining step in the bond cleavage mechanism (see above). Other isomerisation reactions of quadruply bonded dimolybdenum complexes in solution may provide some clues in favour of one of the mechanisms.

In the Introduction it was stated that $\text{Mo}_2\text{Cl}_2(\text{O}_2\text{CCMe}_3)_2(\text{PEt}_3)_2$ ⁶⁴ existed in two isomeric forms (see figure 1.9). It was reported that these isomers interconverted in solution although no rates or mechanisms were given. An internal flip can be ruled out as this will not interconvert the isomers. Green et al⁶⁵ also isolated isomers of this type and reported slow isomerisation in solution as observed by nmr. A mechanism involving a minimum of at least two bond cleavages is required to interconvert the isomers, although which two bonds would be broken is not known.

Another complex for which two geometric isomers have been synthesised is $\text{Mo}_2(\text{S}_2\text{PEt}_2)_4$ ¹³⁵, these are depicted in figure 3.14. The C_{2v} isomer has two bridging and two chelating ligands while the D_{4h} form has all four ligands bridging. Synthesis of the C_{2v} isomer is given below



The D_{4h} form was made by dissolving the C_{2v} isomer in tetrahydrofuran and cooling the saturated solution to -5°C , where crystals of the D_{4h} isomer are formed. The formula for the D_{4h} isomer is actually $\text{Mo}_2(\text{S}_2\text{PEt}_2)_4 \cdot \text{THF}$ where there is a very long Mo-O axial bond (3.107 Å). In tetrahydrofuran solution at room temperature, there is an equilibrium of the two isomers. This is monitored by ^{31}P

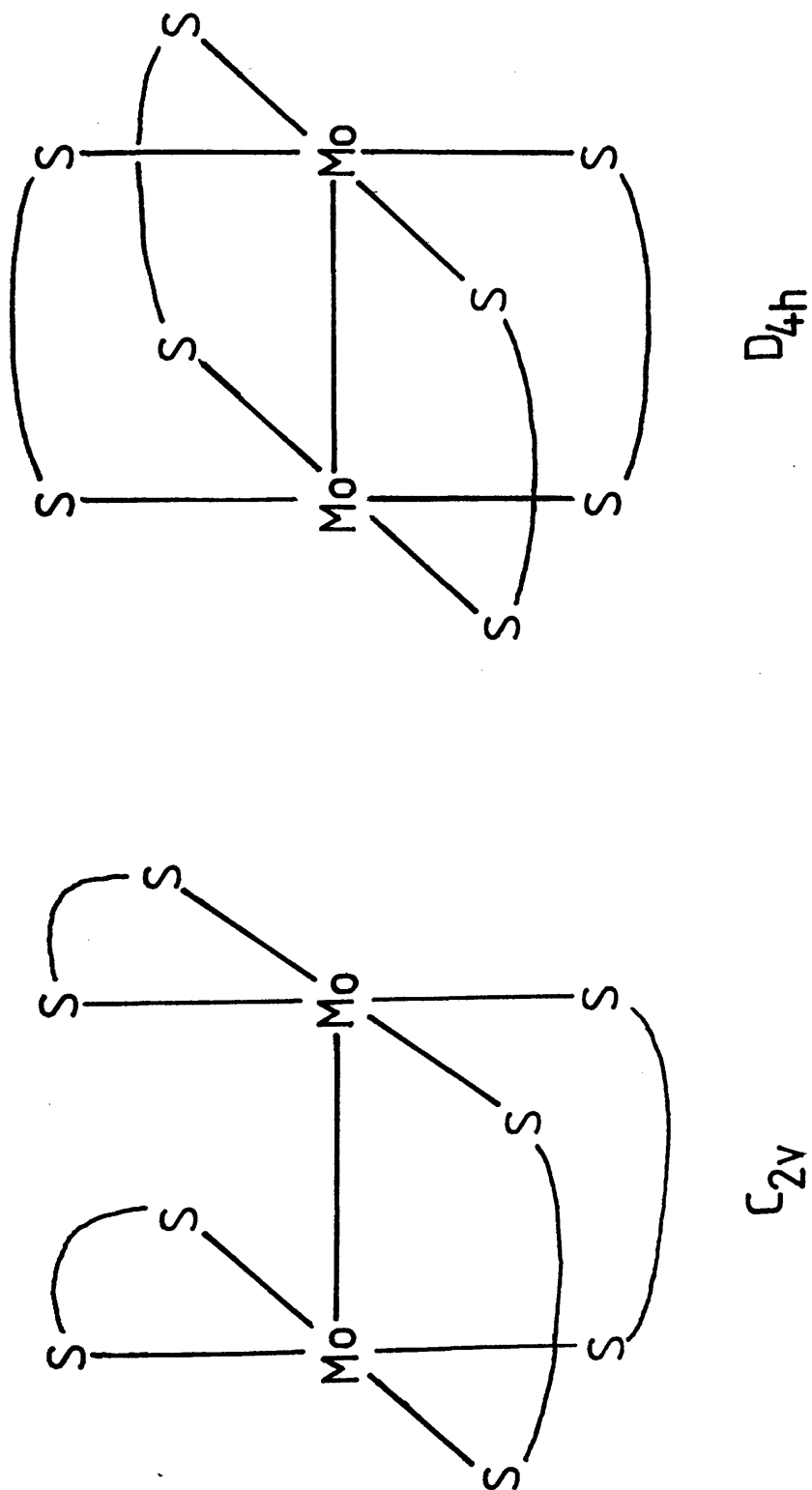


Figure 3.14 Two geometric isomers observed for $\text{Mo}_2(\text{S}_2\text{PEt}_2)_4^-$.

nmr. No mechanism was put forward for the interconversion of the isomers. An internal flip would not result in the desired isomerisation, this is depicted in figure 3.15. This illustrates a schematic diagram for the C_{2v} isomer (figure 3.15(a)), a 90° rotation in the plane parallel to that of the paper converts it to figure 3.15(b) which is another C_{2v} isomer where the ligands that were chelating in (a) are now bridging and vice versa. A different 90° rotation converts (a) to (c) in figure 3.15, (c) is a new isomer where all four ligands are now chelating. However the ^{31}P nmr suggests no presence of a third isomer. A bond rupture mechanism could proceed very easily by dissociation of one end of a chelating ligand in the C_{2v} isomer. This free end of the ligand could then make an $S_{\text{N}}2$ attack at the opposite molybdenum displacing one end of the other chelating ligand, which would then bond to the other molybdenum thereby completing the tetrabridged structure. The reverse process could easily be applied. This mechanism is almost identical to that proposed by Fraser et al for the solution isomerisation of $\alpha\text{-Mo}_2\text{Cl}_4(\text{dppe})_2$.

An interesting recent discovery has been the reverse isomerisation reaction, $\beta \rightarrow \alpha$, in certain complexes. One such compound which displays this phenomenon is $\text{Mo}_2\text{Cl}_4(\text{S-chairphos})_2$ ¹⁰¹. The α isomer of this complex is stable in solvents such as dichloromethane, acetonitrile

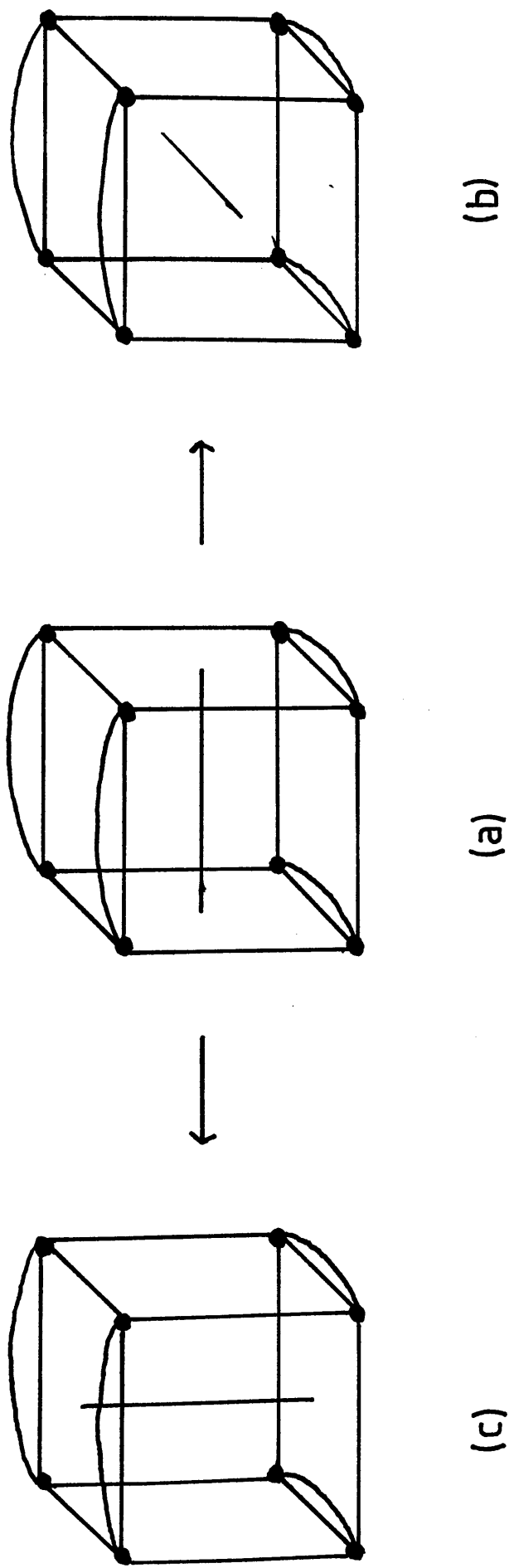


Figure 3.15 Internal flip mechanism for $\text{Mo}_2(\text{S}_2\text{PEt}_2)_4$.

and methanol. However when it is dissolved in benzene or toluene, the β isomer is formed (it is definitely a staggered β isomer as it displays optical activity under the δ - δ^* transition). When the β isomer is redissolved in the above non-aromatic solvents, the α isomer is formed. Both of these isomers are air sensitive. The energy difference between the two isomers must be fairly small for this interconvertability to occur.

This reverse isomerisation is also displayed in $\text{Mo}_2\text{Cl}_4(\text{dtpd})_2$ ¹³⁶. The dtpd ligand is very similar in structure to dppe. One major difference between the α and β isomers of $\text{Mo}_2\text{Cl}_4(\text{dtpd})_2$ and those of $\text{Mo}_2\text{Cl}_4(\text{dppe})_2$ is that the isomers of the former complex are much more soluble. α - $\text{Mo}_2\text{Cl}_4(\text{dtpd})_2$ isomerises to the β form when dissolved in dichloromethane, however when a solution of the pure β isomer in the same solvent is mixed carefully with methanol then crystallisation of the less soluble α isomer occurs. Thus both isomers can interconvert with ease. The energy difference between the two isomers must be fairly small and interconversion can take place if the right conditions are chosen.

4 Conclusions

The mechanism for the solid state isomerisation of $\alpha\text{-Mo}_2\text{Cl}_4(\text{dppe})_2$ appears to be the Mo_2 flip. The precedent of rotating metal fragments in the solid state by metal clusters and the Hückel calculation on $\text{Mo}_2\text{Cl}_4(\text{PH}_3)_4$ seem sufficient evidence. In solution the facts tend to favour the bond breaking mechanism, as all the examples of the isomerisation in solution of other dimolybdenum complexes appear to have the bond cleavage mechanism as the only realistic pathway to isomerisation.

The kinetic parameters for the solid state and solution isomerisation of $\alpha\text{-Mo}_2\text{Cl}_4(\text{dppe})_2$ are drastically different. The activation energy is much larger in the solid state as much higher temperatures are required to achieve the same rate in this phase compared to the solution. The entropy of activation is more difficult to define, a large positive value means that the transition state is more disordered and has more degrees of freedom to rotate. Thus in the solid state reaction, perhaps the Mo_2 unit is whizzing about rapidly. The fact the difference in the entropy of activation is very large in the different phases is perhaps indicative that there are separate mechanisms occurring in each phase

The energy difference between respective α and β isomers must be fairly small and most can probably interconvert, although this has only been observed in a few cases. However there will be isomers where interconversion is virtually impossible because of severe steric crowding in the α isomer, e.g. $\alpha\text{-Mo}_2\text{Cl}_4(\text{S,S-dppb})_2$.

1 General Overview

This chapter deals with partial or total ligand substitution of various quadruply bonded dimolybdenum complexes and the novel points raised by these reactions. It is important to note here that some of the complexes made below are air sensitive and appear to analyse very poorly, including one characterised by X-ray crystallography ⁷¹. Cotton et al ⁷¹ have worked on similar classes of complexes and have also experienced this problem. Therefore the analysis of these complexes can be regarded with some scepticism. Characterisation of these species has been based mainly on the spectral data collected.

2 Structure of [Mo₂(O₂CCH₃)₂(CH₃CN)₆][BF₄]₂ and its reaction with dppm

The complex [Mo₂(O₂CCH₃)₂(CH₃CN)₆][BF₄]₂ has recently been synthesised and structurally characterised by X-ray crystallography by two independent groups of workers ^{71,72}. The structure of the [Mo₂(O₂CCH₃)₂(CH₃CN)₆]²⁺ cation is shown in figure 4.1. The two acetate groups are in a cis arrangement and two of the six acetonitrile molecules are attached axially to the metal-metal bond. Interestingly, the solution ¹H nmr ⁷² of this complex displays only one signal for the methyl protons of the acetonitrile molecules, indicating that all six

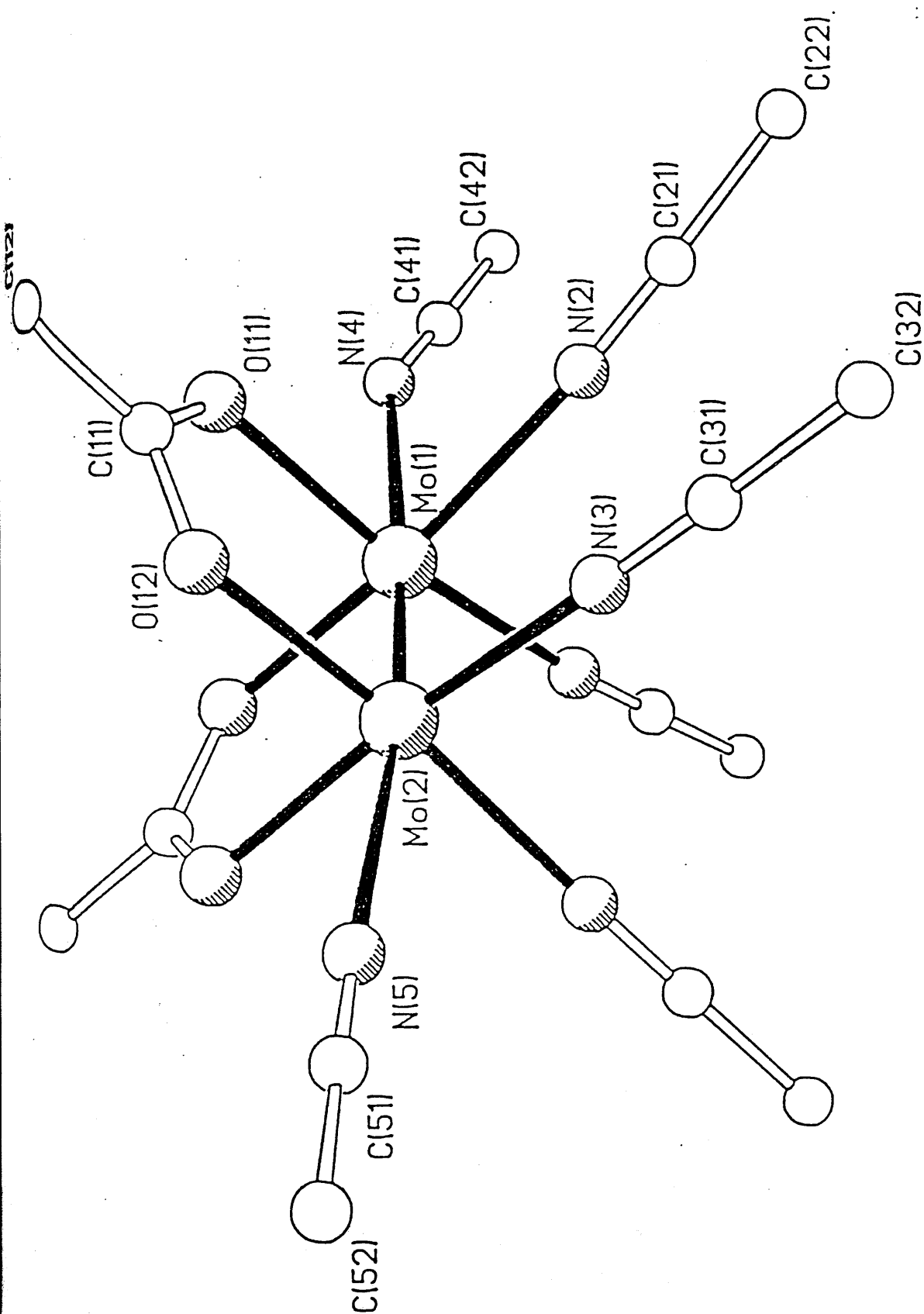


Figure 4.1 Crystal structure of the $[\text{Mo}_2(\text{O}_2\text{CCH}_3)_2(\text{CH}_3\text{CN})_6]^{2+}$ cation.

acetonitriles are equivalent in solution. This implies that the acetonitriles in this complex are labile and may be susceptible to substitution by various ligands. This complex was made analytically pure by Pimblett ⁷², but Cotton et al ⁷¹ could not obtain good reproducible analytical results despite solving the crystal structure.

Pimblett ¹³⁷ reacted $[\text{Mo}_2(\text{O}_2\text{CCH}_3)_2(\text{CH}_3\text{CN})_6][\text{BF}_4]_2$ with dppm to give an air sensitive purple product which was characterised from spectra and analysis as $[\text{Mo}_2(\text{O}_2\text{CCH}_3)_2(\text{dppm})(\text{CH}_3\text{CN})_2][\text{BF}_4]_2$. The structure of this complex was thought to contain cis acetate groups, with the dppm ligand bridging across the metal-metal bond. This complex was not structurally characterised and will be discussed later.

3 Reaction of $[\text{Mo}_2(\text{O}_2\text{CCH}_3)_2(\text{CH}_3\text{CN})_6][\text{BF}_4]_2$ with dmpe

In this project $[\text{Mo}_2(\text{O}_2\text{CCH}_3)_2(\text{CH}_3\text{CN})_6][\text{BF}_4]_2$ was reacted with the less sterically bulky ligand, dmpe, to see if any further substitution could take place. In fact the product from this reaction is an air stable orange solid. The infrared spectrum, figure 4.2, indicates the presence of acetate and diphosphine ligands. However there is no indication of the presence of acetonitrile. Analysis suggests the complex has the formula

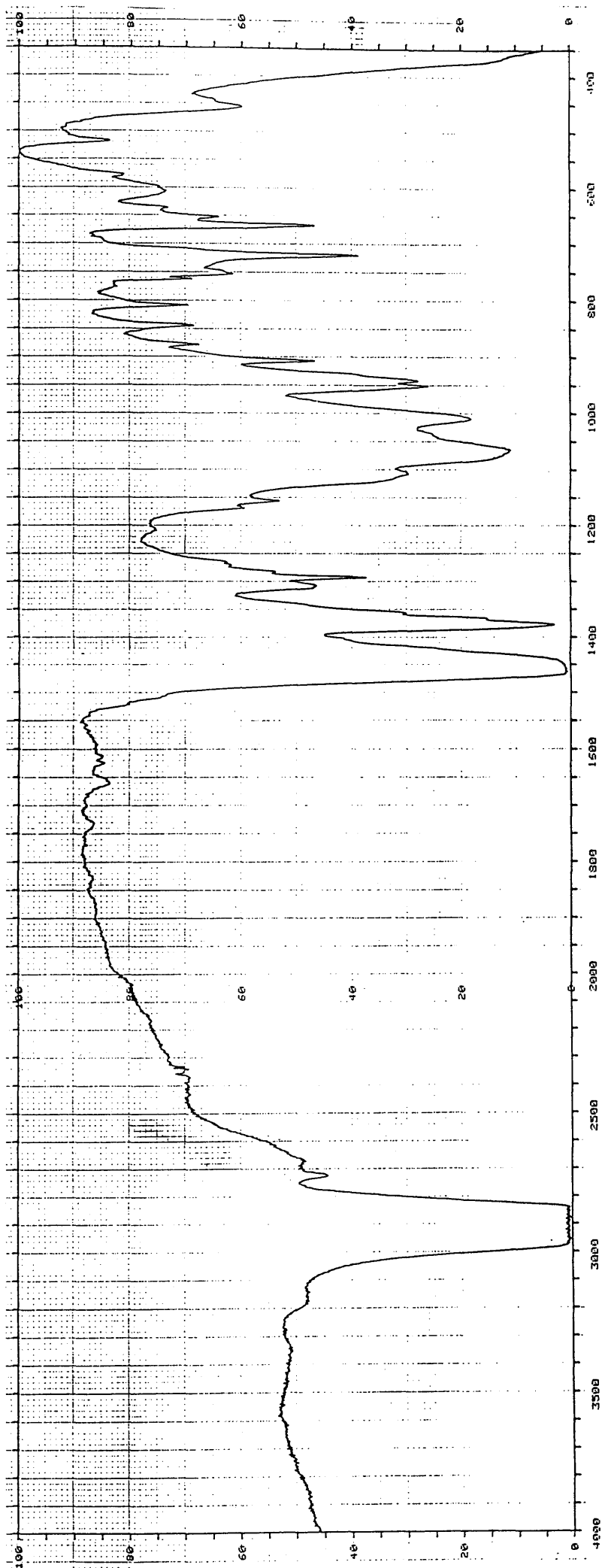


Figure 4.2 ir spectrum of $[\text{Mo}_2(\text{O}_2\text{CCH}_3)_2(\text{dmpe})_2][\text{BF}_4]_2$.

$[\text{Mo}_2(\text{O}_2\text{CCH}_3)_2(\text{dmpe})_2][\text{BF}_4]_2$, although the carbon analysis is somewhat high. There are three possibilities for the structure of the $[\text{Mo}_2(\text{O}_2\text{CCH}_3)_2(\text{dmpe})_2]^{2+}$ cation, these are depicted in figure 4.3. In figure 4.3(a), the acetate groups are trans to each other and the dmpe ligands are bridging the quadruple bond. There is a cis arrangement of acetates in figure 4.3(b), again the dmpe ligands are bridging the metal-metal bond. In figure 4.3(c), the dmpe ligands each chelate to a different molybdenum atom while the acetate groups are cis to each other. A discussion of the spectra of the cation will help to elucidate the structure.

The ^1H nmr of $[\text{Mo}_2(\text{O}_2\text{CCH}_3)_2(\text{dmpe})_2][\text{BF}_4]_2$ was recorded in dichloromethane and is shown in figure 4.4. The singlet at 2.84 p.p.m can be ascribed to the six acetate methyl protons and is comparable with the signal at 2.82 p.p.m in $[\text{Mo}_2(\text{O}_2\text{CCH}_3)_2(\text{CH}_3\text{CN})_6][\text{BF}_4]_2$. The signals due to the protons in the dmpe ligand may be assigned as follows; the protons in the carbon backbone of the ligand give rise to the broad resonance at 2.0 p.p.m; while the quintet at 1.34 p.p.m arises from the P-Me protons. These P-Me protons display an $A_3A'_3BB'$ coupling which implies strongly coupled phosphorus atoms. The coupling constant ($^2J_{\text{pp}}$) is generally ten times larger for trans than for cis phosphorus atoms ¹³⁸; this favours the structure depicted in figure 4.3(a). The $^{31}\text{P}\{-^1\text{H}\}$ nmr of this complex displays a singlet at 4.81 p.p.m. Table 4.1 shows

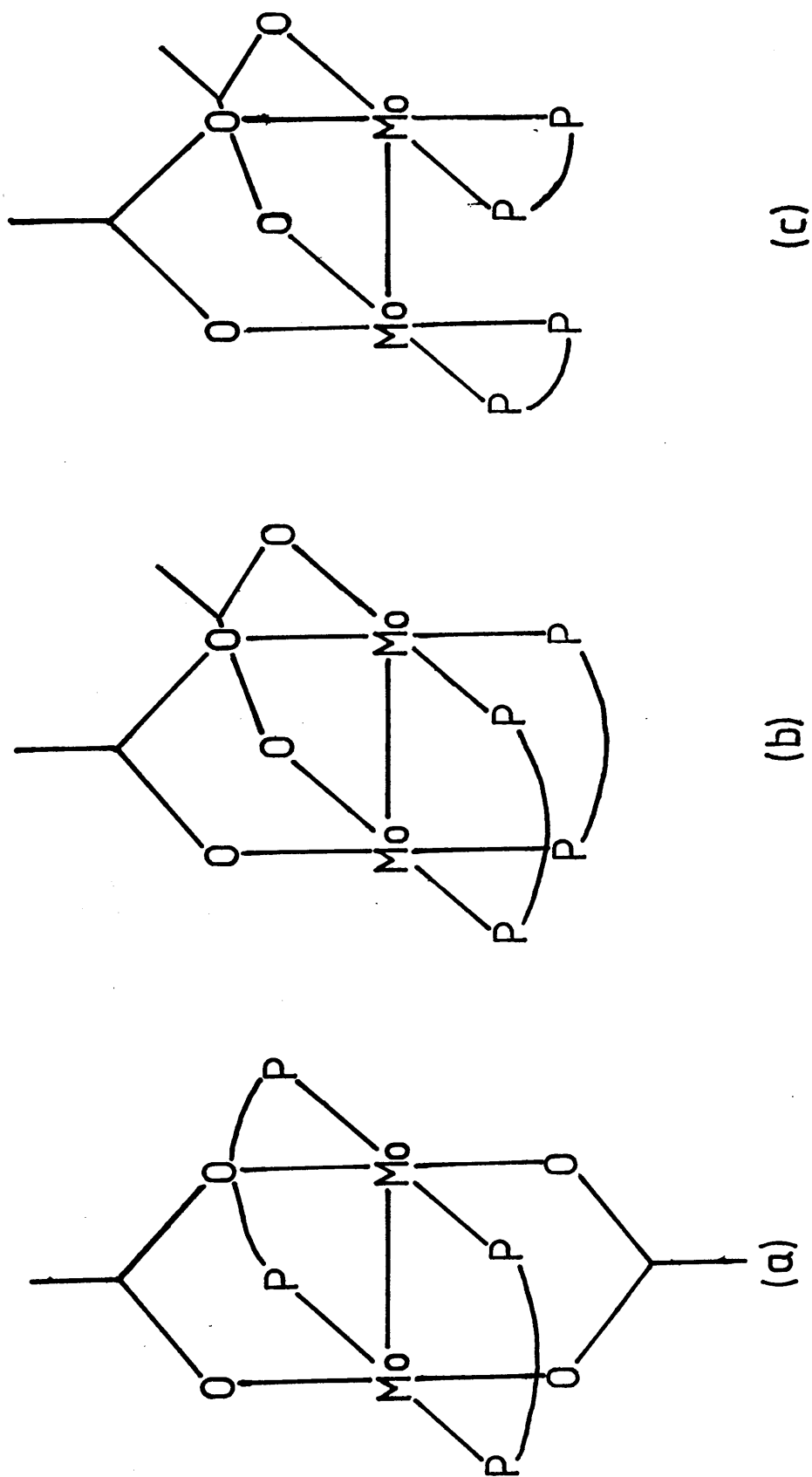


Figure 4.3 Possible structures of the $[\text{Mo}_2(\text{O}_2\text{CCH}_3)_2(\text{dmpe})_2]^{2+}$ cation.

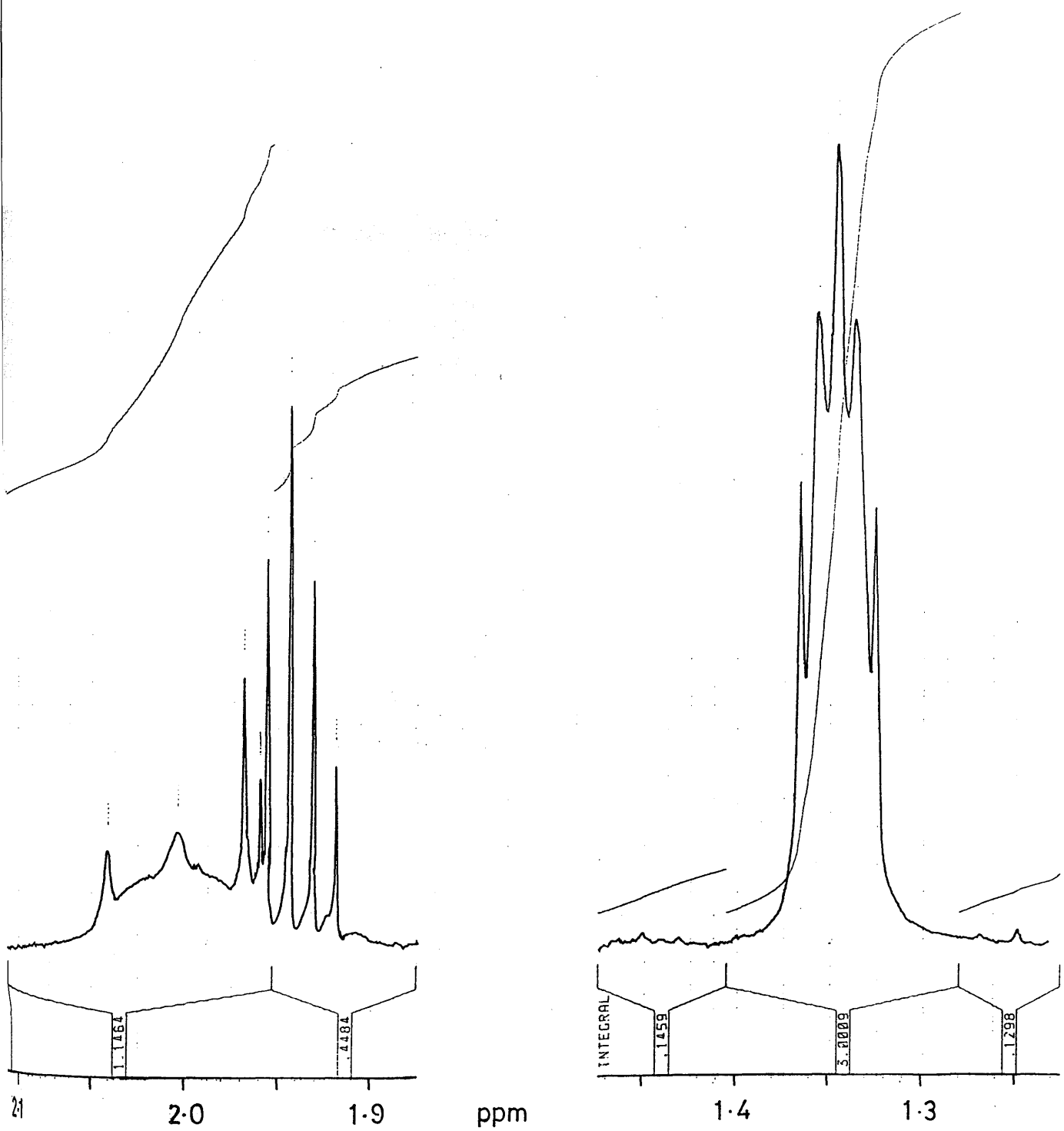


Figure 4.4 nmr spectrum of $[\text{Mo}_2(\text{O}_2\text{CCH}_3)_2(\text{dmpe})_2][\text{BF}_4]_2$.

Table 4.1 Chemical Shifts in the ^{31}P nmr of Some Multiply Bonded Dimetal Complexes Containing Diphosphine Ligands (Values vs 85% H_3PO_4)

<u>Complex</u>	<u>δ</u>	<u>Ref.</u>
$\beta\text{-Mo}_2\text{Cl}_4(\text{dppm})_2$	+ 16.14	139
$\beta\text{-Mo}_2\text{Br}_4(\text{dppm})_2$	+ 14.85	139
$\beta\text{-Mo}_2\text{I}_4(\text{dppm})_2$	+ 12.43	139
$\beta\text{-Mo}_2\text{Cl}_4(\text{dmpm})_2$	- 0.77	85
$\beta\text{-Mo}_2\text{I}_4(\text{dppe})_2$	+ 14.9	90
$[\text{Mo}_2(\text{O}_2\text{CCH}_3)_2(\text{dmpe})_2]^{2+}$	+ 4.81	this work
$\beta\text{-Re}_2\text{Cl}_4(\text{dppm})(\text{dppe})$	+3.0, -5.7	140
$\alpha\text{-Re}_2\text{Cl}_4(\text{dppee})_2$	+ 29.6	104
$\beta\text{-Re}_2\text{Cl}_4(\text{dppee})_2$	+ 5.6	104

that this value is similar to those of complexes with two trans diphosphine ligands. Thus the spectroscopy of $[\text{Mo}_2(\text{O}_2\text{CCH}_3)_2(\text{dmpe})_2][\text{BF}_4]_2$ suggests a structure containing trans diphosphine and trans acetate ligands. This was confirmed by X-ray crystallography.

4 Crystal Structure of $[\text{Mo}_2(\text{O}_2\text{CCH}_3)_2(\text{dmpe})_2][\text{BF}_4]_2$

The $[\text{Mo}_2(\text{O}_2\text{CCH}_3)_2(\text{dmpe})_2][\text{BF}_4]_2$ complex was recrystallised from acetonitrile and grew as translucent orange prisms. The details of the collection of the results are described in the experimental section. The

molecule actually crystallises as $[\text{Mo}_2(\text{O}_2\text{CCH}_3)_2(\text{dmpe})_2][\text{BF}_4]_2 \cdot \text{CH}_3\text{CN}$. There are two independent molecules, **1a** and **1b**, in the unit cell and these are shown in figures 4.5(a) and (b) respectively. A view down the metal-metal bond of molecule **1a** is depicted in figure 4.6. The two cations, **1a** and **1b**, are virtually identical having trans acetate and trans dmpe ligands. Both molecules have a twist angle of 0° , this is a direct effect of the acetate groups which tend to produce eclipsed structures. A list of the main bond lengths and bond angles of the two molecules is shown in table 4.2. The Mo-Mo bond lengths are very similar for both complexes, 2.099(1) Å for **1a** and 2.096(1) Å for **1b**. These bond lengths are similar to other quadruply bonded dimolybdenum complexes with two trans carboxylate ligands (see table 1.2).

The most significant difference between **1a** and **1b** is the C-C bond length in the dmpe ligand backbone. In **1a** this bond length is normal (1.46 Å) whereas in **1b** it is very short (1.20 Å) and the anisotropic thermal parameters for C(7) and C(8) are very large. This phenomenon occurs commonly in dmpe complexes^{23,141} and is most likely due to a ring flipping process between the λ and δ configurations of the six membered rings (see chp 5 sect.6 for notation on bridging rings), or a static conformational disorder.

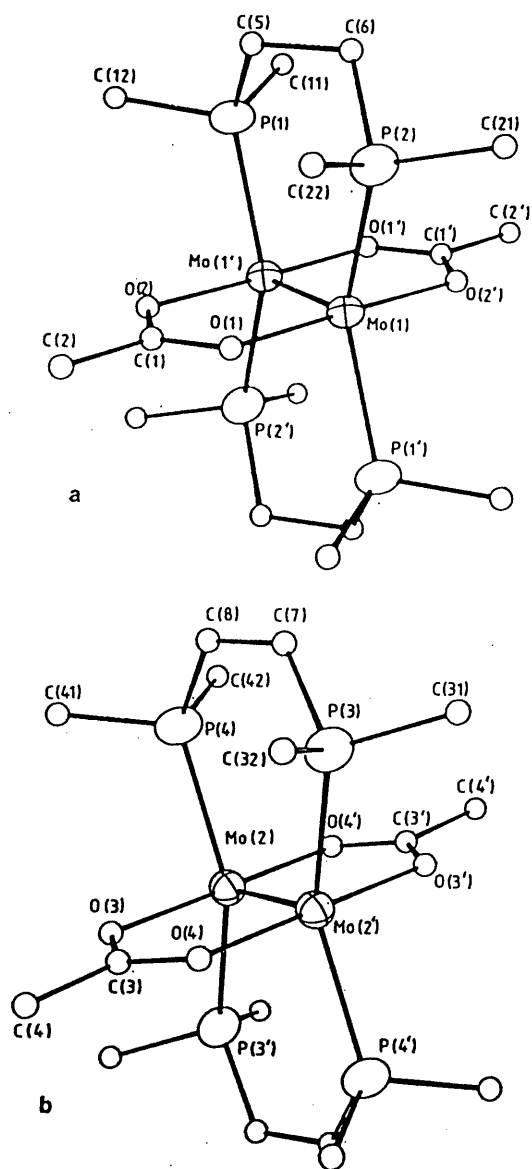


Figure 4.5 Crystal structure of the $[\text{Mo}_2(\text{O}_2\text{CCH}_3)_2(\text{dmpe})_2]^{2+}$ cation.

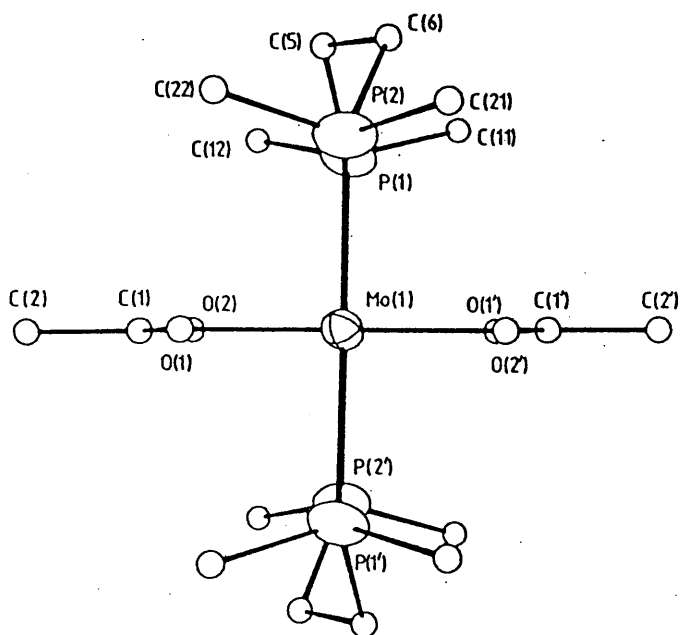


Figure 4.6 View down the Mo-Mo bond of molecule 1a.

Table 4.2 Selected Bond Lengths (Å) and Angles (°) for the
Complex [Mo₂(O₂CCH₃)₂(dmpe)₂][BF₄]₂.CH₃CN

Bond Lengths

Molecule 1a		Molecule 1b	
Mo(1)-Mo(1')	2.099(1)	Mo(2)-Mo(2')	2.096(1)
Mo(1)-P(1')	2.542(3)	Mo(2)-P(3')	2.549(3)
Mo(1)-P(2)	2.552(3)	Mo(2)-P(4)	2.544(3)
Mo(1)-O(1)	2.106(6)	Mo(2)-O(3)	2.124(6)
Mo(1)-O(2')	2.100(6)	Mo(2)-O(4')	2.116(6)
C(1)-O(1)	1.28(1)	C(3)-O(3)	1.27(1)
C(1)-O(2)	1.28(1)	C(3)-O(4)	1.26(1)
C(1)-C(2)	1.48(1)	C(3)-C(4)	1.49(1)
P(1)-C(5)	1.83(1)	P(3)-C(7)	1.75(1)
P(1)-C(11)	1.80(1)	P(3)-C(31)	1.81(1)
P(1)-C(12)	1.82(1)	P(3)-C(32)	1.79(1)
P(2)-C(6)	1.84(1)	P(4)-C(8)	1.79(1)
P(2)-C(21)	1.81(1)	P(4)-C(41)	1.80(1)
P(2)-C(22)	1.80(1)	P(4)-C(42)	1.80(1)
C(5)-C(6)	1.46(1)	C(7)-C(8)	1.20(1)

Table 4.2 continuedBond Angles

Molecule 1a		Molecule 1b	
Mo(1)-Mo(1')-P(1)	106.3(1)	Mo(2)-Mo(2')-P(3)	107.5(1)
Mo(1')-Mo(1)-P(2)	107.5(1)	Mo(2')-Mo(2)-P(4)	106.7(1)
Mo(1)-Mo(1')-O(2)	91.9(2)	Mo(2)-Mo(2')-O(4)	91.9(2)
Mo(1')-Mo(1)-O(1)	91.9(2)	Mo(2')-Mo(2)-O(3)	91.1(2)
Mo(1)-O(1)-C(1)	117.3(6)	Mo(2)-O(3)-C(3)	117.9(6)
Mo(1')-O(2)-C(1)	117.5(6)	Mo(2')-O(4)-C(3)	117.8(6)
O(1)-C(1)-O(2)	121.5(8)	O(3)-C(3)-O(4)	121.8(8)
O(1)-C(1)-C(2)	119.9(9)	O(3)-C(3)-C(4)	118.8(9)
O(2)-C(1)-C(2)	118.6(9)	O(4)-C(3)-C(4)	120.1(8)

These two fused rings have opposite configurations and therefore the complex has no overall chirality.

A major difference between $[\text{Mo}_2(\text{O}_2\text{CCH}_3)_2(\text{dmpe})_2]^{2+}$ and other dmpe complexes is the Mo-Mo-P bond angle which is 106.9° in the cationic species. This value is significantly larger than in $\beta\text{-Mo}_2\text{Cl}_4(\text{dmpe})_2$ (98.4°)⁹¹ and $\beta\text{-Mo}_2\text{Br}_4(\text{dmpe})_2$ (101.3°)²³, both of these complexes have staggered conformations with twist angles of 40.0° and 36.8° respectively. The larger bond angle in the cationic species is expected because in order to be able to be eclipsed, the Mo-Mo-P angle must be splayed back more than in the staggered complexes which have longer Mo-Mo bond lengths. The Mo-Mo-O bond angles in the $[\text{Mo}_2(\text{O}_2\text{CCH}_3)_2(\text{dmpe})_2]^{2+}$ cation are all very close to 90° ; this is a common feature in all dimolybdenum complexes containing carboxylate ligands.

The six membered rings formed by the dmpe ligands and the dimolybdenum unit take up a novel half chair conformation; this is shown to good effect in figures 4.5 and 4.6. The fused double ring system can be considered as a heteronuclear equivalent of 1,2,3,4,5,6,7,8 octahydronaphthalene. This will be discussed more fully in the next chapter along with analogous chiral complexes. The structural skeleton of the $[\text{Mo}_2(\text{O}_2\text{CCH}_3)_2(\text{dmpe})_2]^{2+}$ cation must be very rigid because the nmr solution spectrum is unchanged when cooled to -40°C .

The electronic absorption spectrum of $[\text{Mo}_2(\text{O}_2\text{CCH}_3)_2(\text{dmpe})_2]^{2+}$ is shown in figure 4.7. The δ - δ^* transition occurs at $19\,880\text{ cm}^{-1}$ and has an extinction coefficient of $1\,332\text{ mol}^{-1}\text{ l cm}^{-1}$. It is more intense than the δ - δ^* transition of $\text{Mo}_2(\text{O}_2\text{CCH}_3)_4$ ($\epsilon \sim 100\text{ mol}^{-1}\text{ l cm}^{-1}$), this is due to the intensity stealing mechanism operating because the Mo-Mo-P bond angle deviates considerably from 90° (see chp 1 sect.1.3). However it is not as intense as in some other complexes (e.g. $\text{Mo}_2\text{Cl}_4(\text{PMe}_3)_4$ where $\epsilon \sim 3\,110\text{ mol}^{-1}\text{ l cm}^{-1}$)²⁶, because the presence of two acetate groups means that there are only four Mo-Mo-L bond angles which deviate from 90° , whereas in $\text{Mo}_2\text{Cl}_4(\text{PMe}_3)_4$ there are eight and therefore more orbital mixing. Thus $[\text{Mo}_2(\text{O}_2\text{CCH}_3)_2(\text{dmpe})_2]^{2+}$ is of intermediate intensity and illustrates the dependence of other factors apart from δ overlap on the intensity of the δ - δ^* transition.

The resonance Raman spectrum (488.0 nm excited) was also recorded and displayed a short progression in the Mo-Mo stretching vibration with a wavenumber of 391 cm^{-1} . This value is just lower than that found in $\text{Mo}_2(\text{O}_2\text{CCH}_3)_4$ (406 cm^{-1}) and is consistent with a short and strong metal-metal bond.

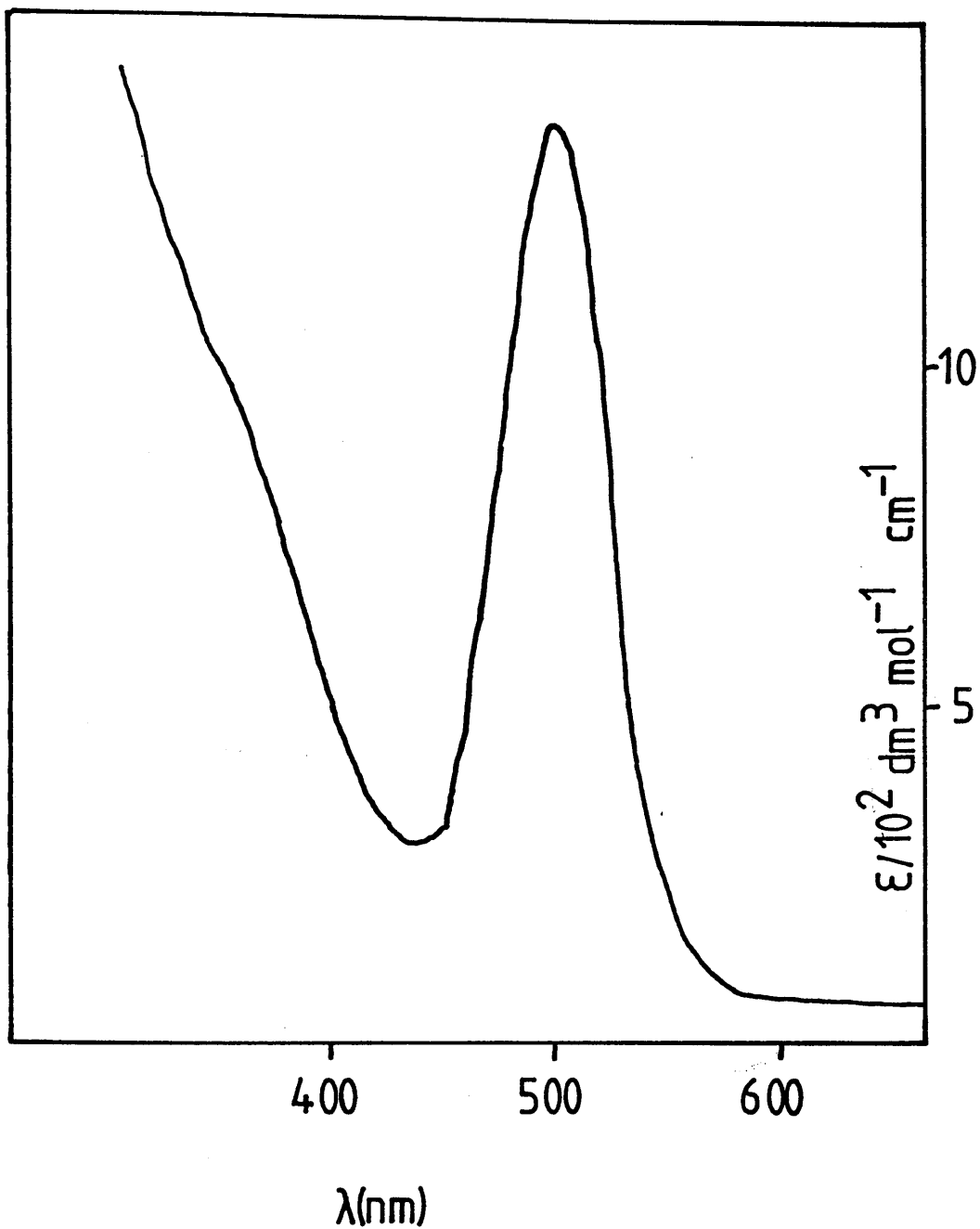


Figure 4.7 Absorption spectrum of $[\text{Mo}_2(\text{O}_2\text{CCH}_3)_2(\text{dmpe})_2]^{2+}$ in CH_3CN .

5 Mechanism of the reaction of $[\text{Mo}_2(\text{O}_2\text{CCH}_3)_2(\text{CH}_3\text{CN})_6]^{2+}$ with Diphosphine Ligands

In the reaction of dmpe with $[\text{Mo}_2(\text{O}_2\text{CCH}_3)_2(\text{CH}_3\text{CN})_6]^{2+}$, an interesting situation arises in which the reactant has all of the acetates in the cis arrangement whereas in the product all the molecules have trans acetates. This is the first example of a reaction involving a quadruply bonded dimolybdenum bis-carboxylate species having 100% conversion from cis to trans. There are examples where interconversion takes place between geometric isomers (e.g. $\text{Mo}_2\text{Cl}_2(\text{O}_2\text{CCMe}_3)_2(\text{PEt}_3)_2$ and $\text{Mo}_2\text{Cl}_2(\text{O}_2\text{CCH}_3)_2(\text{PX}_3)_2$). However in these cases ^{64,65} 100% conversion is not achieved, only an equilibrium.

The reaction of $[\text{Mo}_2(\text{O}_2\text{CCH}_3)_2(\text{CH}_3\text{CN})_6]^{2+}$ with S,S-dppb produces a purple solid which analyses close to the formula $[\text{Mo}_2(\text{O}_2\text{CCH}_3)_2(\text{S,S-dppb})(\text{CH}_3\text{CN})_2][\text{BF}_4]_2$. The S,S-dppb ligand is definitely present in a bridging mode because there is a measurable cd spectrum under the δ - δ^* transition. In fact the complex appears very similar to the $[\text{Mo}_2(\text{O}_2\text{CCH}_3)_2(\text{dppm})(\text{CH}_3\text{CN})_2]^{2+}$ cation ¹³⁷. Both of these complexes are designated to have cis acetate groups because of the similarity of their spectra to that of $[\text{Mo}_2(\text{O}_2\text{CCH}_3)_2(\text{CH}_3\text{CN})_6]^{2+}$, see table 4.3. However there is no reason to suspect that trans-bis diphosphine complexes should not exist containing the ligands dppm and S,S-dppb.

Table 4.3 Selected Electronic Spectral Data For
Dimolybdenum Complexes with two Acetate Groups

<u>Complex</u>	<u>Colour</u>	<u>δ-δ^*(nm)</u>	
$[\text{Mo}_2(\text{O}_2\text{CCH}_3)_2(\text{dppm})(\text{CH}_3\text{CN})_2]^{2+}$	purple	541	<u>cis</u>
$[\text{Mo}_2(\text{O}_2\text{CCH}_3)_2(\text{S,S-dppb})(\text{CH}_3\text{CN})_2]^{2+}$	purple	536	<u>cis</u>
$[\text{Mo}_2(\text{O}_2\text{CCH}_3)_2(\text{CH}_3\text{CN})_6]^{2+}$	red	531	<u>cis</u> *
$[\text{Mo}_2(\text{O}_2\text{CCH}_3)_2(\text{dmpe})_2]^{2+}$	orange	503	<u>trans</u> *
$[\text{Mo}_2(\text{O}_2\text{CCH}_3)_2(\text{S,S-dppb})_2]^{2+}$	orange	492	<u>trans</u>

* - from crystal structure

Indeed trans eclipsed structures are found in $\beta\text{-Mo}_2\text{Cl}_4(\text{dppm})_2$ ⁸³ and in one of crystallographic forms of $\beta\text{-Mo}_2\text{I}_4(\text{dppe})_2$ ⁹⁰. A cis-bis diphosphine complex (as in figure 4.3(a)) is extremely unlikely because of the unfavourable interactions arising between the adjacent substituents on the phosphorus atoms.

The first step of the reaction of $[\text{Mo}_2(\text{O}_2\text{CCH}_3)_2(\text{CH}_3\text{CN})_6]^{2+}$ with diphosphine ligands will be the displacement of two acetonitrile molecules which will be replaced by a single bridging diphosphine ligand. In the case of the dmpe ligand, in order to complete the reaction to the trans product there are two possibilities. Firstly the monosubstituted cis complex can isomerise to a

monosubstituted trans complex, then another dmpe ligand can displace the remaining two acetonitrile molecules to give the disubstituted complex. The other possibility is that the monosubstituted cis complex can be attacked by a dmpe ligand between the cis acetate groups to give the trans disubstituted product.

The first possibility appears untenable because if a trans monosubstituted complex is formed, then this could easily be attacked by dpmm or S,S-dppb to give the trans disubstituted complex. However solutions of $[\text{Mo}_2(\text{O}_2\text{CCH}_3)_2(\text{CH}_3\text{CN})_6]^{2+}$ with S,S-dppb and $[\text{Me}_3\text{O}][\text{BF}_4]$ show no change over a period of several days indicating that the cis monosubstituted complex does not isomerise at all, thus ruling out the first mechanism. The second mechanism appears more plausible because dmpe is a small ligand, therefore it can easily attack between the cis acetates, whereas the more bulky ligands with phenyl groups find this impossible. Thus in the case of the dpmm and S,S-dppb ligands the reaction does not proceed beyond the first step.

Therefore in order to make $[\text{Mo}_2(\text{O}_2\text{CCH}_3)_2(\text{S,S-dppb})_2]^{2+}$, a different preparative route must be undertaken. When $\text{Mo}_2(\text{O}_2\text{CCH}_3)_4$ is reacted with excess S,S-dppb in the presence of $[\text{Me}_3\text{O}][\text{BF}_4]$, an orange solution is obtained.

The electronic spectrum of this complex has the δ - δ^* transition energy at 492 nm, see table 4.2. The solution is plagued with $\text{Mo}_2(\text{O}_2\text{CCH}_3)_4$ impurity but it almost certainly contains the $[\text{Mo}_2(\text{O}_2\text{CCH}_3)_2(\text{S,S-dppb})_2]^{2+}$ cation because of the similarity to the spectrum of $[\text{Mo}_2(\text{O}_2\text{CCH}_3)_2(\text{dmpe})_2]^{2+}$. The $\text{Mo}_2(\text{O}_2\text{CCH}_3)_4$ impurity will have little effect on the spectrum of desired cation because the intensity of the δ - δ^* transition is extremely weak for $\text{Mo}_2(\text{O}_2\text{CCH}_3)_4$. Also there appears to be no sign of any $[\text{Mo}_2(\text{O}_2\text{CCH}_3)_2(\text{S,S-dppb})(\text{CH}_3\text{CN})_2]^{2+}$ (at 536 nm) in the solution. In this reaction the $\text{Mo}_2(\text{O}_2\text{CCH}_3)_4$ will probably be stepwise substituted thereby favouring formation of the thermodynamically more stable trans isomer which has two bridging six membered rings. The optical activity of these complexes containing the S,S-dppb ligand will also be discussed in the next chapter.

6 Reaction of $[\text{Mo}_2(\text{O}_2\text{CCH}_3)_2(\text{CH}_3\text{CN})_6][\text{BF}_4]_2$ with NH_3

The lability of the acetonitrile ligands in the $[\text{Mo}_2(\text{O}_2\text{CCH}_3)_2(\text{CH}_3\text{CN})_6]^{2+}$ cation was again demonstrated when it was reacted with ammonia. A reaction definitely takes place as a golden yellow solution is obtained. The electronic absorption spectrum of this solution is shown in figure 4.8. There is a shift to higher energy for the δ - δ^* transition and there is no sign of any band at 531 nm, this indicates that all of the $[\text{Mo}_2(\text{O}_2\text{CCH}_3)_2(\text{CH}_3\text{CN})_6][\text{BF}_4]_2$ has reacted. The ir spectrum

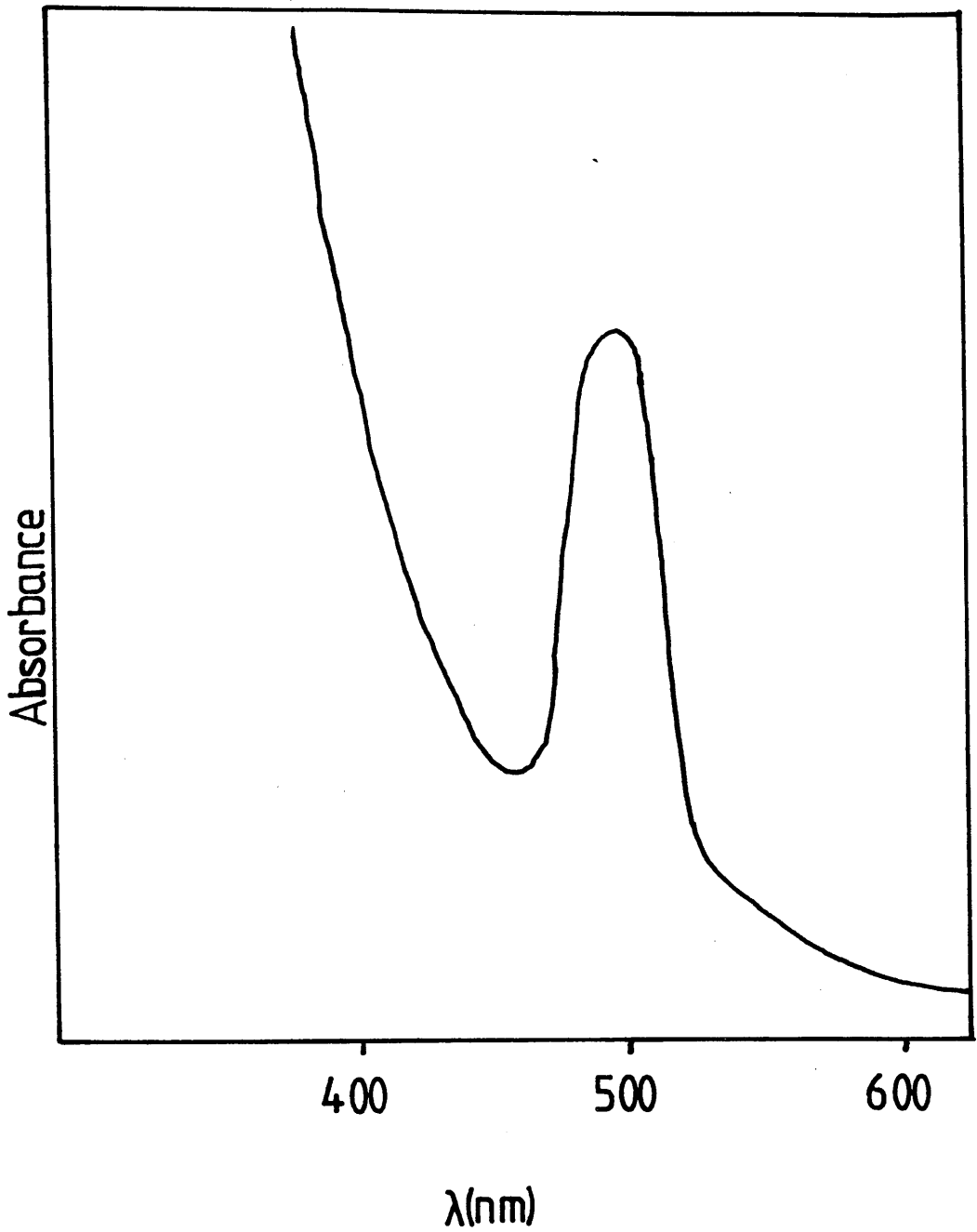


Figure 4.8 Absorption spectrum of $[\text{Mo}_2(\text{O}_2\text{CCH}_3)_2(\text{NH}_3)_4]^{2+}$ in CH_3CN .

of the product from this reaction is shown in figure 4.9, the bands at $3\ 350\ \text{cm}^{-1}$ and $1\ 650\ \text{cm}^{-1}$ are due to the NH_3 stretches and NH_3 degenerate deformation respectively. There is no acetonitrile in this complex (i.e. no bands at $2\ 100\ \text{cm}^{-1}$). Therefore it appears that all of the acetonitrile in the $[\text{Mo}_2(\text{O}_2\text{CCH}_3)_2(\text{CH}_3\text{CN})_6]^{2+}$ cation has been replaced by ammonia. The most probable formula for the product is $[\text{Mo}_2(\text{O}_2\text{CCH}_3)(\text{NH}_3)_4][\text{BF}_4]_2$, although the the complex is air sensitive and analyses poorly. However all the spectra indicate a complex of the above formula, this is not surprising in view of the lability of the acetonitrile in the reactant molecule. The product will only have four ammonia molecules as ammonia does not usually bind axially in dimolybdenum complexes. It cannot be stated with any certainty whether the product contains cis or trans acetate groups.

7 Reactions of $\text{Mo}_2(\text{TFMS})_4$

The complex $\text{Mo}_2(\text{TFMS})_4$ has been used as a precursor to make other quadruply bonded dimolybdenum complexes, because the triflate anion is a weakly coordinating ligand and can be easily substituted. It is made from the reaction of $\text{Mo}_2(\text{O}_2\text{CCH}_3)_4$ with HTFMS and the product can be sublimed for further purification. Abbott et al ¹²³ first

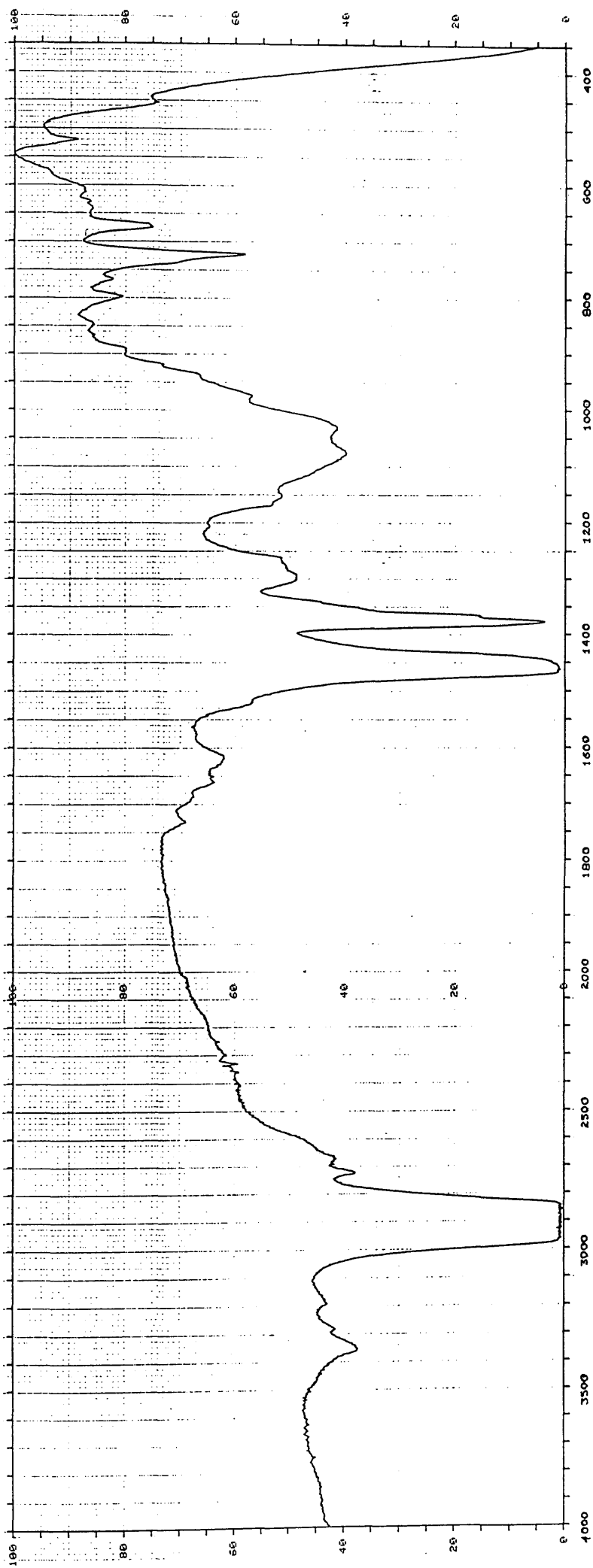


Figure 4.9 ir spectrum of $[\text{Mo}_2(\text{O}_2\text{CCH}_3)_2(\text{NH}_3)_4][\text{BF}_4]_2$.

synthesised $\text{Mo}_2(\text{TFMS})_4$, however they state that it is plagued with acetate impurity. In this project the synthesis proceeded well with no major impurity, the elemental analysis appeared to confirm a pure product.

8 Reaction of $\text{Mo}_2(\text{TFMS})_4$ with DMF

When $\text{Mo}_2(\text{TFMS})_4$ is dissolved in DMF, a deep red solution is formed. The product from this reaction is a red solid which can be recrystallised from dichloromethane. This solid is thermochromic, it is red at room temperature and orange at liquid nitrogen temperatures. The electronic spectrum of the red product is shown in figure 4.10; the $\delta\text{-}\delta^*$ transition occurs at 517 nm. The product is stable in air for only a few minutes. The analysis of this complex was good and indicates a formula of $\text{Mo}_2(\text{DMF})_8(\text{TFMS})_4$. The ir spectrum is shown in figure 4.11 and can be compared with free DMF and the quadruply bonded complex $\text{Mo}_2\text{Cl}_4(\text{DMF})_4$ ¹²⁸, this is summarised in table 4.4.

Table 4.4 Selected ir data of Free DMF and Related Complexes.

<u>Complex</u>	<u>C=O Stretch (cm^{-1})</u>
DMF	1 672
$\text{Mo}_2\text{Cl}_4(\text{DMF})_4$	1 637
$[\text{Mo}_2(\text{DMF})_8][\text{TFMS}]_4$	1 645

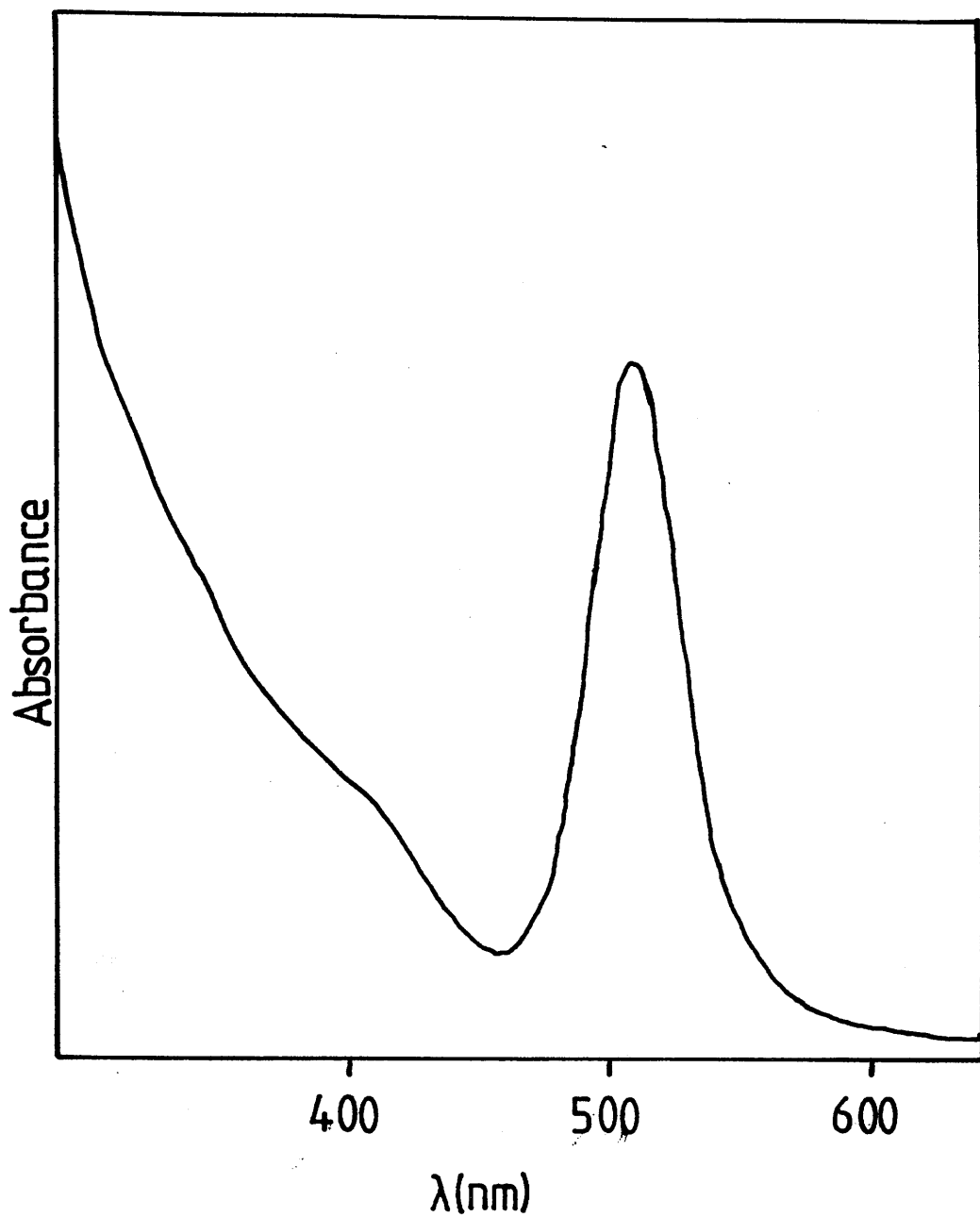


Figure 4.10 Absorption spectrum of $[\text{Mo}_2(\text{DMF})_8]^{4+}$ in CH_2Cl_2 .

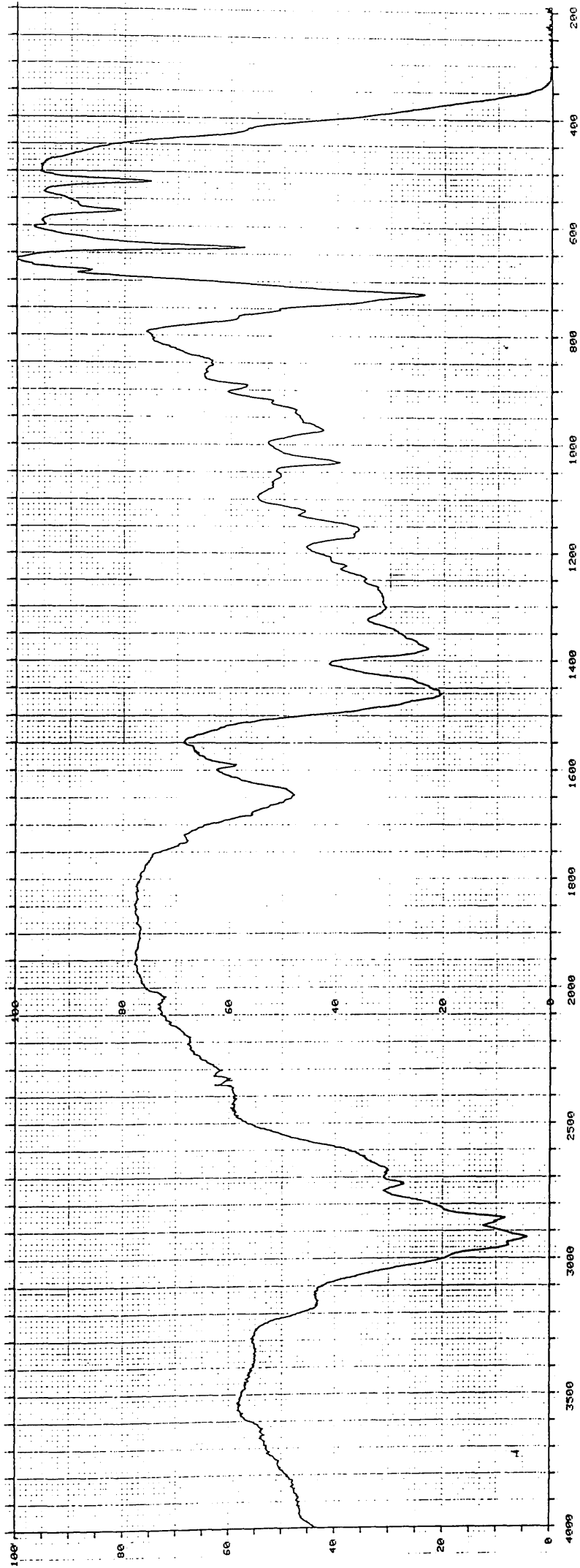
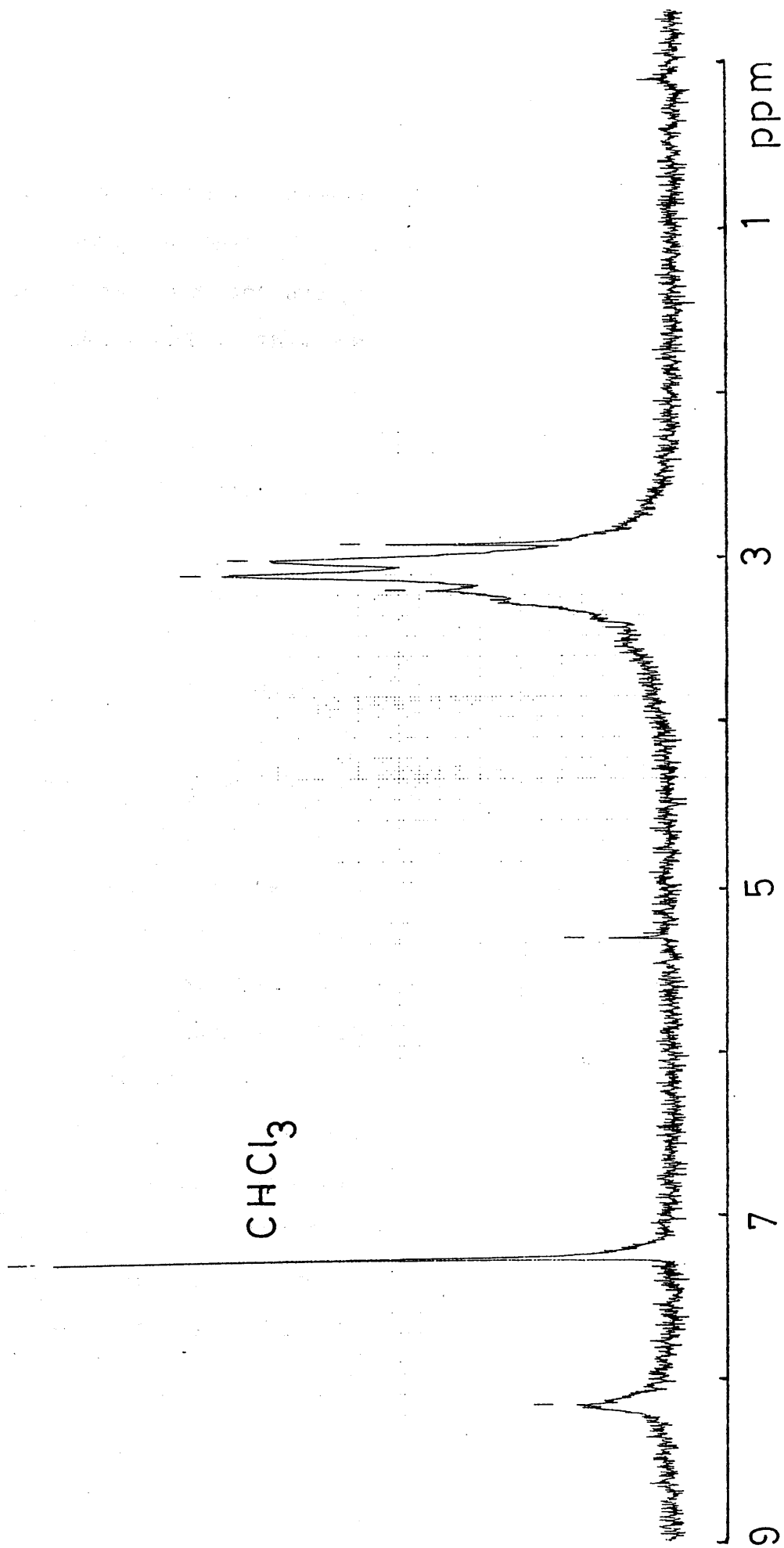


Figure 4.11 ir spectrum of $\text{Mo}_2(\text{DMF})_8(\text{TFMS})_4$.

In $\text{Mo}_2\text{Cl}_4(\text{DMF})_4$, the C=O stretch occurs at 1637 cm^{-1} which signifies a weaker C=O bond than in free DMF. This implies that metal-ligand coordination occurs through the oxygen atom. In $\text{Mo}_2(\text{DMF})_8(\text{TFMS})_4$, the C=O stretch is also weaker, thus in this complex all eight DMF molecules will bond to the molybdenum atoms through the oxygen atoms, while the triflate species will be in an anionic bonding arrangement.

The ^1H nmr of free DMF has two signals in the methyl region of the spectrum, at 2.97 and 2.88 p.p.m., and the amide proton signal is at 8.02 p.p.m. Thus at room temperature there is no free rotation about the N-C bond and the molecule will not possess a plane of symmetry. In the ^1H nmr of $\text{Mo}_2(\text{DMF})_8(\text{TFMS})_4$ in figure 4.12, there appears a little free DMF but not a significant amount. There is no sign of any acetate ligand in the spectrum. In the amide region of the spectrum, there is a broad signal at 8.14 p.p.m. However in the methyl region there are two main signals surrounded by some side bands, these side bands will include some impurities and also free ligand that is present. These two methyl signals, at 2.98 and 3.08 p.p.m., arise from the methyl groups in complexed DMF. All the proton signals in the complexed species are shifted downfield by ~ 0.1 p.p.m. compared to the free ligand; this is due to the diamagnetic anisotropy of the quadruple bond.

Figure 4.12 nmr spectrum of $\text{Mo}_2(\text{DMF})_8(\text{TFMS})_4$.



9 Mo₂(TFMS)₄ with CH₃CN

A deep purple solution is observed when Mo₂(TFMS)₄ is dissolved in CH₃CN. The solid from this reaction can be recrystallised from CH₃CN and analyses very close to the formula Mo₂(CH₃CN)₈(TFMS)₄. This complex has been made before although a slightly different method ¹¹⁴ was used. The spectra of both complexes are identical and the δ-δ* transition occurs at 555 nm.

10 Reaction of Mo₂(CH₃CN)₈(TFMS)₄ with NH₃

Mo₂(CH₃CN)₈(TFMS)₄ was reacted with ammonia in acetonitrile in the hope of a substitution reaction taking place. A reaction occurs as a brown solution is obtained, the product is extremely air sensitive. The ir spectrum of the product is shown in figure 4.13, ammonia is definitely present (bands at 3 350 and 1 650 cm⁻¹) while there is no sign of any acetonitrile. The electronic absorption spectrum is shown in figure 4.14, the δ-δ* transition occurs at 478 nm. This spectrum is very similar to Mo₂(en)Cl₄ ¹¹⁰. The most likely formula is Mo₂(NH₃)₈(TFMS)₄, although the elemental analysis of the product is low for nitrogen and high for carbon. Thus the product probably contains the [Mo₂(NH₃)₈]⁴⁺ cation, however it is still to be isolated in a pure form.

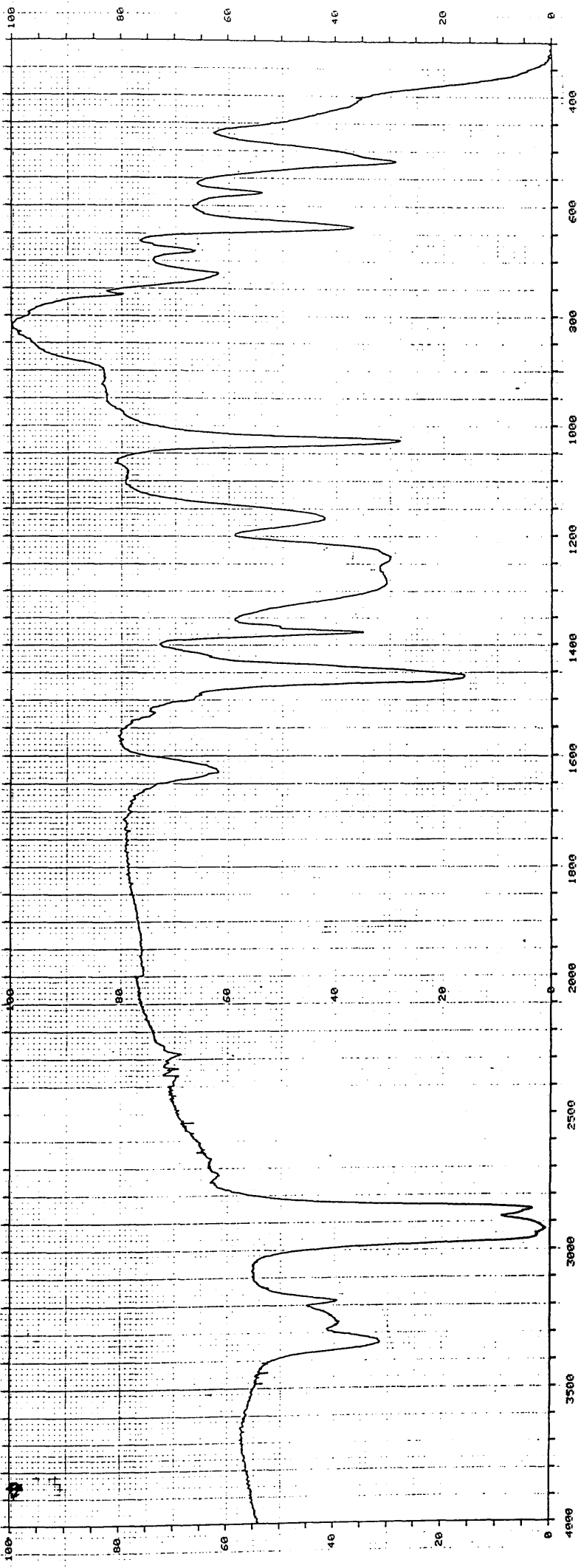


Figure 4.13 ir spectrum of $\text{Mo}_2(\text{NH}_3)_8(\text{TFMS})_4$.

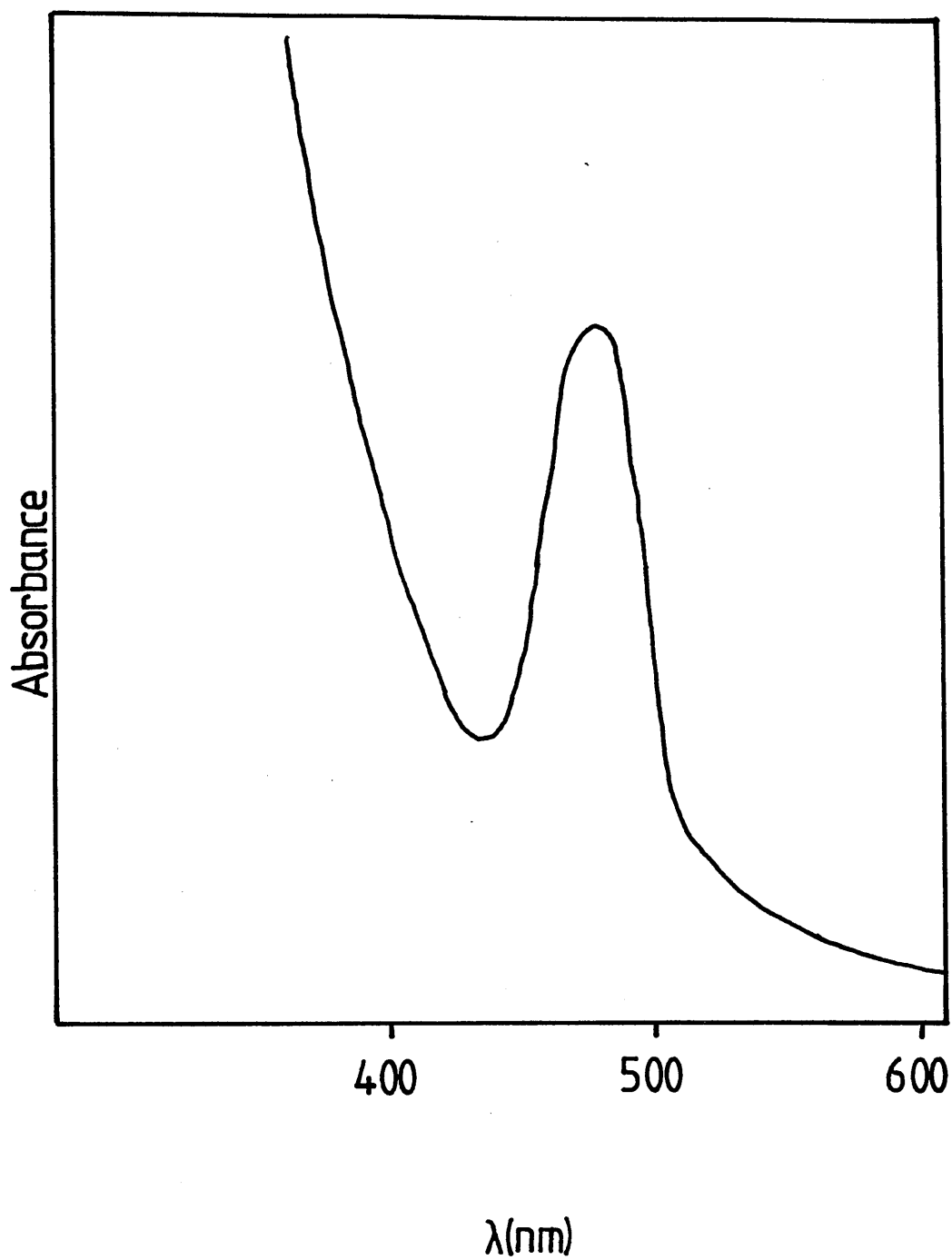


Figure 4.14 Absorption spectrum of $[\text{Mo}_2(\text{NH}_3)_8]^{4+}$ in CH_3CN .

**Chapter Five: OPTICAL ACTIVITY IN DIMOLYBDENUM
COMPLEXES CONTAINING BRIDGING CHIRAL
BIDENTATE LIGANDS**

1 General Overview

Considerable interest has centred on the optical activity of complexes containing a quadruple bond. The optical activity usually arises from the presence of a chiral ligand attached to the dimetal unit. In certain cases where the complexes have an eclipsed structure, the chirality of the ligand does not greatly affect the chromophore (i.e. the Mo-Mo bond). Examples of this type include $[\text{Mo}_2(\text{L-leucine})_4]^{4+}$ ¹⁴², $\alpha\text{-Mo}_2\text{Cl}_4(\text{R-dppp})_2$ ¹²⁹ and $\beta\text{-Mo}_2\text{Cl}_4(\text{S-peap})_2$ ¹⁴³. In other cases the ligands ensure that the Mo-Mo chromophore is intrinsically dissymmetric. This is the situation in complexes where the ligand forces the complex to stagger giving a twist in the clockwise or anticlockwise direction. Figure 5.1 shows the Λ (anticlockwise) and Δ (clockwise) configurations of $\beta\text{-Mo}_2\text{Cl}_4(\text{dppe})_2$. In this case the ligand is achiral and both configurations are present in equal numbers. However the doubly C-methylated derivative of this ligand, S,S-dppb, forces the complex to take either the Λ or Δ configuration because of the chirality of the ligand. This will be discussed in more detail below.

2 Circular Dichroism Spectra

The optical activity of these staggered chiral complexes is normally detected by measuring the cd

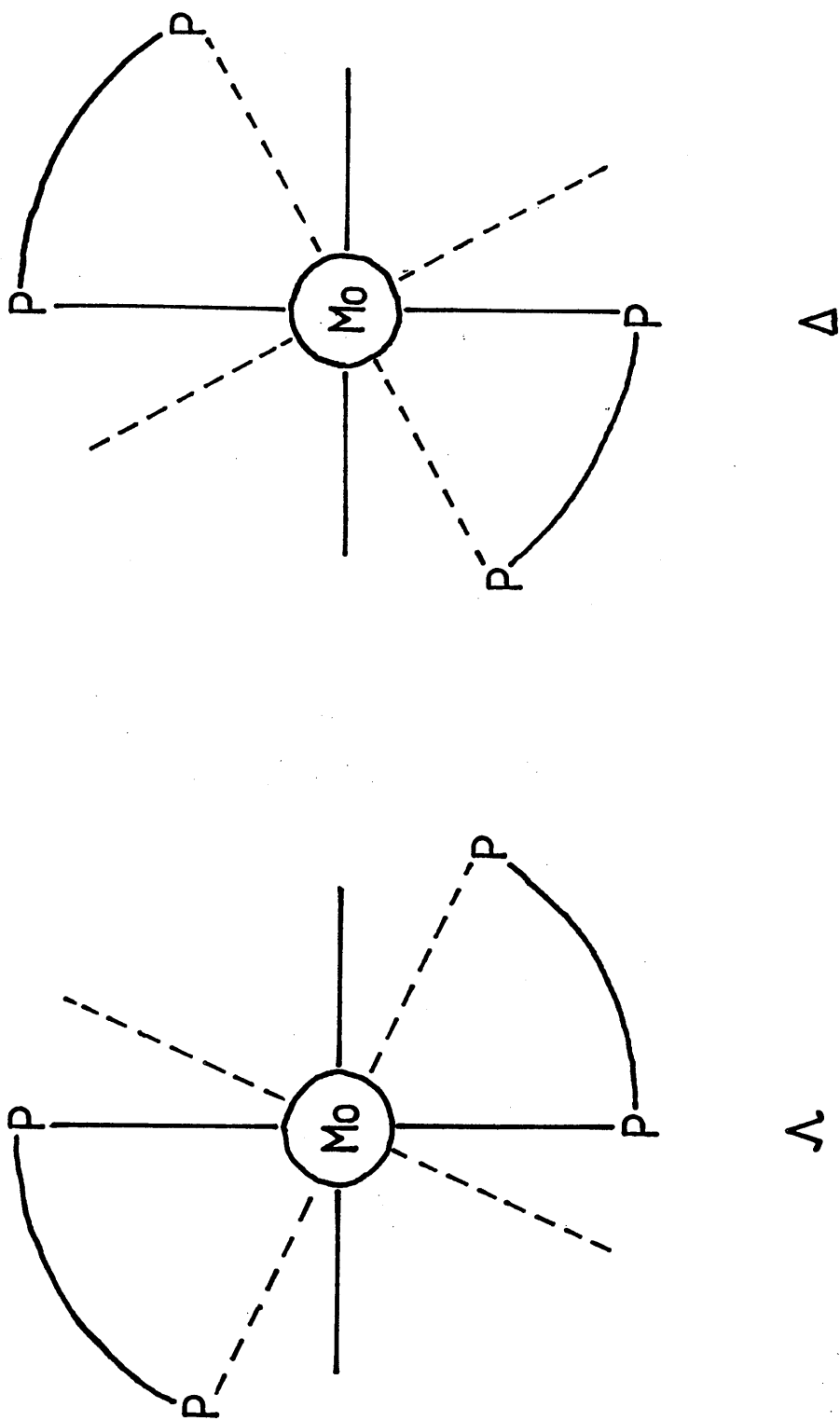


Figure 5.1 Λ and Δ configurations of $\beta\text{-Mo}_2\text{Cl}_4(\text{dppe})_2$.

spectrum. When plane polarised light crosses an optically active medium, the left and right circularly polarised components interact differently with the chiral molecules. Therefore the refractive indices of the left (n_l) and right (n_r) components are different and one component is slowed down more than the other. Thus when leaving the optically medium, the two components are out of phase by a certain angle. Also when the frequency of the electromagnetic radiation is close to an absorption band of the molecule being studied; the extinction coefficients (ϵ_l and ϵ_r) of the two circularly polarised components are not identical. Therefore as well as emerging at different angles, the electric vectors also have different magnitudes. Thus the two components recombine to form elliptically, not plane, polarised light. These are the fundamentals of circular dichroism spectroscopy and are explained in greater detail elsewhere ¹⁴⁴.

3 The δ - δ^* Transition

The lowest energy electronic transition for quadruply bonded complexes is the δ - δ^* transition (chp 1). The transient charge distribution for this transition is depicted in figure 1.6; this is simply obtained by multiplying the phases of the two orbitals involved. Figure 1.6 shows a complex with a fully eclipsed geometry. This picture is formally equivalent to the group

theoretical statement that the product of the symmetries of the $\delta(b_{1g})$ and $\delta^*(b_{2u})$ orbitals transform as $z(a_{2u})$ in D_{4h} symmetry. The representations in D_{2h} (e.g. for eclipsed $\beta\text{-Mo}_2\text{X}_4(\text{P}\tilde{\text{P}})_2$ complexes) are $b_{1g}(\delta)$, $a_u(\delta^*)$ and $b_{1u}(z)$. However when the complex is configurationally chiral, the symmetry of the chromophore drops to D_4 or D_2 and the products of the δ and δ^* orbital symmetries transform as b_1 and a_2 respectively. These representations are electric and magnetic dipole allowed along or around the metal-metal bond and so the transition can show circular dichroism ⁹⁴.

When the ligators are twisted with respect to each other about the metal-metal bond the shortest path of the electron becomes a helix. The metal localised model ⁹⁴ can be used to help predict the structure of the complex from the sign of the $\delta\text{-}\delta^*$ transition in the cd spectrum. Figure 5.2 shows the result of twists producing the Λ configuration of a $\beta\text{-Mo}_2\text{X}_4(\text{L}\tilde{\text{L}})_2$ chromophore. In figure 5.2(a) the twist angle between the front and rear ligators is between 0° and 45° when viewed down the metal-metal bond. Here the charge displacement is that of a left handed helix. In figure 5.2(b), the twist angle is between 45° and 90° and the charge displacement is that of a right handed helix. The chromophore is not chiral at 0° , 45° and 90° ; at these angles there is no net helicity. The absolute sign of the cd associated with the $\delta\text{-}\delta^*$

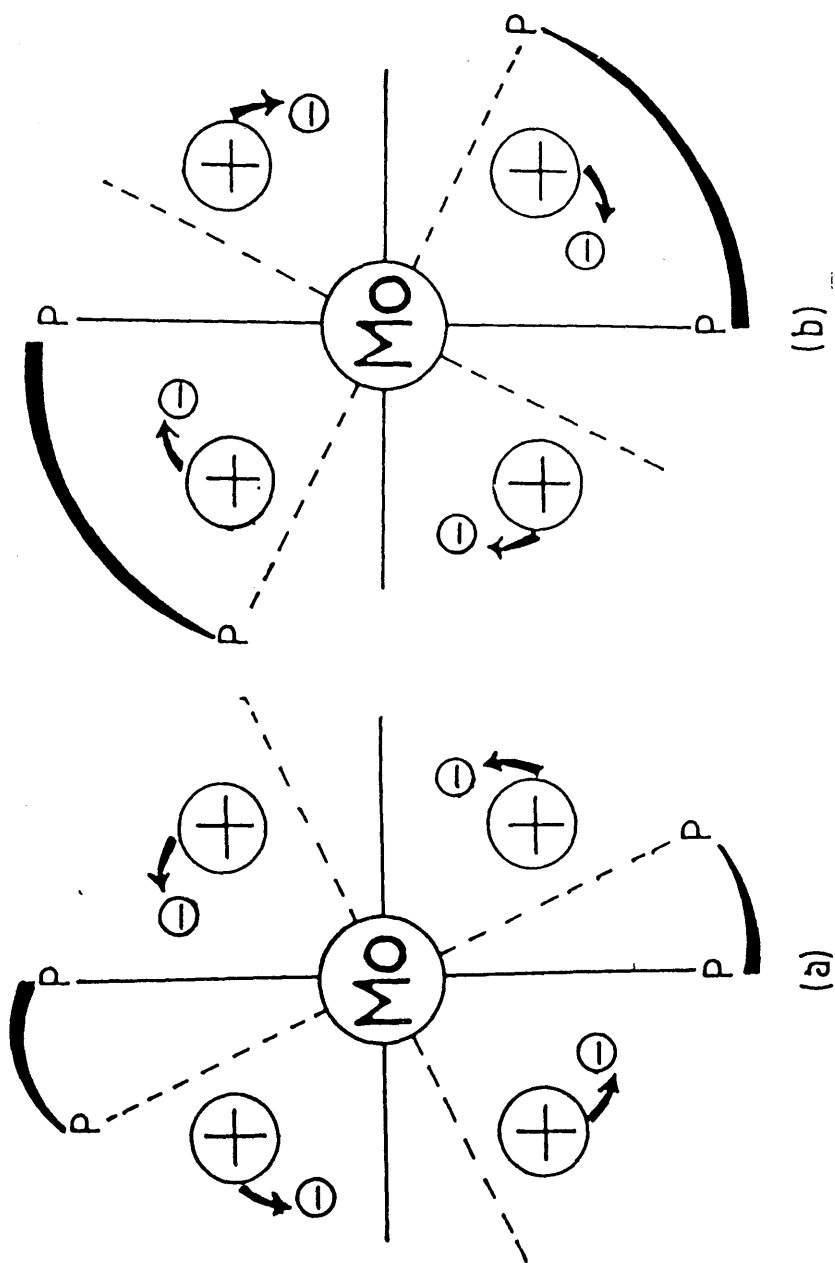


Figure 5.2 Helical charge distribution for the δ - δ^* transition set up from twisting the rear MoX_2P_2 group (a) anticlockwise $< 45^\circ$, (b) anticlockwise $> 45^\circ$.

transition can be derived from the helicity of the charge displacement. In figure 5.2(a), there is a left handed helical charge displacement around and along the metal-metal bond. However the $\delta\text{-}\delta^*$ transition is excited by light propagated perpendicular to the metal-metal bond and any helix has the opposite helicity when viewed perpendicular to the helix axis. Therefore in figure 5.2(a), right circularly polarised light will interact more strongly with the right handed helical charge displacement. This means that the extinction coefficient of the right component (ϵ_r) will be greater than ϵ_l . Therefore the differential extinction coefficient $\Delta\epsilon$ (which is defined as $\epsilon_l - \epsilon_r$) will be negative for figure 5.2(a), whereas $\Delta\epsilon$ will be positive for figure 5.2(b). Thus a sign rule can be built up for the $\delta\text{-}\delta^*$ transition depending on the twist angle and the configuration of the chromophore. This sign rule is shown in figure 5.3, the sign of the cd is that of the sectors containing the rear set of ligators. There are nodal planes at 0° , 45° and 90° .

4 The $\delta\text{-}d_{x^2-y^2}$ Transition

The next lowest energy transition in many quadruply bonded complexes is the $\delta\text{-}d_{x^2-y^2}$ transition⁹⁴. The transient charge distribution for this transition is shown in figure 5.4. This involves a rotation of charge about

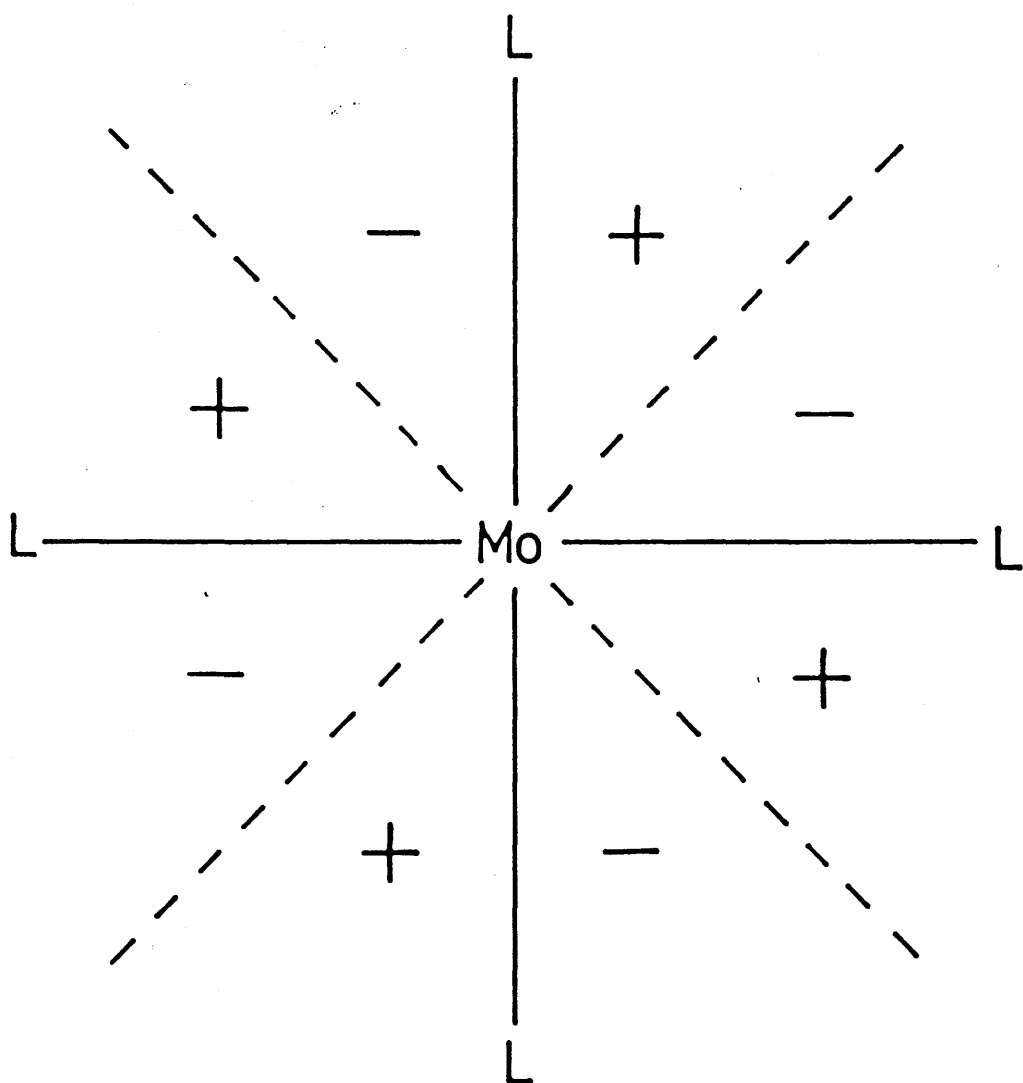


Figure 5.3 Sign rule for the δ - δ^* transition.

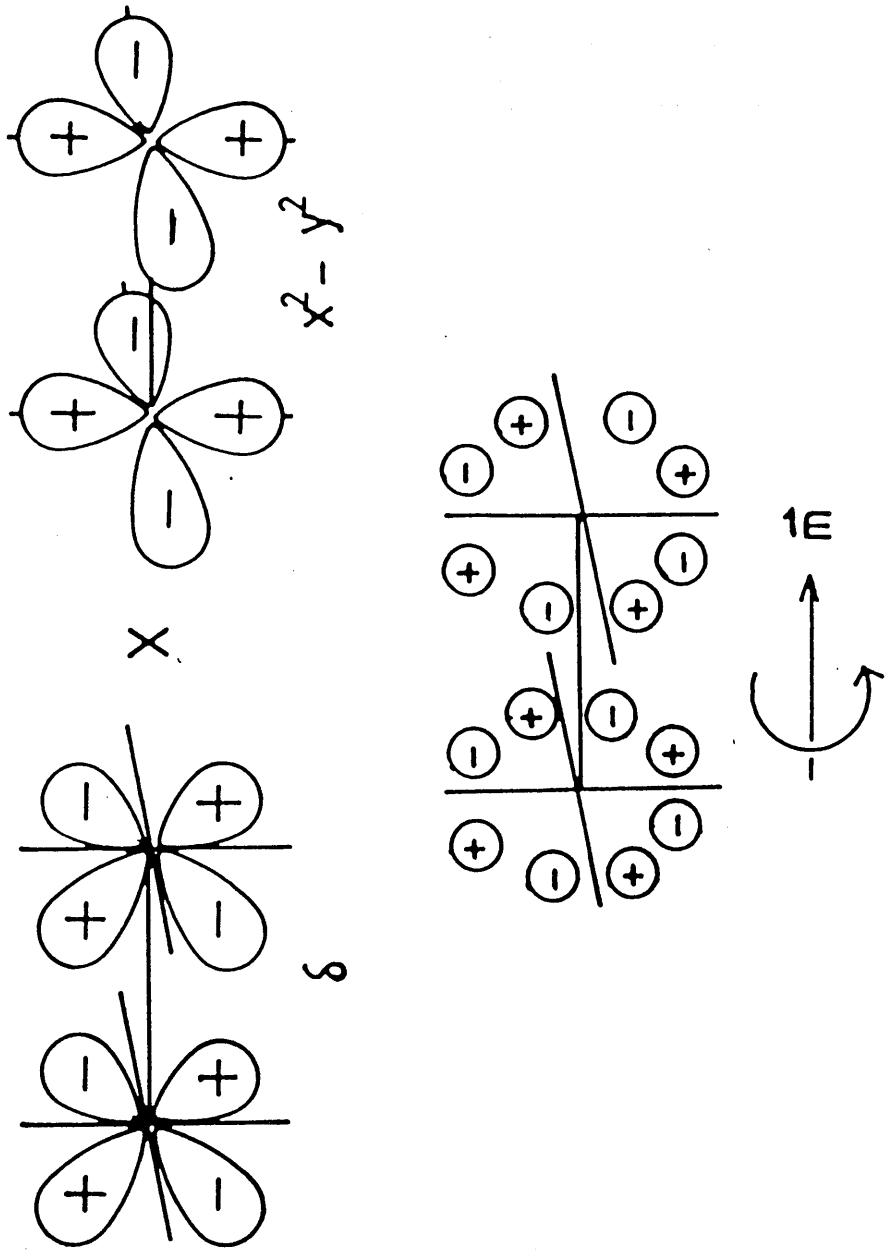


Figure 5.4 Phase multiplication and transient charge distribution for the δ - $d_{x^2-y^2}$ transition.

the metal-metal bond and is therefore magnetic dipole allowed. Rotating the two halves of the molecule will also make the transition electric dipole allowed. The same procedure can be used with this transition as with that used above for the δ - δ^* transition. Figure 5.5(a) depicts a λ configuration with a twist angle of between 0° and 45° , here a right handed helical charge displacement arises. Figure 5.5(b) has a twist angle of between 45° and 90° in the counterclockwise direction, this results in a left handed helical charge displacement. Again a sign rule can be constructed and this is shown in figure 5.6. The sign rule for the δ - $d_{x^2-y^2}$ transition has the same nodal planes as in figure 5.4 but has opposite signs. Thus it is predicted that the sign of the cd under the δ - δ^* transition should be opposite to that of the δ - $d_{x^2-y^2}$ transition for quadruply bonded complexes.

5 Magnitude of Dissymmetry Factors

The magnitude of the dissymmetry caused by rotation about the chromophore can be quantified. The helical charge displacement can be thought of in terms of an electric and magnetic dipole transition. The translational motion of the electron (i.e. along the metal-metal bond) is the electric dipole transition and the rotational motion is the magnetic dipole transition. The electric dipole transition moment, μ , is dependent on the δ overlap

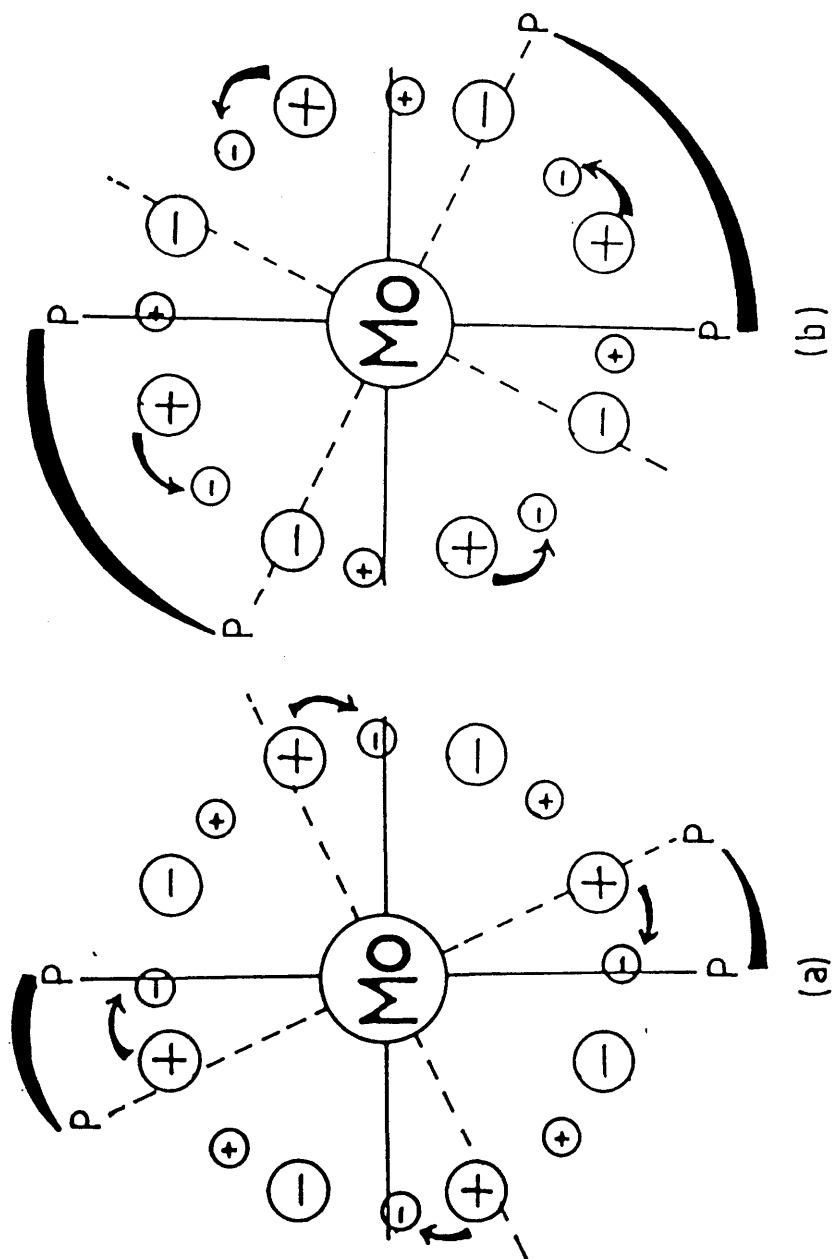


Figure 5.5 Helical charge distribution for the δ - $d_{x^2-y^2}$ transition set up from twisting the rear MoX_2P_2 group (a) anticlockwise $< 45^\circ$, (b) anticlockwise $> 45^\circ$.

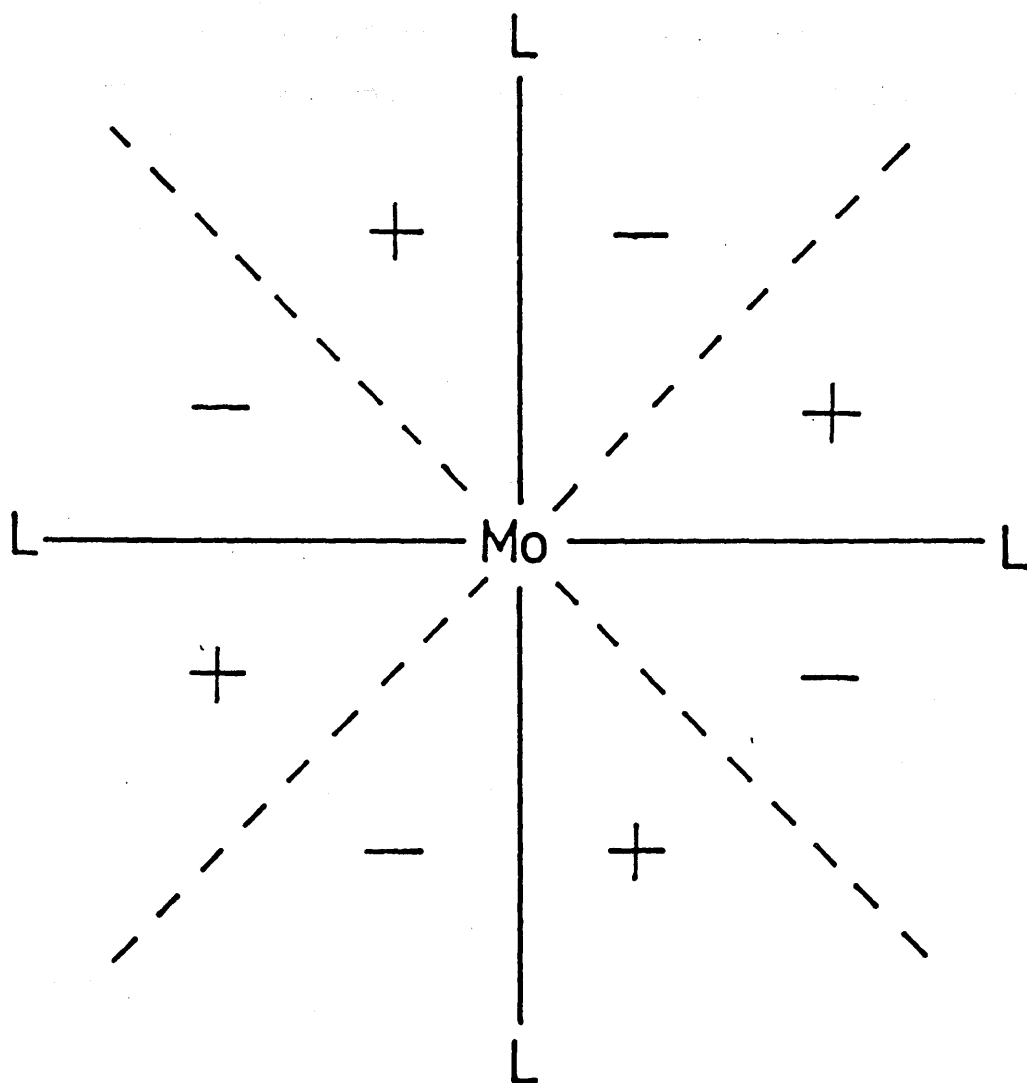


Figure 5.6 . Sign rule for the δ - $d_{x^2-y^2}$ transition.

between the two metal atoms and can be written as

$$\mu(X) = \mu_{\max} \cos 2X$$

The magnetic dipole transition moment, $m(X)$, is also dependent on δ overlap and has a maximum at 45° and minima at 0° and 90° , and is written as

$$m(X) = m_{\max} \sin 2X$$

The dipole strength, D , of an electronic transition is proportional to $\langle \mu \rangle^2$, while the rotational strength, R , is proportional to the product of μ and m . Thus

$$D(X) = D_{\max} \cos^2 2X$$

$$R(X) = R_{\max} \cos 2X \sin 2X$$

The dissymmetry factor (called the g value) is expressed as

$$g = 2R/D = \Delta\epsilon/\epsilon$$

Using the above equations it is possible to express a value for g in terms of the twist angle, X ,

$$g = g_{\max} \tan 2X$$

These equations are summarised pictorially in figure 5.7. It can be seen that g is at a minimum at twists of 0° and 90° , however as the twist approaches 45° the g value tends to infinity.

6 Conformations and Configurations

The above equations can help in determining the nature of the twist in chiral quadruply bonded complexes. However the information is not totally unambiguous. For example a complex which gives a negative cd under the $\delta-\delta^*$ transition could have a Λ configuration with a twist angle of between 0° and 45° , or a Δ configuration with a twist angle of between 45° and 90° . X-ray crystallography can easily solve this problem. However when this is not possible an examination of scale models and consideration of the conformations of the bridging rings are required.

The bridging rings formed in $\beta\text{-Mo}_2\text{X}_4(\text{L}\sim\text{L})_2$ complexes have already been looked at in previous chapters. In most of the cases that will be discussed, six membered rings are involved. These rings usually prefer to be in the chair conformation as in cyclohexane (figure 5.8). Several other conformations are possible, including the boat, but the chair is the most stable. If any substituents are now added to the six membered ring as in methylcyclohexane, then the methyl group will have a

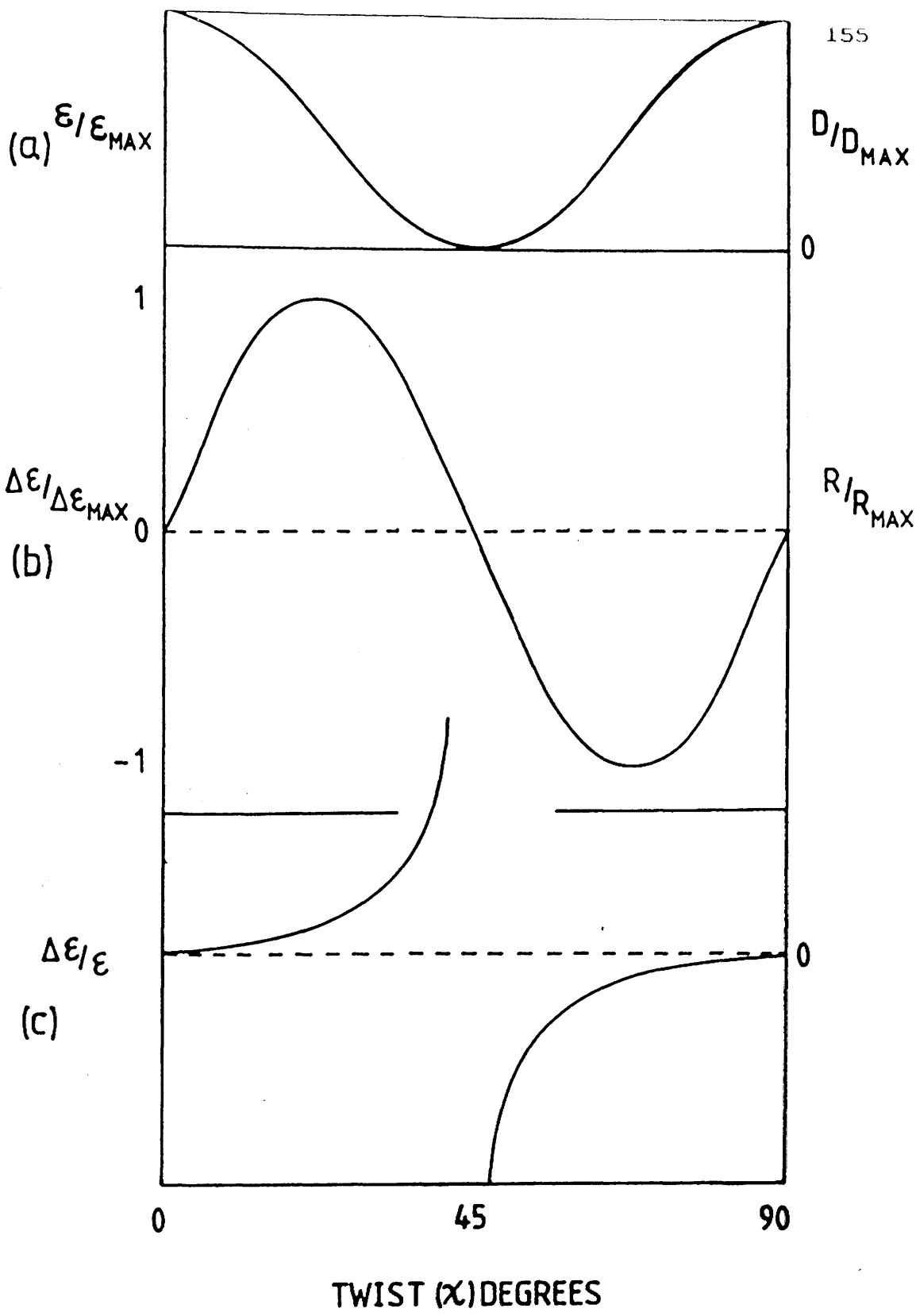


Figure 5.7 Graphic representation of ϵ , $\Delta\epsilon$ and g . The dependence of (a) dipole strength, (b) rotational strength and (c) dissymmetry factor on twist angle X .

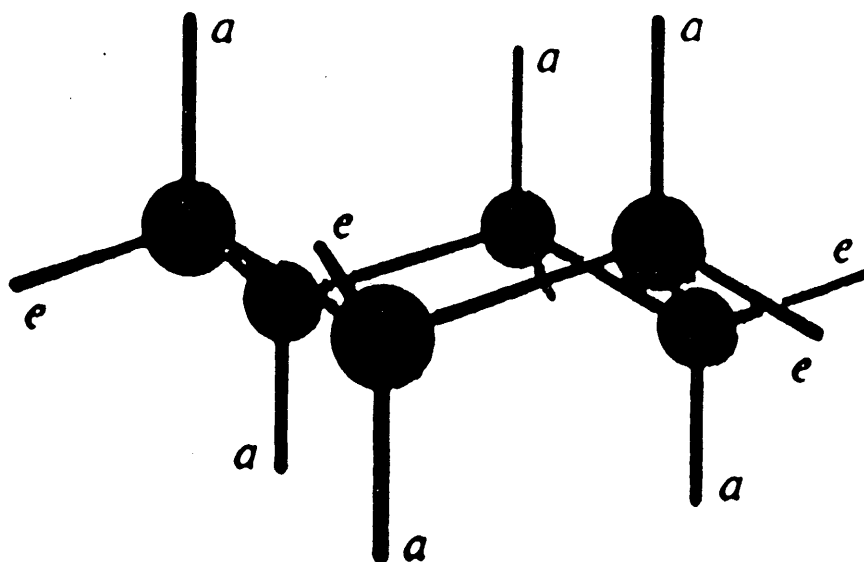


Figure 5.8 Cyclohexane in the chair conformation.

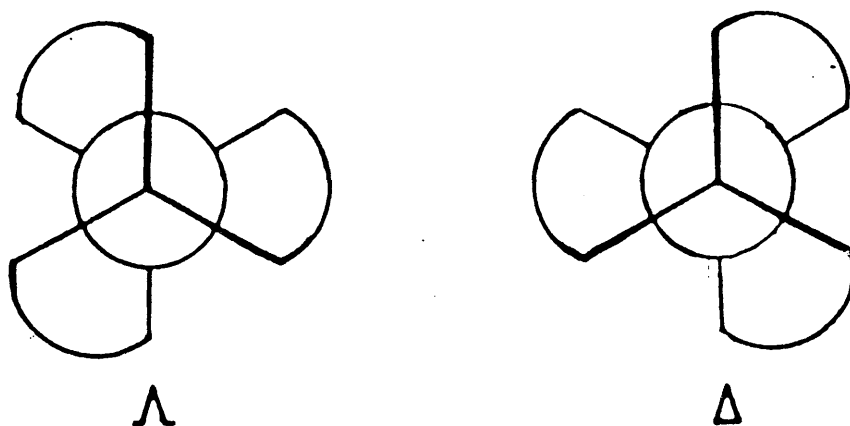
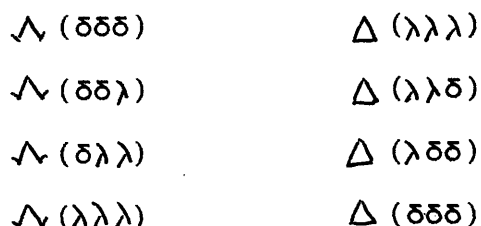


Figure 5.9 Λ and Δ configurations of octahedral trischelates. The absolute configuration is defined according to the twist of the helices.

tendency to take up an equatorial position. These considerations can help in deciding which conformation is present in these β complexes.

Firstly when labelling the configuration and conformation of complexes it is best to look at the system used for mononuclear trischelate octahedral complexes. Here the chromophores can also be dissymmetric with either a λ or δ configuration, see figure 5.9. The rings formed by the chelating ligand can also be assigned individual configurations (λ or δ). Figure 5.10 shows the two enantiomeric forms ¹⁴⁵ of the skew five membered chelate rings as found in $[\text{Co}(\text{en})_3]^{3+}$. The configuration of the individual rings is simply derived from the X-C-C-X torsion angle. These two different forms of chirality lead, in the case of octahedral trischelates, to four pairs of diastereomers



This system can be applied to quadruply bonded complexes where the six membered rings can be treated as five membered rings, as above, if the central point of the metal-metal bond is taken to be a metal atom. In this way

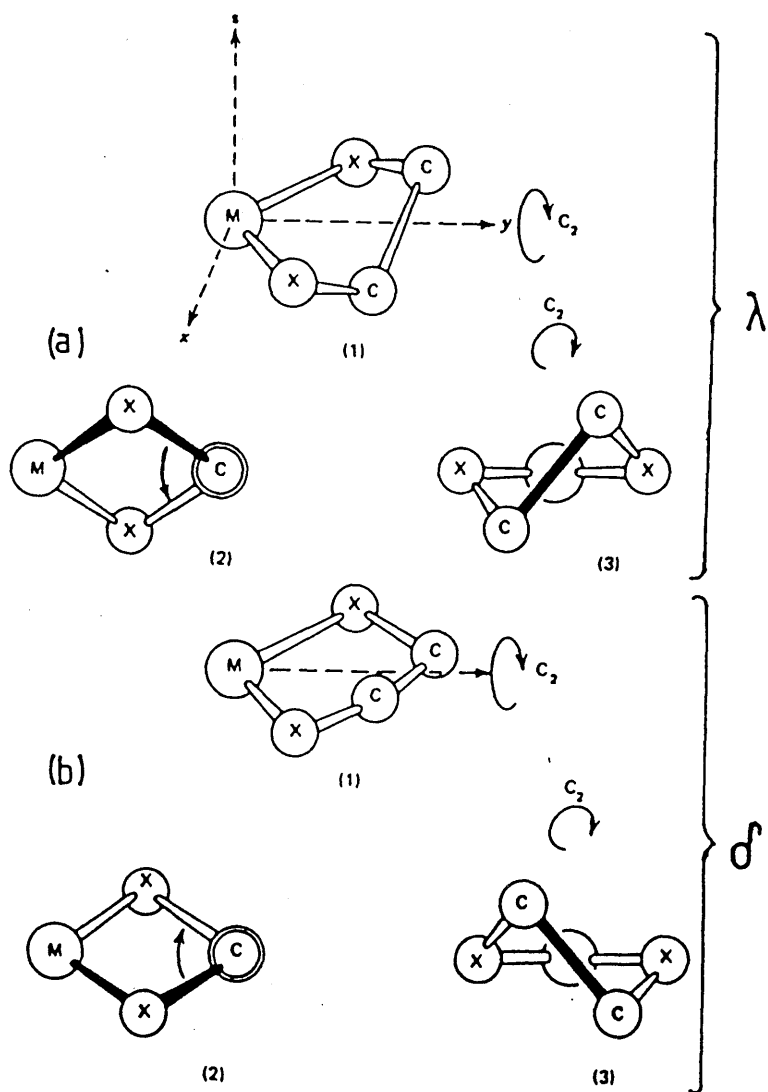


Figure 5.10 The two enantiomeric conformations of the symmetric skew five-membered chelate rings.

the rings in these complexes can be designated as λ or δ as in figure 5.11; again this can be derived by looking at the P-C-C-P torsion angle. Thus in quadruply bonded β isomers with six membered rings there are three pairs of diastereomers possible.



In the crystal structure of $\beta\text{-Mo}_2\text{Cl}_4(\text{dppe})_2$ ⁸⁸, four of these diastereomers are observed. The complex has two orientations: 87% of the molecules are in the major orientation where the bridging rings possess a chair conformation while the minor orientation (13%) has the bridging rings in the skew boat conformation. Within the major orientation, figure 5.12, there are equal numbers of $\Delta(\lambda\lambda)$ and $\Lambda(\delta\delta)$. Whereas the minor orientation, figure 5.13, has equal numbers of $\Delta(\delta\delta)$ and $\Lambda(\lambda\lambda)$. The two other diastereomers, $\Lambda(\delta\lambda)$ and $\Delta(\lambda\delta)$, were not observed, presumably because they are too high in energy. It is interesting to note that there are two different conformations present in sizeable numbers. This confirms that the chair conformation is the most stable but also shows that the difference in energy between various conformers is small (cf chp 1 sect.2.2 on $\beta\text{-Mo}_2\text{I}_4(\text{dppe})_2$). The average twist angle in $\beta\text{-Mo}_2\text{Cl}_4(\text{dppe})_2$ is 60° .

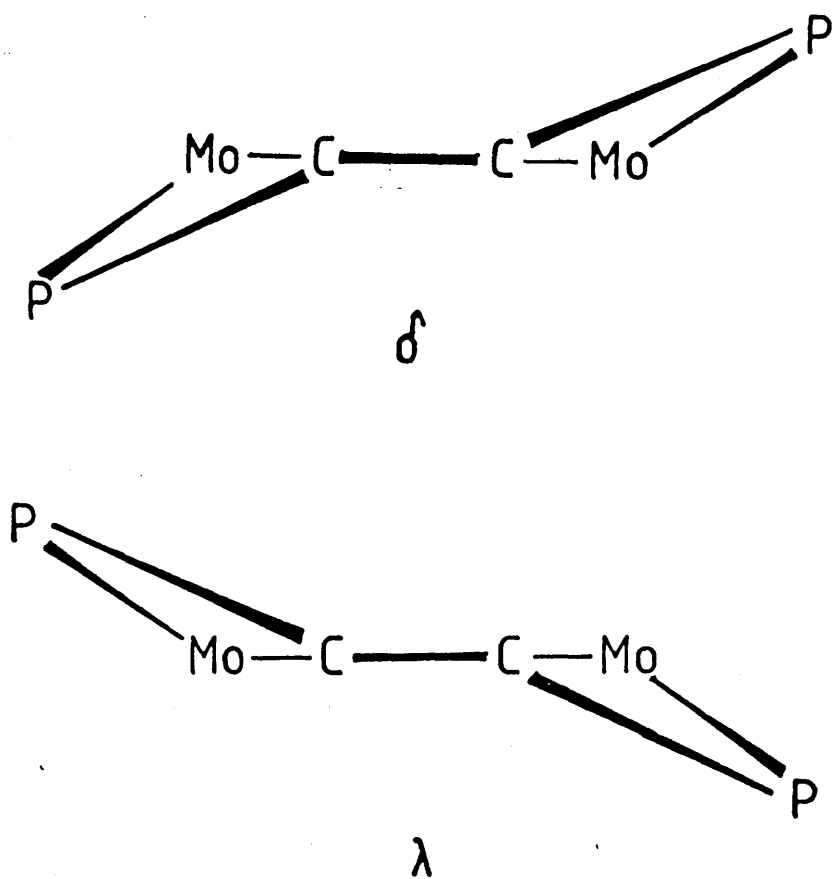


Figure 5.11 The δ and λ conformations of the six-membered $\text{Mo}_2\text{P}_2\text{C}_2$ heteronuclear rings.

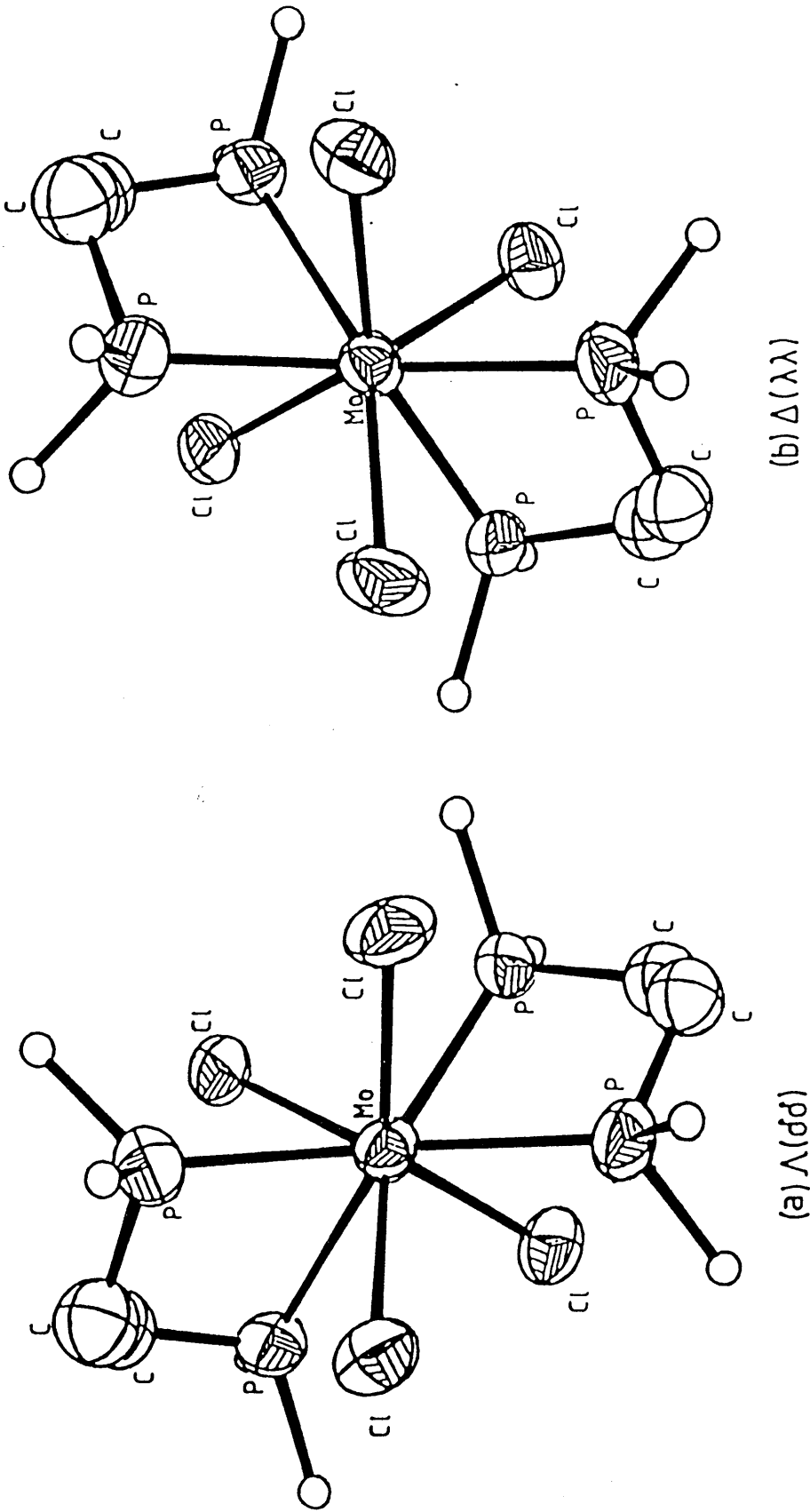


Figure 5.12 (a) $\Lambda(\delta\delta)$ and (b) $\Delta(\lambda\lambda)$ configurations of $\beta\text{-Mo}_2\text{Cl}_4(\text{dppe})_2$.

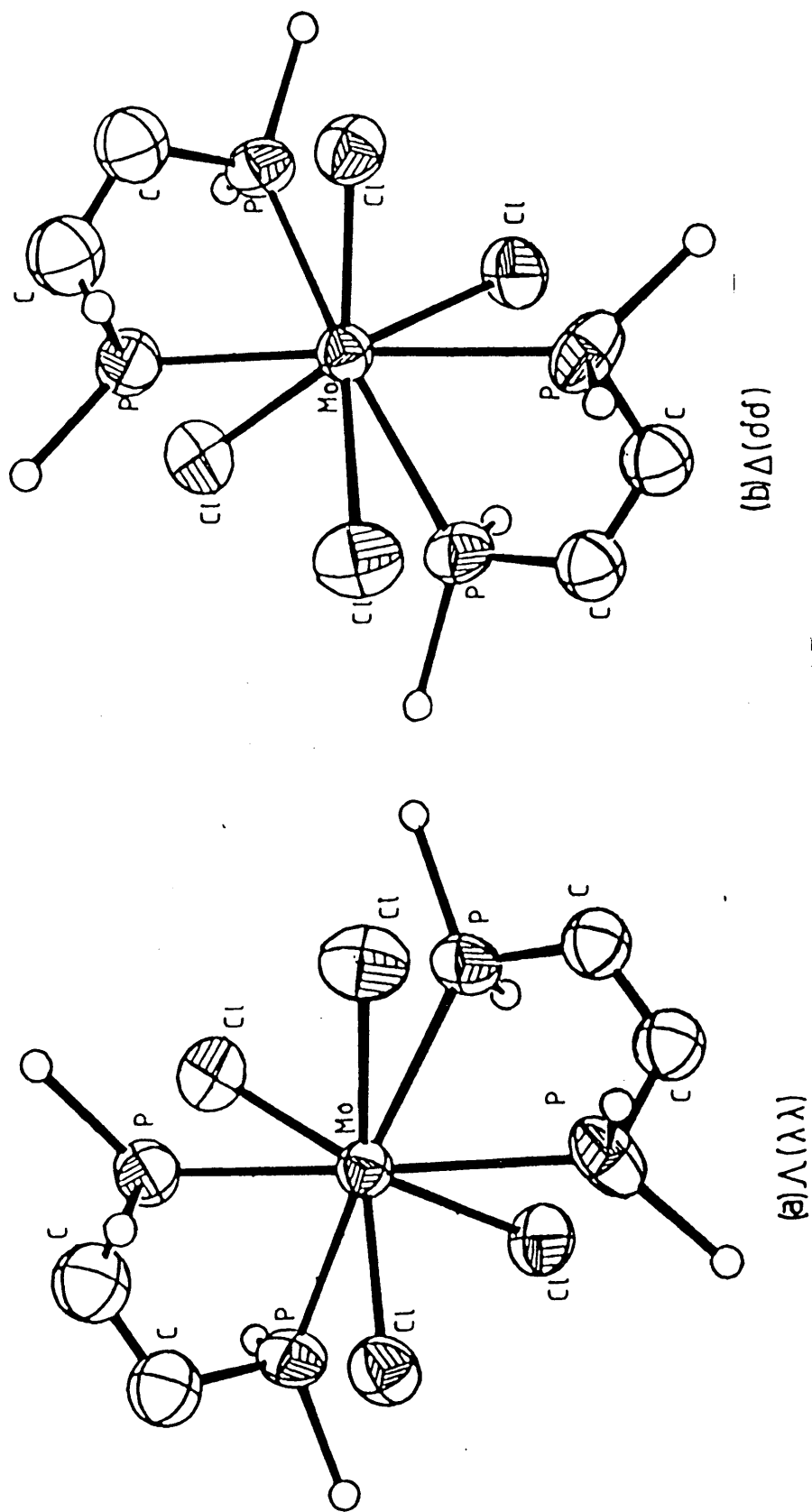


Figure 5.13 (a) $\Lambda(\lambda\lambda)$ and (b) $\Delta(\delta\delta)$ configurations of $\beta\text{-Mo}_2\text{Cl}_4(\text{dppe})_2$.

When the chiral ligand, S,S-dppb, is incorporated into a β isomer then the complex will be forced to take the Λ or Δ configuration. The absorption and cd spectra of $\beta\text{-Mo}_2\text{Cl}_4(\text{S,S-dppb})_2$ ⁹³ are shown in figure 5.14. The first and second lowest energy transitions are of opposite sign in the cd spectrum, this confirms that the $\delta\text{-d}_{x^2-y^2}$ transition is the second lowest energy transition in these complexes. $\beta\text{-Mo}_2\text{Cl}_4(\text{S,S-dppb})_2$ has a negative cd under the $\delta\text{-}\delta^*$ transition, this indicates that it has either a Λ configuration with twist angle of between 0° and 45° , or a Δ configuration with twist angle between 45° and 90° . The above models can help to determine which conformation will result. It would be expected that the chair conformation would occur in each six membered ring. However now there are two methyl groups in each ring which will prefer to be in the more favourable equatorial position if possible. The $\Delta(\lambda\lambda)$ configuration places all four methyls in the unfavourable axial position, while $\Lambda(\delta\delta)$ has all four methyls in the equatorial position. However the $\Lambda(\delta\delta)$ configuration would be expected to have a twist angle of 60° as in $\beta\text{-Mo}_2\text{Cl}_4(\text{dppe})_2$. Unfortunately this places the complex in the positive sector for the $\delta\text{-}\delta^*$ transition. The sign of the cd can be explained if it is assumed that the twist angle is tightened to less than 45° which will produce a slightly distorted chair but the methyls will remain equatorial. The energy difference in distorting the chair should be small. This proposed configuration is confirmed by the crystal structure determination of

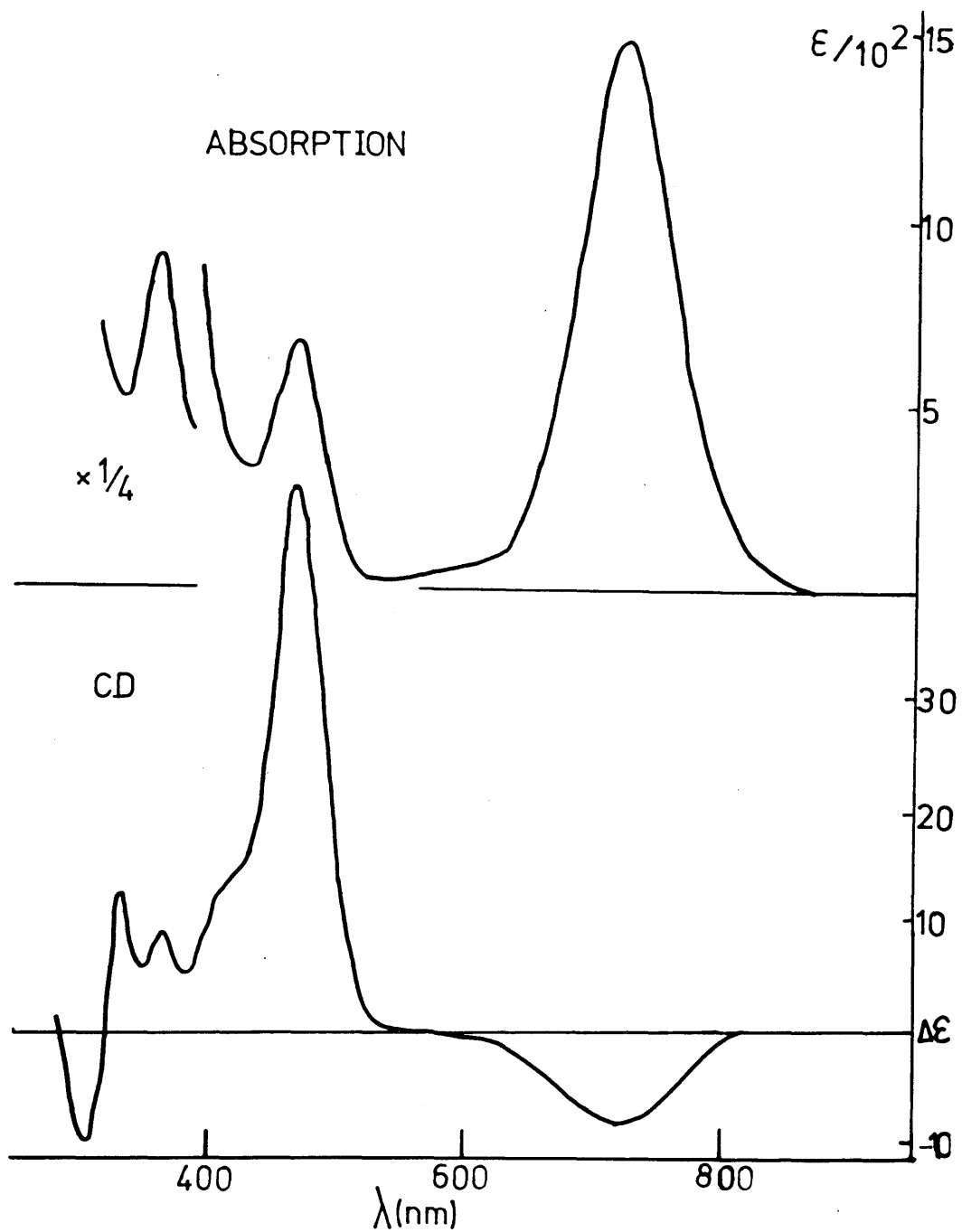


Figure 5.14 Absorption and cd spectra of $\beta\text{-Mo}_2\text{Cl}_4(\text{S,S-dppb})_2$ in CH_2Cl_2 .

$\beta\text{-Mo}_2\text{Cl}_4(\text{S,S-dppb})_2$ ⁹³ which is shown in figure 5.15. Here the distorted chair conformation can be readily seen and the twist angle is 23° with configuration $\Lambda(\delta\delta)$ as predicted.

In fact even one methyl group in the ligand backbone is enough to tighten the twist angle to less than 45° , because $\beta\text{-Mo}_2\text{Cl}_4(\text{R-dppp})_2$ ¹²⁹ displays a positive cd under the $\delta\text{-}\delta^*$ transition. The ligand R-dppp will produce the opposite configuration to that seen in $\beta\text{-Mo}_2\text{Cl}_4(\text{S,S-dppb})_2$. Therefore in $\beta\text{-Mo}_2\text{Cl}_4(\text{R-dppp})_2$, the $\Delta(\lambda\lambda)$ configuration will place both methyls in the equatorial position, and since the configuration is Δ the twist angle must be less than 45° in order to place the rear set of ligands in the positive sector for the $\delta\text{-}\delta^*$ transition. In fact for $\beta\text{-Mo}_2\text{Cl}_4(\text{R-dppp})_2$, χ will be approximately 27° . This can be interpolated from the plot of $\delta\text{-}\delta^*$ transition energy vs $\cos 2\chi$ for this family of complexes (figure 1.7).

7 Results and Discussion

7.1 $\beta\text{-Mo}_2\text{Cl}_4(\text{R-phenphos})_2$

One of the first complexes made during this project was $\beta\text{-Mo}_2\text{Cl}_4(\text{R-phenphos})_2$. It was hoped to compare its properties with $\beta\text{-Mo}_2\text{Cl}_4(\text{R-dppp})_2$ to see what the significance was of replacing a methyl group by a phenyl

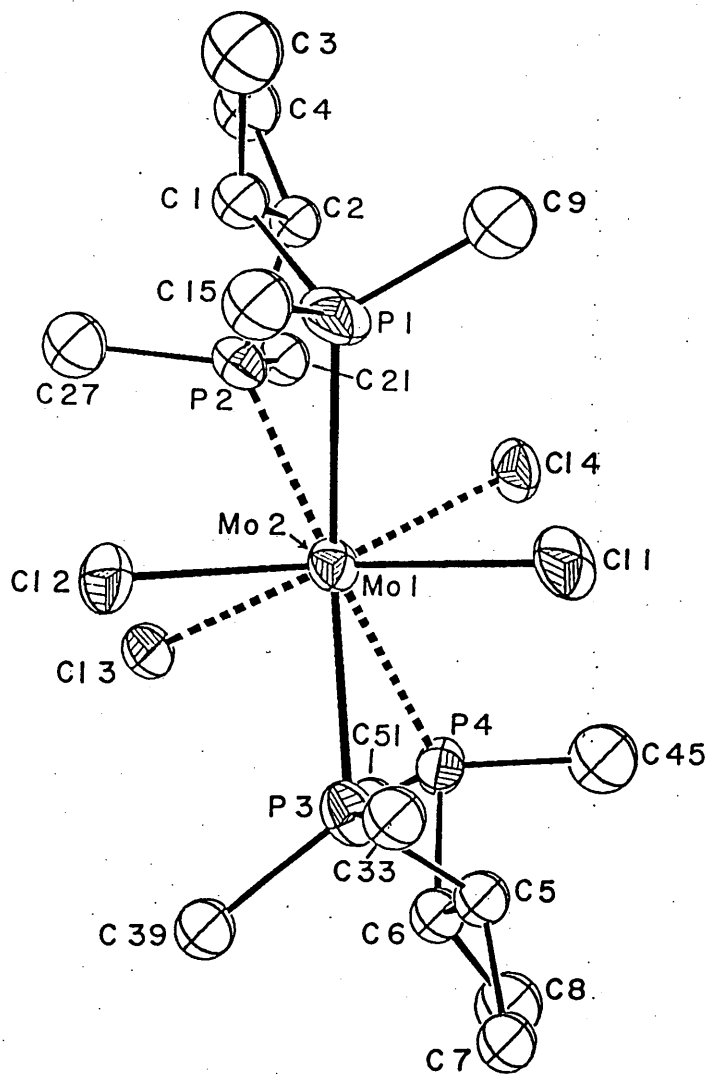


Figure 5.15 View down the Mo-Mo bond of $\beta\text{-Mo}_2\text{Cl}_4(\text{S,S-dppb})_2$.

group on the ligand backbone. Figure 5.16 shows the absorption and cd spectra of $\beta\text{-Mo}_2\text{Cl}_4(\text{R-phenphos})_2$ in dichloromethane. Table 5.1 lists the $\delta\text{-}\delta^*$ and $\delta\text{-}d_{x^2-y^2}$ transition energies and g values for a multitude of quadruply bonded dimolybdenum complexes containing diphosphine or diamine ligands. The signs and magnitudes of these values are very similar for $\beta\text{-Mo}_2\text{Cl}_4(\text{R-dppp})_2$ and $\beta\text{-Mo}_2\text{Cl}_4(\text{R-phenphos})_2$. This means that both of these complexes will have very similar configurations. Thus $\beta\text{-Mo}_2\text{Cl}_4(\text{R-phenphos})_2$ will have a Δ configuration with a twist of approximately 27° . There appears to be very little difference when the methyl is replaced by the phenyl, indicating that the phenyl group also tightens the twist angle when compared to $\beta\text{-Mo}_2\text{Cl}_4(\text{dppe})_2$.

7.2 $\beta\text{-Mo}_2\text{Cl}_4(\text{S,S-skewphos})_2$

The complex $\beta\text{-Mo}_2\text{Cl}_4(\text{S,S-skewphos})_2$ was synthesised with some considerable difficulty since it is very air sensitive. The most intriguing property of this complex is its behaviour in different solvents. The electronic absorption and cd spectra of $\beta\text{-Mo}_2\text{Cl}_4(\text{S,S-skewphos})_2$ in dichloromethane and methanol are shown in figures 5.17 and 5.18 respectively. The spectra in dichloromethane are similar to those of $\beta\text{-Mo}_2\text{Cl}_4(\text{S,S-dppb})_2$ (see table 5.1). Therefore in this solvent the complex appears to be a

Table 5.1 Energies ($\tilde{\nu}$) and g values for the δ - δ^* and δ - $d_{x^2-y^2}$ transitions of chiral dimolybdenum complexes in CH_2Cl_2 (except * in MeOH and † in MeCN)

	δ - δ^*		δ - $d_{x^2-y^2}$		ref.
	$\tilde{\nu}$ ($\times 10^{-3}$ cm^{-1})	g ($\times 10^3$)	$\tilde{\nu}$ ($\times 10^{-3}$ cm^{-1})	g ($\times 10^2$)	
β -[Mo ₂ Cl ₄ (S,S-dppb) ₂]	13.70	-5.8	21.05	+7.3	93
β -[Mo ₂ Cl ₄ (R-dppp) ₂]	13.33	+7.5	21.74	-6.7	129
β -[Mo ₂ Cl ₄ (R-phenphos) ₂]	13.20	+6.0	21.51	-6.2	this work
β -[Mo ₂ Cl ₄ (S-chairphos) ₂]	14.33	-2.0	21.28	+1.1	101
β -[Mo ₂ Cl ₄ (S,S-skewphos) ₂]	13.89	-10.8	20.83	+3.7	this work
β -[Mo ₂ Br ₄ (S,S-dppb) ₂]	13.24	-3.2	20.70	+8.5	129
β -[Mo ₂ Br ₄ (R-dppp) ₂]	12.82	+3.0	20.83	-4.5	129
β -[Mo ₂ (R-pn) ₄] ⁴⁺	20.96	-9.1	27.78	+17.0	111
β -[Mo ₂ Cl ₄ (S,S-skewphos) ₂]*	16.13	-6.4	21.19	+3.1	this work
[Mo ₂ (OAc) ₂ (S,S-dppb)(MeCN) ₂] ²⁺ †	18.79	+0.3	-	-	this work
[Mo ₂ (OAc) ₂ (S,S-dppb) ₂] ²⁺ †	20.32	+1.1	-	-	this work
[Mo ₂ (OAc) ₂ (R-pn)(MeCN) ₂] ²⁺ †	20.83	+0.4	-	-	this work
[Mo ₂ (OAc) ₂ (R-pn) ₂] ²⁺ †	21.32	+0.5	-	-	this work

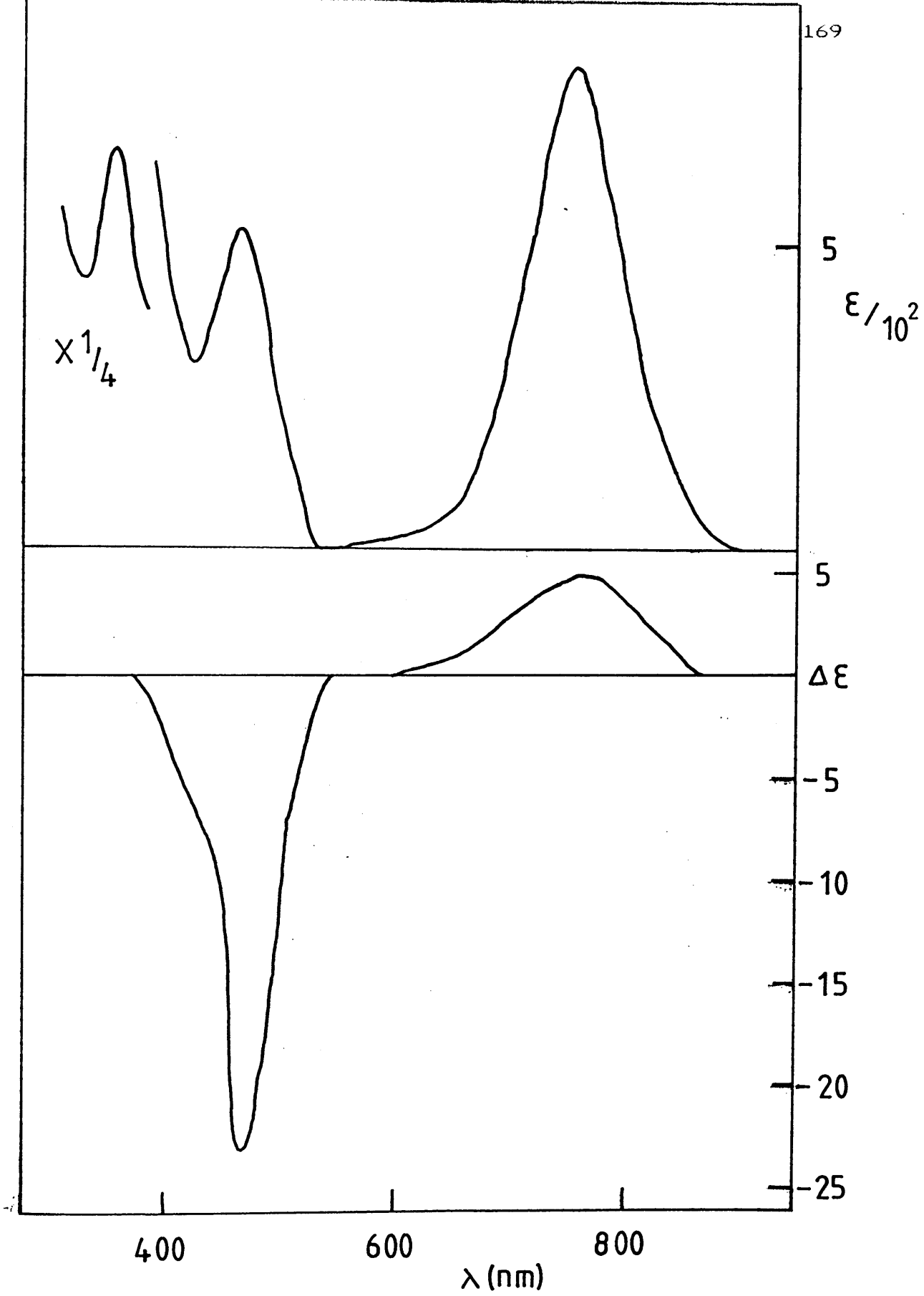


Figure 5.16 Absorption and cd spectra of $\beta\text{-Mo}_2\text{Cl}_4(\text{R-phenphos})_2$ in CH_2Cl_2 .

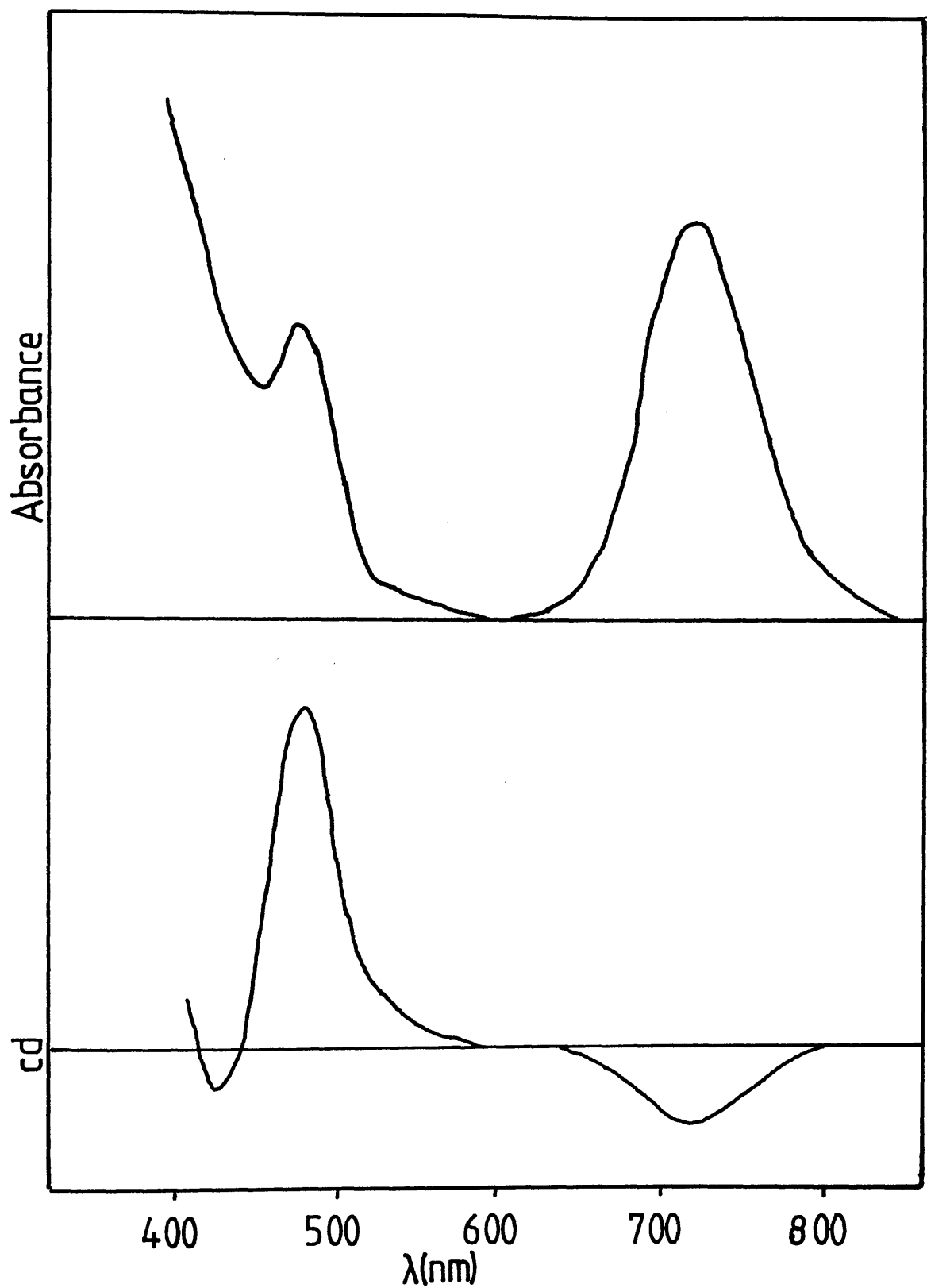


Figure 5.17 Absorption and cd spectra of $\beta\text{-Mo}_2\text{Cl}_4(\text{S,S-skewphos})_2$ in CH_2Cl_2 .

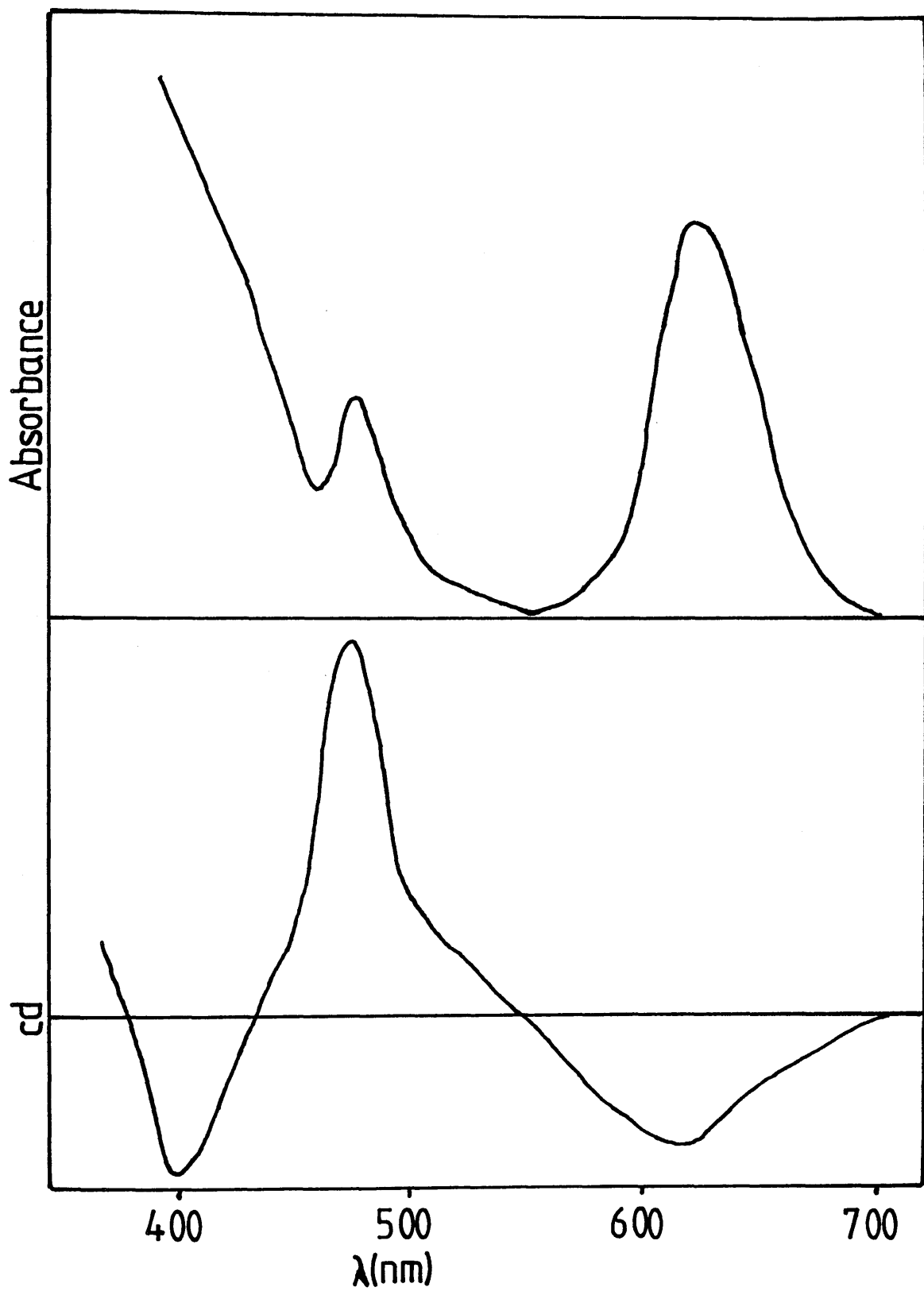


Figure 5.18 Absorption and cd spectra of $\beta\text{-Mo}_2\text{Cl}_4(\text{S,S-skewphos})_2$ in CH_3OH .

typically staggered β isomer. In methanol, β - $\text{Mo}_2\text{Cl}_4(\text{S,S-skewphos})_2$ displays a δ - δ^* transition at a high energy ($16.13 \times 10^3 \text{ cm}^{-1}$), there is no question of this being an α isomer because there is a significant g factor for this transition which is comparable to other staggered β isomers. Therefore it appears that there are two distinct β isomers of $\text{Mo}_2\text{Cl}_4(\text{S,S-skewphos})_2$, each one stabilised by a different solvent. The two β isomers have a large energy difference between the respective δ - δ^* transitions but the signs of the cd spectra are the same. The negative cd signals under the δ - δ^* transitions indicate that either β isomer can have a Δ configuration with twist angle between 45° and 90° , or a Λ configuration with twist angle between 0° and 45° . There appears to be stable conformations in both of these sectors because of the flexibility of the bridging rings due to the long ligand backbone. A study of scale models indicates a stable rotameric form in the Δ configuration with a twist angle of about 70° , here the seven membered rings take up a chair type conformation with all four methyls in equatorial positions. From the plot of δ - δ^* transition energies vs $\cos 2X$ for this family of complexes, then the β isomer of $\text{Mo}_2\text{Cl}_4(\text{S,S-skewphos})_2$ in dichloromethane is predicted to have a configuration of $\Lambda(22^\circ)$ or $\Delta(68^\circ)$. From the discussion above on scale models, the latter configuration appears a good candidate. The β isomer present in methanol has a very high δ - δ^*

transition energy, in fact the above plot predicts a twist of 0° or 90° . This cannot be the case as the magnitude of the g factor indicates considerable staggering from the eclipsed conformation. Obviously this illustrates the unreliability of some of the plots concerning the δ overlap and shows the limitations of predicting X from the δ - δ^* transition energy. Therefore the methanol isomer is staggered but not as much as the other β isomer (because of the smaller g factor). This is the first example of different rotamers of this type being stabilised in different solvents, although this phenomenon has been observed in the solid state (cf. β - $\text{Mo}_2\text{I}_4(\text{dppe})_2$).

7.3 β - $\text{Mo}_2\text{Cl}_4(\text{DIOP})_2$

β - $\text{Mo}_2\text{Cl}_4(\text{DIOP})_2$ displays similar properties to that of β - $\text{Mo}_2\text{Cl}_4(\text{S,S-skewphos})_2$. The former complex is very air sensitive and soluble in a number of solvents. The DIOP ligand has a very long backbone, P-C-C-C-C-P, therefore the eight membered bridging rings formed across the dimolybdenum unit are expected to be quite flexible. The absorption and cd spectra of β - $\text{Mo}_2\text{Cl}_4(\text{DIOP})_2$ in various solvents indicate that more than one species is present in each solution. This is not surprising because in large ring systems there will be little energy difference between various conformers. Therefore the flexibility of the eight membered ring means that no one conformation is

dominant and several rotamers can exist in the same solvent.

7.4 $[\text{Mo}_2(\text{O}_2\text{CCH}_3)_2(\text{S,S-dppb})_x(\text{CH}_3\text{CN})_{4-2x}]^{2+}$ ($x = 1$ or 2)

Very interesting properties arise from the spectra of the cations, $[\text{Mo}_2(\text{O}_2\text{CCH}_3)_2(\text{S,S-dppb})(\text{CH}_3\text{CN})_2]^{2+}$ and $[\text{Mo}_2(\text{O}_2\text{CCH}_3)_2(\text{S,S-dppb})_2]^{2+}$, both of which have not been fully purified and are air sensitive. The former cation is thought to contain the acetate groups in a cis arrangement while the latter will probably have a trans acetate structure. These structural assignments are made on the basis of similarities between the spectra of these cations with other complexes (see chp 4). Both complexes definitely have the chiral diphosphine ligands attached in a bridging structure because each cation has a measurable cd signal under the respective δ - δ^* transition.

The electronic absorption and cd spectra of $[\text{Mo}_2(\text{O}_2\text{CCH}_3)_2(\text{S,S-dppb})(\text{CH}_3\text{CN})_2]^{2+}$ and $[\text{Mo}_2(\text{O}_2\text{CCH}_3)_2(\text{S,S-dppb})_2]^{2+}$ are shown in figures 5.19 and 5.20 respectively. Table 5.1 shows that the magnitudes of the δ - δ^* transitions of the two cations being discussed are relatively small compared to that of $\beta\text{-Mo}_2\text{Cl}_4(\text{S,S-dppb})_2$. This is not unexpected because $[\text{Mo}_2(\text{O}_2\text{CCH}_3)_2(\text{S,S-dppb})_2]^{2+}$ will have a very similar structure to $[\text{Mo}_2(\text{O}_2\text{CCH}_3)_2(\text{dmpe})_2]^{2+}$ which is eclipsed.

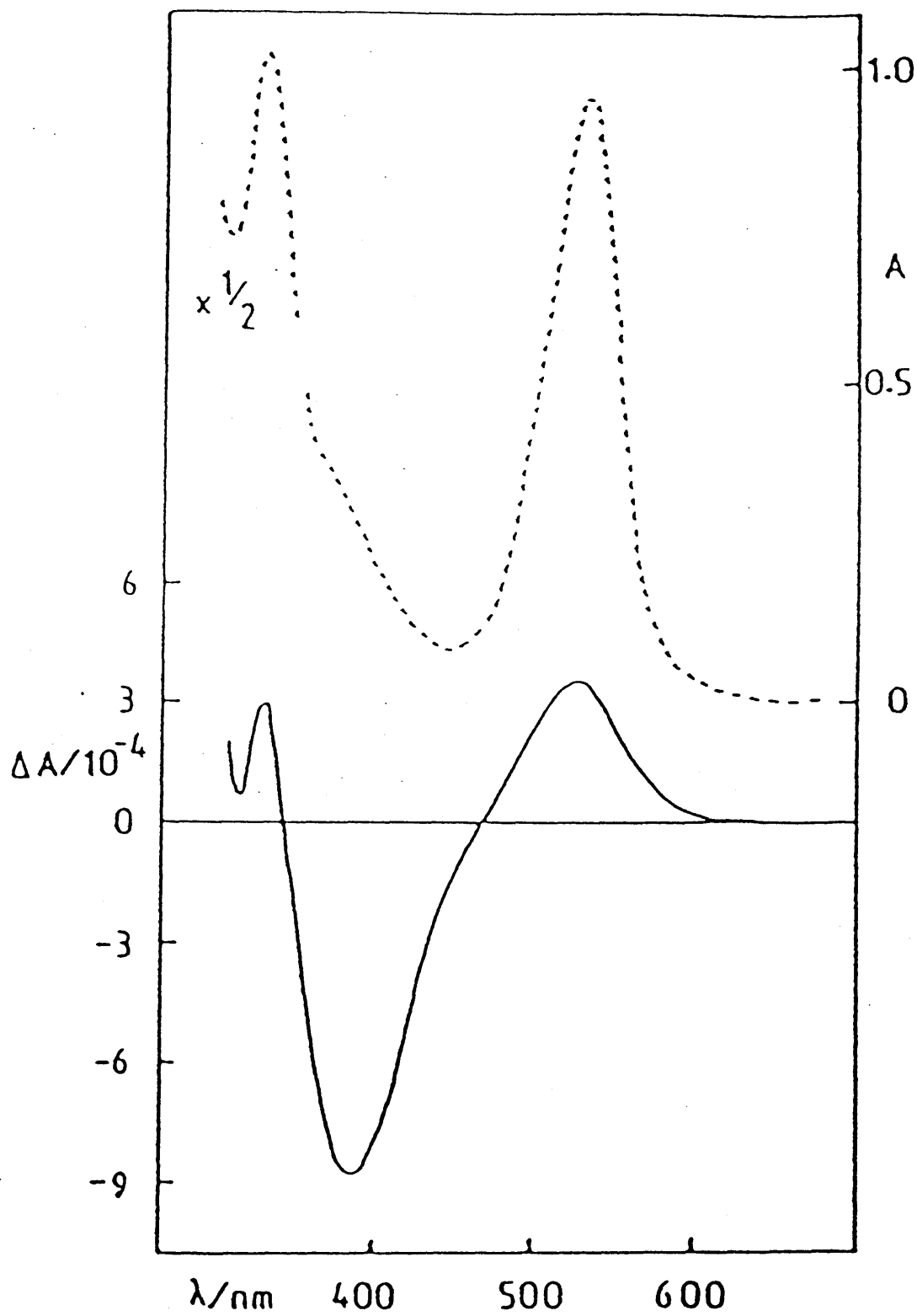


Figure 5.19 Absorption and cd spectra of $[\text{Mo}_2(\text{O}_2\text{CCH}_3)_2(\text{S,S-dppb})(\text{CH}_3\text{CN})_2]^{2+}$ in CH_3CN .

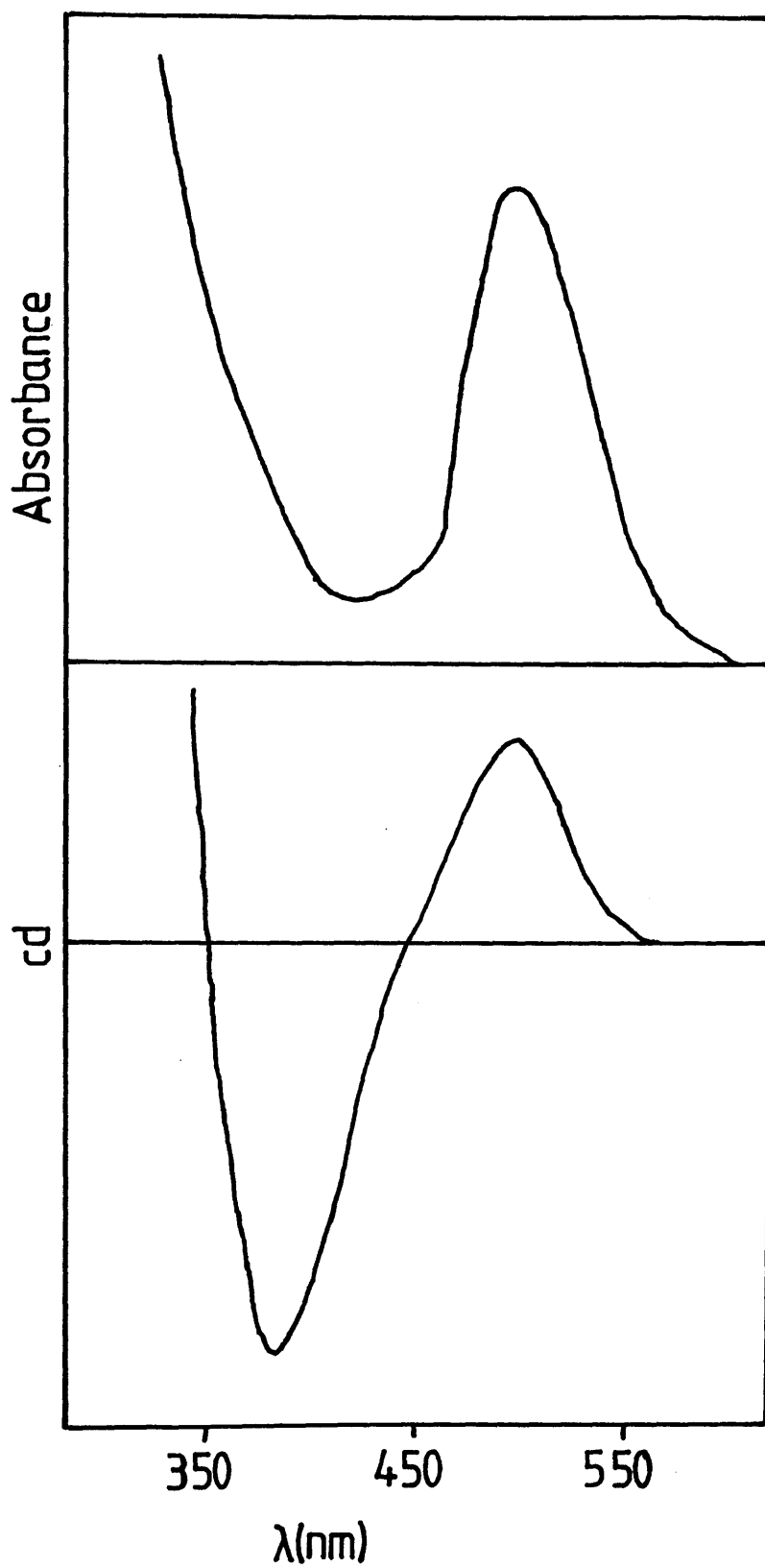


Figure 5.20 Absorption and cd spectra of $[\text{Mo}_2(\text{O}_2\text{CCH}_3)_2(\text{S,S-dppb})_2]^{2+}$ in CH_3CN .

Therefore it might have been expected that $[\text{Mo}_2(\text{O}_2\text{CCH}_3)_2(\text{S,S-dppb})_2]^{2+}$ would show no optical activity under the $\delta\text{-}\delta^*$ transition. The fact that it does means that it must be twisted by a few degrees, but the rigid eclipsing effect of the acetate groups means that it can be no more than this.

The most striking aspect of the spectra of these two cations is that the signs of the $\delta\text{-}\delta^*$ and the $\delta\text{-}d_{x^2-y^2}$ transitions are both opposite to those observed for $\beta\text{-Mo}_2\text{Cl}_4(\text{S,S-dppb})_2$. As the twist will only be a few degrees in both of the cations and the sign of the $\delta\text{-}\delta^*$ transition is positive, then from the sector rule (figure 5.3) both cations must have the Δ configuration. This is opposite to $\beta\text{-Mo}_2\text{Cl}_4(\text{S,S-dppb})_2$ which has a Λ configuration. The conformations of the bridging rings in $[\text{Mo}_2(\text{O}_2\text{CCH}_3)_2(\text{S,S-dppb})_2]^{2+}$ will be similar to those in $[\text{Mo}_2(\text{O}_2\text{CCH}_3)_2(\text{dmpe})_2]^{2+}$ as in figure 4.5. Scale models show that the $\Delta(\lambda\lambda)$ configuration (the λ 's apply only to the six membered rings, the rings formed by the acetates are ignored) with a twist of only a few degrees has all four methyls in the axial position. However $\Delta(\delta\delta)$ with a small twist has all four methyls equatorial. This latter configuration ties in with the observed spectra and appears free of any steric congestion. However the $\Lambda(\delta\delta)$ configuration with a small twist appears equally stable and also has all four methyls equatorial, although this

would give rise to a negative cd signal under the δ - δ^* transition. As yet there is no apparent reason why the $\Delta(\delta\delta)$ configuration is preferred. The $[\text{Mo}_2(\text{O}_2\text{CCH}_3)_2(\text{S,S-dppb})(\text{CH}_3\text{CN})_2]^{2+}$ cation has a very similar cd spectrum to $[\text{Mo}_2(\text{O}_2\text{CCH}_3)_2(\text{S,S-dppb})_2]^{2+}$, therefore the former complex will have a $\Delta(\delta)$ configuration. The g factor for $[\text{Mo}_2(\text{O}_2\text{CCH}_3)_2(\text{S,S-dppb})_2]^{2+}$ is significantly larger than the monophosphine cation, this is probably due to the greater staggering effect of the two S,S-dppb ligands which together can exert a greater twist than a single one.

7.5 $[\text{Mo}_2(\text{O}_2\text{CCH}_3)_2(\text{R-pn})_x(\text{CH}_3\text{CN})_{4-2x}]^{2+}$ (x = 1 or 2)

The first quadruply bonded dimolybdenum complex to be made containing a diamine ligand was $\text{Mo}_2(\text{en})_4\text{Cl}_4$ ¹¹⁰. As stated in the Introduction, this complex was initially predicted as having chelating ligands present (figure 1.15(a)) rather than bridging ligands (figure 1.15(b)). The methylated derivative, $\text{Mo}_2(\text{R-pn})_4\text{Cl}_4$ ¹¹¹, has since been made and this complex displays a strong cd signal under the δ - δ^* transition. This evidence is indicative of a twisted structure with bridging ligands rather than a conformation with chelating ligands which would tend to have an eclipsed structure. It is expected that $\text{Mo}_2(\text{en})_4\text{Cl}_4$ has a similar structure.

When $[\text{Mo}_2(\text{O}_2\text{CCH}_3)_2(\text{CH}_3\text{CN})_6][\text{BF}_4]_2$ is reacted with R-pn in acetonitrile, an air sensitive complex is obtained. The electronic absorption and cd spectra of this complex are shown in figure 5.21. The g factor for the δ - δ^* transition of this complex (4×10^{-4}) is very small compared to $\text{Mo}_2(\text{R-pn})_4\text{Cl}_4$ (see table 5.1). The measurable cd signal indicates that there is at least one bridging R-pn ligand present. The twist angle will be very small because of the eclipsing nature of the acetate groups. In the ir spectrum of this complex, acetonitrile is present (at 2100 cm^{-1}) thus the formula of this species is most likely to be $[\text{Mo}_2(\text{O}_2\text{CCH}_3)_2(\text{R-pn})(\text{CH}_3\text{CN})_2][\text{BF}_4]_2$. The elemental analysis of this complex is poor as with other complexes in this series. The structure is expected to be similar to that of the $[\text{Mo}_2(\text{O}_2\text{CCH}_3)_2(\text{S,S-dppb})(\text{CH}_3\text{CN})_2]^{2+}$ cation.

The reaction of $\text{Mo}_2(\text{O}_2\text{CCH}_3)_4$ with R-pn in the presence of $[\text{Me}_3\text{O}][\text{BF}_4]$ produces a golden yellow solution. The electronic absorption and cd spectra of this solution are shown in figure 5.22. This solution is plagued with $\text{Mo}_2(\text{O}_2\text{CCH}_3)_4$ impurity, however the δ - δ^* transition appears at slightly higher energy than $[\text{Mo}_2(\text{O}_2\text{CCH}_3)_2(\text{R-pn})(\text{CH}_3\text{CN})_2]^{2+}$, possibly indicating more extensive substitution. The reactions of R-pn with $\text{Mo}_2(\text{O}_2\text{CCH}_3)_4$ and the $[\text{Mo}_2(\text{O}_2\text{CCH}_3)_2(\text{CH}_3\text{CN})_6]^{2+}$ cation appear to be analogous with those for the S,S-dppb. Thus the golden yellow solution will almost certainly contain the $[\text{Mo}_2(\text{O}_2\text{CCH}_3)_2(\text{R-pn})_2]^{2+}$ cation.

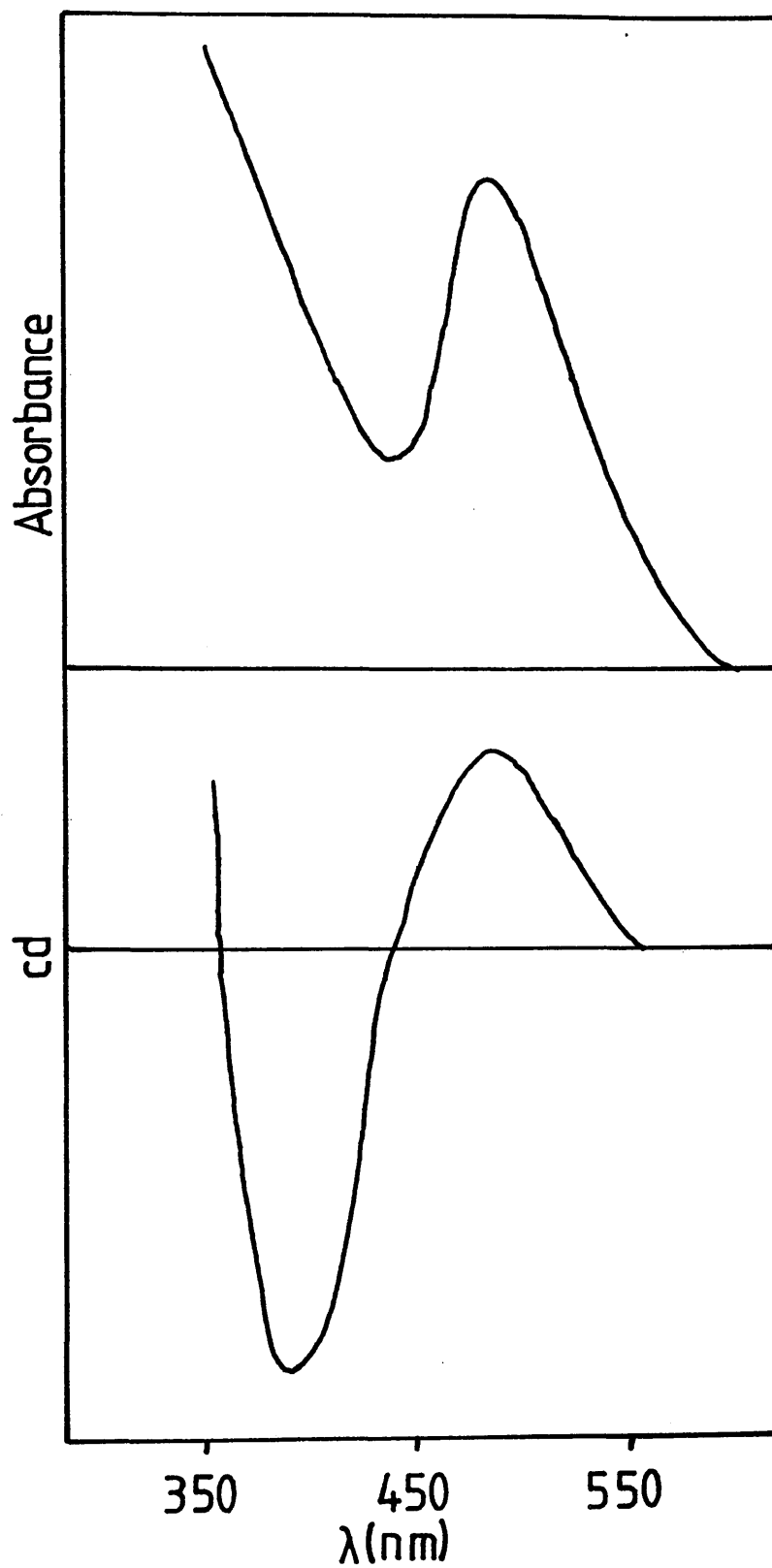


Figure 5.21 Absorption and cd spectra of $[\text{Mo}_2(\text{O}_2\text{CCH}_3)_2(\text{R-pn})(\text{CH}_3\text{CN})_2]^{2+}$ in CH_3CN .

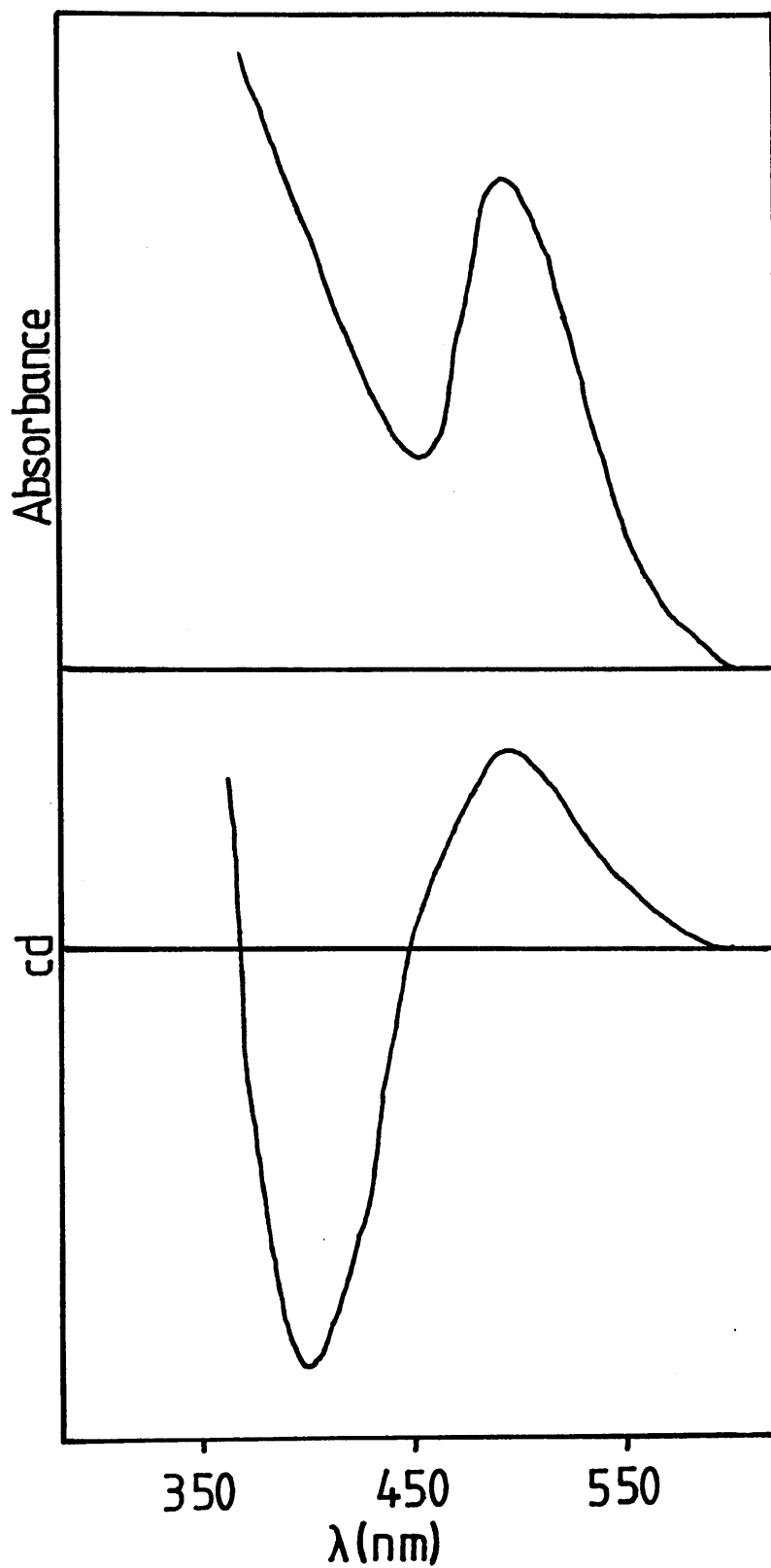


Figure 5.22 Absorption and cd spectra of $[\text{Mo}_2(\text{O}_2\text{CCH}_3)_2(\text{R-pn})_2]^{2+}$ in CH_3CN .

The sign of the cd signal under the δ - δ^* transition for both $[\text{Mo}_2(\text{O}_2\text{CCH}_3)_2(\text{R-pn})(\text{CH}_3\text{CN})_2]^{2+}$ and $[\text{Mo}_2(\text{O}_2\text{CCH}_3)_2(\text{R-pn})_2]^{2+}$ is positive. The sign of the cd under the same transition for $\text{Mo}_2(\text{R-pn})_4\text{Cl}_4$ is negative and this complex is predicted to have a Δ configuration with twist angle of between 45° and 90° . Since both cations being discussed must have very small twists, then they will also have the Δ configuration as derived from the sector rule (figure 5.3). In fact the configurations of these cations should be almost identical to the analogous S,S-dppb complexes. The most surprising fact is that R-pn does not react with $[\text{Mo}_2(\text{O}_2\text{CCH}_3)_2(\text{CH}_3\text{CN})_6]^{2+}$ to give the trans bis R-pn complex, as R-pn is a small ligand and might be expected to react in the same manner as the dmpe ligand.

REFERENCES

1. Cotton F.A., Curtis N.F., Harris C.B., Johnson B.F.G., Lippard S.J., Mague J.T., Robinson W.R., Wood J.S., Science, 1964, 145, 1305.
2. Cotton F.A., Inorg. Chem., 1965, 4, 334.
3. Cotton F.A., Harris C.B., Inorg. Chem., 1965, 4, 330.
4. Cotton F.A., Walton R.A., "Multiple Bonds Between Metal Atoms", Wiley Interscience, 1982, p.29.
5. Garner C.D., Senior R.G., J.Chem.Soc.Chem.Commun., 1974, 580.
6. Matson M.S., Wentworth R.A.D., J.Amer.Chem.Soc., 1974, 96, 7837.
7. Garner C.D., Senior R.G., King T.J., J.Amer.Chem.Soc., 1976, 98, 3526.
8. Katovic V., Templeton J.L., Hoxmeier R.J., J.Amer.Chem.Soc., 1975, 97, 5300.
9. Katovic V., McCarley R.E., J.Amer.Chem.Soc., 1978, 100, 5586.
10. Cotton F.A., Hanson B.E., Inorg.Chem., 1978, 17, 3237.
11. Bursten B.E., Cotton F.A., Cowley A.H., Hanson B.E., Lattman M., Staneley G.G., J.Amer.Chem.Soc., 1979, 101, 6244.
12. Cotton F.A., Walton R.A., "Multiple Bonds Between Metal Atoms", Wiley Interscience, 1982, p.18.

13. Gray H.B., Trogler W.C., Acc.Chem.Res., 1978, 11, 232.
14. Brencic J.V., Cotton F.A., Inorg.Chem., 1969, 8, 7.
15. Cotton F.A., Walton R.A., "Multiple Bonds Between Metal Atoms", Wiley Interscience, 1982, p.342.
16. Cotton F.A., Fanwick P.E., Fitch J.W., Glicksman H.D., Walton R.A., J.Amer.Chem.Soc., 1979, 100, 1752.
17. Chisholm M.H., Cotton F.A., Acc.Chem.Res., 1978, 11, 356.
18. Cotton F.A., Frenz B.A., Ebner J.R., Walton R.A., J.Chem.Soc.Chem.Commun., 1974, 4.
19. Cotton F.A., Frenz B.A., Ebner J.R., Walton R.A., Inorg.Chem., 1976, 15, 1630.
20. Agaskar P.A., Cotton F.A., Dunbar K.R., Falvello L.R., Tetrack S.M., Walton R.A., J.Amer.Chem.Soc., 1986, 108, 4850.
21. Fanwick P.E., Tetrack S.M., Walton R.A., Inorg.Chem., 1986, 25, 4546.
22. Mulliken R.S., J.Chem.Phys., 1939, 7, 20.
23. Campbell F.L.III, Cotton F.A., Powell G.L., Inorg.Chem., 1985, 24, 177.
24. Hopkins M.D., Zietlow T.C., Miskowski V.M., Gray H.B., J.Amer.Chem.Soc., 1985, 107, 510.
25. Hopkins M.D., Gray H.B., J.Amer.Chem.Soc., 1984, 106, 2468.

26. Hopkins M.D., Schaefer W.P., Bronikowski M.J., Woodruff W.H., Miskowski V.M., Dallinger R.F., Gray H.B., J.Amer.Chem.Soc., 1987, 109, 408.
27. Hopkins M.D., Gray H.B., Miskowski V.M., Polyhedron, 1987, 6, 705.
28. Fanwick P.E., Martin D.S., Cotton F.A., Webb T.R., Inorg.Chem., 1977, 16, 2103.
29. Clark R.J.H., Franks M.L., J.Amer.Chem.Soc., 1975, 97, 2691.
30. Slater J.C., Adv.Quantum.Chem., 1972, 6, 1.
31. Johnson K.H., Adv.Quantum.Chem., 1973, 7, 143.
32. Rosch N., Klemperer W.G., Johnson K.H., Chem.Phys.Letts., 1973, 23, 149.
33. Case D.A., Annu.Rev.Phys.Chem., 1982, 33, 151.
34. Mortola A.P., Moskowitz J.W., Rosch N., Int.J.Quantum.Chem., Symposium No.8, 1974, 161.
35. Norman J.G.Jnr., Kolari H.J., J.Chem.Soc.Chem.Comm., 1974, 303.
36. Norman J.G.Jnr., Kolari H.J., J.Amer.Chem.Soc., 1975, 97, 33.
37. Norman J.G.Jnr., Kolari H.J., J.Chem.Soc.Chem.Comm., 1975, 649.
38. Mortola A.P., Moskowitz J.W., Rosch N., Cowman C.D., Gray H.B., Chem.Phys.Letts., 1975, 32, 283.
39. Cotton F.A., Kalbacher B.J., Inorg.Chem., 1977, 16, 2386.

40. Norman J.G.Jnr., Kolari H.J., Gray H.B., Trogler W.C., Inorg.Chem., 1977, 16, 987.
41. Cotton F.A., Stanley G.G., Inorg.Chem., 1977, 16, 2668.
42. Block T.F., Fenske R.F., Lichtenberger D.L., Cotton F.A., J.Coord.Chem., 1978, 8, 109.
43. Benard M., J.Amer.Chem.Soc., 1978, 100, 2354.
44. Cotton F.A., Extine M.W., J.Amer.Chem.Soc., 1978, 100, 3788.
45. Bursten B.E., Cotton F.A., Fanwick P.E., Stanley G.G., J.Amer.Chem.Soc., 1980, 102, 4579.
46. Cotton F.A., Hubbard J.L., Lichtenberger D.L., Shim I., J.Amer.Chem.Soc., 1982, 104, 679.
47. Bursten B.E., Cotton F.A., Fanwick P.E., Stanley G.G., J.Amer.Chem.Soc., 1983, 105, 3082.
48. Bursten B.E., Cotton F.A., Fanwick P.E., Stanley G.G., Walton R.A., J.Amer.Chem.Soc., 1983, 105, 2606.
49. Arratia-Perez R., Case D.A., Inorg.Chem., 1984, 23, 3271.
50. Noodleman L., Norman J.G.Jnr., J.Chem.Phys., 1979, 70, 4903.
51. Cotton F.A., Norman J.G.Jnr., Stults B.R., Webb T.R., J.Coord.Chem., 1976, 5, 217.
52. Robbin G.A., M.S. thesis, Iowa State University, Ames, Iowa, 1978.

53. Cotton F.A., Mester Z.C., Webb T.R.,
Acta.Crystallogr., 1974, B30, 2768.
54. Cotton F.A., Normam J.G.Jnr., J.Coord.Chem., 1971, 1,
161.
55. Cotton F.A., Norman J.G.Jnr., J.Amer.Chem.Soc., 1972,
94, 5967.
56. Cotton F.A., Extine M.W., Gage L.D., Inorg.Chem.,
1978, 17, 172.
57. Collins D.M., Cotton F.A., Murillo C.A., Inorg.Chem.,
1976, 15, 2950.
58. Cotton F.A., Mott G.N., Organomett., 1982, 1, 302.
59. Lamotte J., Dideberg D., Dupont L., Durbut P.,
Cryst.Struct.Commun., 1981, 10, 59.
60. Garner C.D., Parkes S., Walton I.B., Clegg W.,
Inorg.Chim.Acta, 1978, 31, L451.
61. Potenza J.A., Johnson R.J., San Filippo J.Jnr.,
Inorg.Chem., 1976, 15, 2215.
62. Cotton F.A., Polyhedron, 1985, 4, 1669.
63. Cotton F.A., Fanwick P.E., Inorg.Chem., 1983, 22,
1327.
64. Arenivar J.D., Mainz V.V., Ruben H., Andersen R.A.,
Zalkin A., Inorg.Chem., 1982, 21, 2649.
65. Green M.L.H., Parkin G., Bashkin J., Fail J., Prout
K., J.Chem.Soc.Dal.Trans., 1982, 2519.
66. Cotton F.A., Ilsley W.H., Kaim W., Inorg.Chem., 1981,
20, 930.

67. Girolami G.S., Mainz V.V., Andersen R.A.,
J.Amer.Chem.Soc., 1982, 104, 2041.
68. Agaskar P.A., Cotton F.A., Inorg.Chim.Acta, 1984,
83, L33.
69. Collins D.M., Cotton F.A., Murillo C.A., Inorg.Chem.,
1976, 15, 1861.
70. Cotton F.A., Ilsley W.H., Kaim W., Inorg.Chim.Acta,
1979, 37, L267.
71. Cotton F.A., Reid A.H.Jnr., Schwotzer W.,
Inorg.Chem., 1985, 24, 3965.
72. Pimblett G., Garner C.D., Clegg W.,
J.Chem.Soc.Dal.Trans., 1986, 1257.
73. Abel E.W., Singh A., Wilkinson G., J.Chem.Soc., 1959,
3097.
74. Bannister E., Wilkinson G., Chem. and Ind., 1960,
319.
75. Stephenson T.A., Bannister E., Wilkinson G.,
J.Chem.Soc., 1964, 2538.
76. Holste G., Schafer H., Z.Anorg.Allg.Chem., 1972, 391,
263.
77. Holste G., Z.Anorg.Allg.Chem., 1975, 414, 81.
78. Hochberg E., Walks P., Abbott E.H, Inorg.Chem., 1974,
13, 1824.
79. Brignole E., Cotton F.A., Inorg.Synth., 1972, 13, 81.
80. Lawton D., Mason R., J.Amer.Chem.Soc., 1965, 87, 921.
81. Andersen R.A., Sheldon J.C., Aust.J.Chem., 1965, 18,
271.

82. Cotton F.A., Extine M.W., Felthouse T.R., Kolthammer B.W.S., Lay D.G., J.Amer.Chem.Soc., 1981, 103; 4040.
83. Abbott E.H., Bose K.S., Cotton F.A., Hall W.T., Sekutowski J.C., Inorg.Chem., 1978, 17, 3240.
84. Campbell F.L.III, Cotton F.A., Powell G.L., Inorg.Chem., 1984, 23, 4222.
85. Cotton F.A., Falvello L.R., Harwood W.S., Powell G.L., Walton R.A., Inorg.Chem., 1986, 25, 3949.
86. Cotton F.A., Dunbar K.R., Poli R., Inorg.Chem., 1986, 25, 3700.
87. Agaskar P.A., Cotton F.A., Inorg.Chem., 1986, 25, 15.
88. Agaskar P.A., Cotton F.A., Inorg.Chem., 1984, 23, 3383.
89. Agaskar P.A., Cotton F.A., Derringer D.R., Powell G.L., Root D.R., Smith T.J., Inorg.Chem., 1985, 24, 2786.
90. Cotton F.A., Dunbar K.R., Matusz M., Inorg.Chem., 1986, 25, 3641.
91. Cotton F.A., Powell G.L., Inorg.Chem., 1983, 22, 1507.
92. Campbell F.L.III, Cotton F.A., Powell G.L., Inorg.Chem., 1985, 24, 4384.
93. Agaskar P.A., Cotton F.A., Fraser I.F., Peacock R.D., J.Amer.Chem.Soc., 1984, 106, 1851.
94. Agaskar P.A., Cotton F.A., Fraser I.F., Peacock R.D., Muir K., Manlovich-Muir Lj., Inorg.Chem., 1986, 25, 2511.

95. Aitchison A.A., unpublished results.
96. Cotton F.A., Felthouse T.R., Inorg.Chem., 1981, 20, 3880.
97. Cotton F.A., Felthouse T.R., Lay D.G., J.Amer.Chem.Soc., 1980, 102, 1431.
98. Barder T.J., Cotton F.A., Dunbar K.R., Powell G.L., Schwotzer W., Walton R.A., Inorg.Chem., 1985, 24, 2550.
99. Cole N.F., Cotton F.A., Powell G.L., Smith T.J., Inorg.Chem., 1983, 22, 2618.
100. Fraser I.F., McVitie A., Peacock R.D., J.Chem.Res., 1984, 420.
101. Christie S., Fraser I.F., McVitie A., Peacock R.D., Polyhedron, 1986, 5, 35.
102. Cotton F.A., Shive L.W., Stults B.R., Inorg.Chem., 1976, 15, 2239.
103. Bakir M., Cotton F.A., Simpson C., Walton R.A., unpublished results.
104. Anderson L.B., Bakir M., Walton R.A., Polyhedron, to be published.
105. Cotton F.A., Niswander R.H., Sekutowski J.C., Inorg.Chem., 1978, 17, 3541.
106. Cotton F.A., Inglis T., Kiluer M., Webb T.R., Inorg.Chem., 1975, 14, 2023.
107. Cotton F.A., Ilsley W.H., Inorg.Chem., 1981, 20, 572.
108. Cotton F.A., Rice G.W., Sekutowski J.C., Inorg.Chem., 1979, 18, 1143.

109. Chakravarty A.R., Cotton F.A., Shamsoum E.S.,
Inorg.Chem., 1984, 23, 4216.
110. Bowen A.R., Taube H., Inorg.Chem., 1974, 13, 2245.
111. Fraser I.F., Peacock R.D., Inorg.Chem., 1985, 24,
988.
112. Yang C.H., Dzugan S.J., Goedken V.L.,
J.Chem.Soc.Chem.Comm., 1986, 1313.
113. Mandon D., Giraudon J-M., Toupet L., Sala-Pala J.,
Guerchais J.E., J.Amer.Chem.Soc., 1987, 109, 3490.
114. Mayer J.M., Abbott E.,H., Inorg.Chem., 1983, 22,
2774.
115. Abbott E.H., Schoenewolf F.Jnr., Backstrom T.,
J.Coord.Chem., 1974, 3, 255.
116. Cotton F.A., Reid A.H.Jnr., Schwotzer W., unpublished
results.
117. Cotton F.A., Stanley G.G., Walton R.A., Inorg.Chem.,
1978, 17, 2099.
118. Cotton F.A., private communication.
119. Cotton F.A., Norman J.G.Jnr., J.Coord.Chem., 1971, 1,
161.
120. Brencic J.V., Cotton F.A., Inorg.Chem., 1970, 9, 351.
121. King R.B., Bakos J., Hoff C.D., Marko L.,
J.Org.Chem., 1979, 44, 1729.
122. MacNeil P.A., Roberts N.K., Bosnich B.,
J.Amer.Chem.Soc., 1981, 103, 2273.
123. Abbott E.H., Schoenewolf F.Jnr., Backstrom T.,
J.Coord.Chem., 1974, 3, 255

- 124 Walker N., Stuart D., Acta Crystallogr.Sect.A;
Found.Crystallogr., 1983, 39A, 158.
- 125 Gilmore C.J., J.Appl.Crystallogr., 1984, 17, 42.
- 126 International Tables for X-Ray Crystallography;
Kynoch Press; Birmingham, 1974; Vol. 4.
- 127 Mallinson P.R., Muir K.W., J.Appl.Crystallogr., 1985,
18, 51.
- 128 San Filippo J.Jnr., Snaidoch H.J., Grayson R.L.,
Inorg.Chem., 1974, 13, 2121.
- 129 Fraser I.F., Ph.D. thesis, University of Glasgow,
Glasgow, 1985.
- 130 Basolo F., Pearson R.G., "Mechanisms of Inorganic
Reactions", Second Edition, Wiley, 1967, p.316.
- 131 Johnson B.F.G., J.Chem.Soc.Chem.Commun., 1976, 703.
- 132 Dorn H., Hanson B.E., Motell E., Inorg.Chim.Acta,
1981, 54, L71.
- 133 Wei C.H., Dahl L.F., J.Amer.Chem.Soc., 1969, 91,
1351.
- 134 Cotton F.A., Hunter D.L., Inorg.Chim.Acta, 1974, 11,
L9.
- 135 Burke J.H., Whitwell G.E.II, Lemley J.T.,
Burlitch J.M., Inorg.Chem., 1983, 22, 1306.
- 136 Cotton F.A., Kitagawa S., Inorg.Chem., 1987, 26,
3463.
- 137 Pimblett G., Ph.D. thesis, University of Manchester,
Manchester, 1986.
- 138 Baker M.V., Field L.D., Inorg.Chem., 1987, 26, 2010.

- 139 Harwood W.S., Qi J-S, Walton R.A., Polyhedron, 1986, 5, 15.
- 140 Fanwick P.E., Root D.R., Walton R.A., Inorg.Chem., 1986, 25, 3724.
- 141 Cotton F.A., Falvello L.R., Najjar R.C., Inorg.Chem., 1983, 22, 770.
- 142 Bino A., Cotton F.A., Fanwick P.E., Inorg.Chem., 1980, 19, 1215.
- 143 McVitie A., B.Sc. thesis, University of Glasgow, Glasgow, 1984.
- 144 Noble B.C., Ph.D thesis, University of Glasgow, Glasgow, 1987.
- 145 Hawkins C.J., "Absolute Configuration of Metal Complexes", Wiley-Interscience, 1971, p.9.

